

CEREBRAL BLOOD FLOW IN THE PIG
A STUDY OF XENON-133 CLEARANCE TECHNIQUES

PROEFSCHRIFT

TER VERKRIJGING VAN DE GRAAD VAN DOCTOR IN DE
GENEESKUNDE
AAN DE ERASMUS UNIVERSITEIT ROTTERDAM
OP GEZAG VAN DE RECTOR MAGNIFICUS
PROF. DR. B. LEIJNSE
EN VOLGENS BESLUIT VAN HET COLLEGE VAN DEKANEN
DE OPENBARE VERDEDIGING ZAL PLAATS VINDEN OP
WOENSDAG 14 SEPTEMBER 1977 DES NAMIDDAGS
TE 4.15 UUR PRECIES

DOOR

WILHELMUS ADRIANUS VAN DUYL
GEBOREN TE ROTTERDAM

PROMOTOR : PROF. DR. G. VAN DEN BRINK
CO-REFERENTEN: PROF. DR. K.H. EPHRAÏM
DR. P.R. SAXENA

Ter nagedachtenis aan mijn moeder

CONTENTS

Acknowledgements

List of symbols, abbreviations

<u>Preface</u>	1
 I <u>Introduction</u>	 4
-1 Outline of investigation	4
-2 Anatomy and physiology of cerebral circulation in man	5
-3 Survey of methods to measure cerebral blood flow	10
 II <u>Description of the clearance technique of measuring cerebral blood flow</u>	 15
-1 A review of the development of clearance techniques	15
-2 Application of the residue-detection method	20
-3 Experience with the application of the Xe-133 inhalation technique on patients	33
-4 Heterogeneity of cerebral blood flow	42
-5 Improvements to the Xe-inhalation technique	49
-6 Alternative methods of analysis of the clearance curves	52
 III <u>Methods and materials for the measurement of cerebral blood flow in the pig</u>	 61
-1 Surgery	61
-1-1 Anatomy of cerebral vessels in the pig	61
-1-2 Preparation of the animal	68
-2 Equipment for the measurement of the clearance curves	77
-2-1 The scintillation detector	77
-2-2 Pulse processing	82

VIII

-3	Computer program for the analysis of the clearance curves	89
-3-1	Digital fitting procedure	89
-3-2	Reliability of the parameters of a fitted exponential model	92
-4	Features of a compartmental model in relation to '81-keV' and '31-keV' clearance curves	98
IV	<u>Results of the experiments in vivo</u>	106
-1	Introduction	106
-2	First group of experiments	106
-3	Second group of experiments	122
-4	Third group of experiments	125
-5	Fourth group of experiments	130
-6	Xe-clearance measurements on dogs	139
-7	Summary of conclusions	144
V	<u>Supplementary investigations</u>	146
-1	Multi-exponential character of the clearance curves	146
-1-1	A study of the heterogeneity of cerebral blood flow in the pig	146
-1-2	Some features of multi-exponential clearance curves	154
-1-3	A study of a multi-exponential clearance model	162
-1-4	Inverse Laplace transformation methods for the analysis of multi-exponential clearance curves	167
-1-5	The use of positive power series of time for the analysis of clearance curves	172
-2	Diffusion effects on the clearance curves	177
-2-1	Phenomena related to intertissue transport of Xe-133	177

IX

-2-2 Determination of the solubility coefficient and diffusion coefficient of Xe in cerebral tissue of the pig	184
<u>Appendix I</u> Characteristics of the collimator for 81-keV and 31-keV radiation of Xe-133	199
<u>Appendix II</u> Analysis of the sorption and desorption curves	206
<u>References</u>	216
<u>Summary</u>	225
<u>Samenvatting</u>	227
<u>Curriculum vitae</u>	229

ACKNOWLEDGEMENTS

This thesis is a result of teamwork.

In the early period of the investigations at Leiden I worked with Dr. K. Mechelse, J.A. Tuynman and W. Krul. I regret that we could not proceed with our good and pleasant collaboration.

I was fortunate that Prof.Dr. G. van den Brink offered me the opportunity to start animal experiments for this research and 'placed at my disposal' a vacancy for a person to look after the physiological aspects of these experiments. Again I was fortunate that Drs. A.C.W. Volkers took the job.

All the experiments in-vivo were done in collaboration with him. I never called on his help in vain, although it often meant experimental work lasting until midnight. At the Technical University at Delft I collaborated with Ir. D. Sparreboom. I am grateful to him that so many students could be involved in these investigations. I hope that both Volkers and Sparreboom take this thesis as a success for their own work too.

I was in the favourable position of supervising students, attached to the Medical Electrical Engineering Group at Delft, who worked on individual aspects of this research. Their predoctoral studies furnished my postdoctoral education. Contributions from their studies are referred to in this thesis.

The use of the ratio of the energy peaks of Xe-133 to determine the position of the Xe-source originates from discussions with Ir. M. de Bruin of the Interuniversity Reactor Institute Delft.

I thank Dr. K. Mechelse for his interest in this research and his assistance in the early period.

Dr. E. Lagerwey and Drs. K. Bijleveld taught us the

anaesthesia and surgery of the pig.

The experiments on the dog were done in collaboration with A. Zwart and A. van Dieren of T.N.O.-Utrecht.

The microspheres technique which we used was introduced to our Faculty by Dr. P.R. Saxena. He also placed the electromagnetic flow probe at our disposal. I am grateful for his willingness to be my co-referent.

Dr. D.J. Griffiths not only improved my English text but also gave valuable comments. I thank him for both.

Furthermore I thank I. van Egmond, J.F. Fasotte, C. Goedegebuur, H.G. Jansen, C.J. Leijdekker, L. Meijer, J. Melchior, Mrs. E.S. Mennema, Dr. E. Mulder, W. Rutgers, Drs. R.S. Stoeckart and C.J. Verleg for their services. I wish to express by gratitude to Prof.Dr. G. van den Brink for stimulating me to write this thesis now. Without his decision I am sure that I should never have stopped preparing it.

Further I am happy that Prof.Dr. K.H. Ephraïm was willing to be my co-referent.

The following team typed my manuscript in its final form. Thanks to Miss C.M.J. Postmus, Miss M.G. van Kruining and Mrs. N.J. Dijkdrenth-Duijzend, through whose skill and diligence this thesis was ready just in time.

LIST OF ABBREVIATIONS AND SYMBOLS

c.b.f.	- cerebral blood flow
Ci	- Curie
exp.nr. 43-I	- experiment number; pig 43, 1st injection
Hct	- haematocrit
I.S.I.	- initial slope index
W.H.M.	- width at half maximum
$P_a\text{CO}_2$	- arterial pressure of carbon dioxide (mm Hg)
P_{CO_2}	- percentage carbon dioxide in expired air
A	- coefficient of an exponential term experimental value expressed in pulses per preset time interval area (diffusion measurements)
a	- length of a tissue column
B	- coefficient of the 'slower' exponential term (see A)
C	- coefficient of the 'slowest' exponential term (see A)
c	- concentration
D	- diastolic; diffusion coefficient
d	- differential thickness of a compartment distance between plane source and collimator face
e	- natural logarithmic base = 2.7
F	- absolute cerebral blood flow (cm^3/min)
f	- specific cerebral blood flow ($\text{cm}^3/\text{min}/100 \text{ cm}^3 \text{ tissue}$)
f(x)	- arbitrary function of x
G	- proportionality factor
g	- proportionality factor
$H^*(t)$	- residue function of tracer in tissue
h(t)	- distribution function of transit times

XIV

\underline{h}	- error-vector
i	- tracer infusion rate
K	- constant (see A)
k	- number of parameters
M	- moment about the origin
m	- number of data
n	- number of exponential terms
p	- variable of Laplace transformation
q	- amount of tracer
r	- pulse rate
S	- systolic; sensitivity parameter
$s(x)$	- spread in a set of values of x
T	- period of time; transposition
$T_{\frac{1}{2}}$	- half value time
t	- time
\bar{t}	- mean transit time
$u(t)$	- unit - pulse - response
V	- tissue volume
W	- relative weight of tissue
x	- arbitrary variable
y	- arbitrary variable
α	- decay constant experimental value expressed in (min^{-1})
β	- decay constant of the 'slower' exponential (see α) solubility coefficient
γ	- decay constant of the 'slowest' exponential (see α)
Δ	- part of
σ	- partial differential
ζ	- eigenvalue
λ	- partition coefficient
μ	- linear attenuation coefficient (cm^{-1})
ξ	- eccentricity of the weighted sum of squares

π	- = 3.14
ρ	- correlation coefficient
Σ	- algebraic sum
$\sigma(x)$	- standard deviation of a variable x
τ	- time constant (min)
ϕ	- weighted sum of squares
\sim	- infinity
$*$	- convolution
$!$	- faculty
\bar{x}	- mean value of x
\underline{p}	- vector p

indices

a	- arterial
b	- blood
cap	- capillary
g	- grey cerebral tissue
i	- i-th exponential term
j	- j-th data point
n	- n-th exponential term; n-th moment
s	- solute
t	- tissue
v	- venous
w	- white cerebral tissue
81	- 81-keV
31	- 31-keV
o	- initial value

CEREBRAL BLOOD FLOW IN THE PIG
A STUDY OF XE-133 CLEARANCE TECHNIQUES

PREFACE

As a member of the Department of Electrical Engineering of the Technical University Delft the author was initially involved in 1968 in the development of an apparatus for the measurement of cerebral blood flow on patients by the Xe-133 inhalation technique. The interest in this topic was aroused by members of the Department of Electro-neurology of the Academic Hospital Leiden (head dr.K. Mechelse, neurologist). In collaboration with J.A. Tuynman, neurologist, and W. Krul, medical student, preliminary investigations were performed using a provisory set-up. Results of these experiments are described in this thesis. Because at that time unsufficient funds were available to establish permanent clinical apparatus for these measurements, the experiments were not continued. From the preliminary investigations it was concluded that further basic research on Xe-clearance methods for the measurement of cerebral blood flow was needed. The Xe-133 inhalation technique is an atraumatic alternative to the traumatic Xe-133 injection technique for the measurement of cerebral blood flow. Xe-133 is administered by means of an intracarotid injection in the injection technique. This injection limits the clinical applicability of this method, although measurements made by the injection technique are more reliable than those made by the inhalation technique. Systematic differences between the results of the two methods have been reported. Because the clinical advantages of inhalation technique, more research on the causes of these discrepancies and an improvement of the inhalation technique seemed to be justified.

As soon as the Central Isotope Laboratories of the Medical Faculty of the Erasmus University (head dr.E. Mulder) started its activities in 1971, investigation on Xe-133 clearance methods in the pig was started. The reasons for our choice of the pig as an experimental animal are given in the thesis.

It was initially planned to perform cerebral blood flow measurements with injection and inhalation simultaneously using the radioactive inert gases Kr-85 and Xe-133. The author was enabled to perform these experiments as a member of the Department of Biological and Medical Physics of the Medical Faculty of the Erasmus University (head prof.dr.G. van den Brink). Drs.A.C.W. Volkers of the same department was involved in the work to look after the physiological aspects of the animal experiments. At the beginning we were assisted by dr.K. Mechelse, neurologist and at that time member of the Department of Neurology of the Academic Hospital Dijkzigt, and the veterinary surgeons dr.E. Lagerwey and drs.K Bijleveld, both from the Veterinary Faculty of the University of Utrecht. Since the author is a part time member of the Medical Technology Group of the Department of Electrical Engineering of the Technical University Delft, he supervised a number of engineering students performing studies on individual aspects of the Xe-133 clearance technique in collaboration with ir.D. Sparreboom, member of that Group.

Because the literature did not furnish clear pictures of the anatomy of cerebral vessels of the pig, an angiographic study was carried out in collaboration with J.F. Fasotte, technician of the Department of Experimental Surgery of the Erasmus University (head dr.D.L. Westbroek).

Much attention was given to the Xe-133 injection

technique, because many problems arose in the evaluation of this technique on the pig. Results of that study are described in this thesis. The evaluation of the inhalation technique on the pig was postponed for that reason.

No reference data on the cerebral blood flow of the pig were available until Foreman et al published in 1976 their study of the cerebral blood flow of the pig, performed by the radioactive microsphere technique. They reported a wide overlap of blood flow ranges in grey and white cerebral tissue. This finding furnished a basis for the explanation of the results which we obtained with the Xe-133 injection technique.

Because of the small differences between blood flows in grey and white cerebral tissue, special problems are involved in the interpretation of the Xe-133 clearance curves in the pig, which are not found in normal man. Consequently a comparison of the results of the Xe-133 injection technique with those of the Xe-133 inhalation technique is not representative of a comparison of these techniques applied in man. Therefore it is concluded in this thesis that the pig is not a good experimental animal in which to study Xe-133 clearance methods for the measurement of human cerebral blood flow.

Apart from the unexpected problems with regard to the experimental animal, the regulations concerning the use of radioactive material delayed the planned evaluation of the inhalation technique in comparison with the injection technique.

This thesis gives a description of a variety of physiological experiments and a comparison of possible mathematical models, which hopefully will contribute to further development in the field of measurement of cerebral blood flow.

I-INTRODUCTION

I-1 Outline of investigation.

Cerebrovascular disease is an important cause of death. The number of cerebrovascular complaints is increasing, mainly as a consequence of increasing the mean lifetime. Functioning of the brain is dependent on blood supply. A temporary or prolonged reduction of total or regional cerebral blood flow (c.b.f.) may lead to irreversible damage of cerebral tissue and loss of neurological functions. Therefore the measurement of cerebral blood flow, preferably in different regions, is clinically important. Several methods of measuring c.b.f. have been developed. The applicability of a method in a clinical situation depends on its traumatic aspects. A brief survey of the methods of c.b.f. measurement is given at the end of this chapter. The clinical method used most frequently is the Xe-133 clearance technique. The Xe-133 is administered by three different routes, intra-arterial, intravenous or by inhalation. This thesis mainly deals with the intra-arterial injection technique, evaluated on the pig as experimental animal.

The role of the pig as an experimental animal in human medical research has an increasing importance (Bustad and Mc Clellah, 1966). An interesting review of applications and analogies of the pig in human medical research is given by W.R. Douglas (1972). Because of the similarity of the heart and the circulatory system of the pig to those of man, this animal is of special interest in cardiovascular research. For that reason it could replace the dog in that field. One approach to the understanding of predisposing factors and pathogenetic mechanisms in the development of cerebrovascular

diseases is the study of comparable pathophysiological processes in animals. In this context it is of great interest that cerebral atherosclerosis with consequent cerebral infarction is common in aged pigs (Luginbuhl and Detweiler, 1967). Despite this interest in the pig as experimental animal, little is known of the cerebral circulation of the pig. At the beginning of our experiments we were not aware of this lack of knowledge. Our choice of the pig for the c.b.f. measurements was based on the following considerations;

- 1-the assumption of the similarity of the anatomy and physiology of its cerebral circulation to those of man;
- 2-the availability and price of this animal;
- 3-the size of the cerebrum;
- 4-the advanced research on a stable anaesthesia scheme for the pig carried out by Lagerwey (1973) at the Thorax center of our medical faculty.

I-2 Anatomy and physiology of cerebral circulation in man.

The human brain is supplied with blood via two pairs of arteries, the right and left internal carotid arteries and the right and left vertebral arteries. These vessels are interconnected in the circle of Willis. The internal carotid artery is one of the two branches of the common carotid artery. The other branch, the external carotid artery, mainly supplies extra-cerebral tissue. Collateral circulation between intra- and extra-cranial circulation is not important. The right common carotid artery branches off from the branchiocephalic trunk and the left common carotid artery branches off from the aortic arch. Though the vascular systems of right and left hemispheres are

interconnected via the circle of Willis, normally blood circulates separately in each hemisphere. The circumferential afferent cerebral vessels surround the cerebrum and penetrate the upper grey brain tissue layer (cortex). The arteries are subdivided finally into very small arteries, the arterioles (30-100 μm in diameter). The arteries are capacitance vessels, while the arterioles are resistance vessels. The blood pressure is damped and reduced in these vessels.

The arterioles also control the blood supply to the capillary network by a smooth muscle layer, which enables an adjustment of their diameters. In most capillary networks there are two further flow regulating systems, namely precapillary sphincters and arterio-venous anastomotic vessels. Via the permeable wall of the capillaries metabolic substances (glucose, oxygen) enter the surrounding tissue. Metabolic residues (e.g. carbon dioxide) diffuse from the tissue into the blood. The exchange between the capillaries and the metabolizing cells takes place via an intermediate diffusion medium, the aqueous intercellular fluid. From the assumption of a balance between oxygen consumption and the rate of oxygen transport by diffusion, Krogh (1918) calculated the diameter of the tissue cylinder which is supplied from one capillary. Thus it can be understood, that the capillary density in a particular type of tissue is related to the oxygen consumption in it. The cerebral cortex contains the cell bodies of neurons. By its more grey appearance this type of cerebral tissue can be distinguished by eye from deeper brain tissue. The bordering white brain tissue consists mainly of the axons of the neurons. The white appearance of this tissue originates from the fatty myelin sheets of the axons. The nuclear mass (e.g. thalamus) in the centre of the cerebrum also consists of a mass of cell bodies.

The volume ratio of grey to white brain tissue is about 1:1 (Henneberg, 1910). The total vascular volume is about 5% of the whole cerebrum (Smith et al, 1971), while the capillary volume is less than 3% of the cerebrum (Lierse, 1963).

The venous cerebral drainage system is interconnected very extensively, both internally and with the extracranial venous system. Blood from capillary networks converges to venules. Blood from the venules is collected in a superficial and a deep venous system. These systems end in several blood pools, the venous sinuses. The sinuses empty into the right and left internal jugular veins, the vertebral veins and the internal maxillary veins. Via the superior vena cava, blood returns to the heart.

In man cerebral circulation requires about 15% of the cardiac output (Ph. Bard, 1961). In comparison with the relative weight of the cerebrum to the weight of the whole body this figure is high. The cerebral blood flow is about $50 \text{ cm}^3/\text{min} / 100 \text{ gram tissue}$, while the blood flow of the whole body is about $10 \text{ cm}^3/\text{min} / 100 \text{ gram tissue}$. The cerebrum is exclusively protected against insufficient circulation in an emergency (shock), even at the expense of other organs. The maintenance of a sufficient cerebral circulation is a necessary priority, because the cerebrum has no oxygen storage capacity and lack of oxygen in the central nervous system very soon leads to irreversible damage. That is why the cerebral circulation is controlled by a complex physiological system. In man exercise does not alter c.b.f. (Hedlund et al 1962, Zobl et al 1965), though it increases significantly in regions associated with increased metabolic activity (Risberg and Ingvar, 1973; Olesen, 1971; Tschetter et al, 1970).

From the ratio of perfusion rate F and the arterio-venous pressure difference ΔP a vascular resistance R is often derived by analogy to Ohm's law, i.e. $R = \Delta P / F$. In contrast to this simple relationship, however, the vascular resistance is determined by the physiological control mechanisms, and consequently is neither linear, nor passive. One factor affecting the vascular resistance is the geometrical structure of the vascular network. As already mentioned, the muscular layer of the arterioles controls their diameters. The tone of each arteriole is believed to be controlled neurogenic and by its own interstitial fluid pH. Blood pressure is sensed by baroreceptors, concentrated in a neuroplexus, situated in the internal carotid artery near its origin from the common carotid artery (carotid sinus), and in the aortic arch. It has been shown (e.g. by Kety and Schmidt, 1948) that c.b.f. remains virtually constant over the physiological range of pressure. Thus c.b.f. is protected from both high and low blood pressure. This phenomenon is known as the autoregulation of the cerebral circulation, and is reflected in a non-linear vascular resistance. This autoregulation is in contra-distinction to most other vascular systems, and can be impaired after cerebrovascular accidents (Paulson et al, 1970).

The pulsatile flow seems to meet less resistance in the cerebrum than an equal constant flow (Held et al, 1969), so that one should speak of an impedance rather than a resistance of the vascular system. Furthermore it has been observed (Misrahy and Clark, 1958), that there is a stop-and-go blood flow in the micro-circulatory system, instead of a continuous flow, with a periodic time of 5-25 seconds.

Besides nervous control mechanisms chemical mechanisms related to metabolism are involved in cerebral homeostasis.

The most effective agent is carbon dioxide. Grubb et al (1974) found in monkeys a linear relationship between arterial pressure of carbon dioxide, $P_a\text{CO}_2$ (mmHg), and c.b.f., with the equation: $f = 1.8P_a\text{CO}_2 - 16.75 \text{ cm}^3/\text{min}/100\text{g}$. Inhalation of air containing 5% CO_2 normally results in an increase of c.b.f. of about 50%, while inhalation of 7% CO_2 causes c.b.f. to double (Purves, 1972). In the cerebrum the local regulatory effect of carbon dioxide is vasodilatation, which results in an increase of local perfusion. Local regulation of c.b.f. meets local need for removal of CO_2 or supply of O_2 . This need can be met by an increase of blood perfusion. However, as long as the gas in the capillary blood is not in equilibrium with the extra-capillary space, an increase in residence time of the blood in the capillary network is also effective. As the mean residence time is equal to $V_{\text{cap.}}/F$, an increase in vascular blood volume results in an increase of mean residence time at constant perfusion. Since this increase in capillary blood volume accompanies with a decrease in intercapillary distance, the gas transport rate becomes less limited by diffusion at the same time. In monkeys Grubb et al (1974) found that for a pressure change of one mmHg in $P_a\text{CO}_2$, there was a change in cerebral blood volume of $0.041 \text{ cm}^3/100 \text{ gram}$ perfused tissue. It turns out that gas transport in cerebral tissue is controlled by altering both the perfusion and the capillary blood volume. (Allan et al, 1970; Smith et al, 1971). In monkeys Grubb et al (1974) found a non-linear relationship between vascular mean transit time and c.b.f.. From the clearance measurements with diffusable tracers figures for the specific blood flow are derived, i.e. the ratio of the absolute perfusion rate F divided by perfused tissue volume V .

As the capillary volume is only about 3% of tissue volume, a change in capillary blood volume is not reflected in the figure for specific blood flow. In other words the clearance technique with diffusable tracers does not fully evaluate the physiological adaptation in tissue to assure adequate gas transport. Nevertheless the measurement of c.b.f. according to the clearance technique with diffusable tracers, at different values of the percentage carbon dioxide in respiration air, P_{CO_2} , is of clinical interest, as it constitutes a test of perfusion control function.

I-3 Survey of methods to measure cerebral blood flow.

Many different methods to measure cerebral blood flow are available for clinical application, however, each one has its own particular limitations. A survey is given by e.g. Capon et al (1968). A brief survey of methods, with their principal limitations is given here,

Electromagnetic flow probes.

An annular probe, in which a magnetic field is generated, is placed around a bloodvessel, e.g. the internal carotid artery. The flowing blood cuts the magnetic lines of force, so that an electromagnetic force is generated. This e.m.f. is sensed by electrodes mounted on the probe, located at diametrically opposed points of the lumen of the vessel. The electric signal is calibrated in terms of blood flow. As the calibration is dependent on the local situation of the probe, it is preferable to perform the calibration in each set-up. The zero-flow reference may change in the situation in-vivo, so that a repeated zero-flow test must be carried out. Both, calibration and zero-flow reference

test are not always easy to perform in vivo, and thus limit the applicability and reliability of the electromagnetic flow probes measurements. Furthermore, the exposure of the vessel to the probe may cause vasospasm, and this method is traumatic. It reveals total blood flow only to the region supplied by the vessel.

Ultrasonic Doppler technique.

When an ultrasonic wave impinges upon a blood stream, the frequency of the waves reflected from the moving particles is shifted, because of the Doppler effect. A typical repetitive noise pattern is received which after demodulation with the transmitted frequency it can be calibrated in terms of blood flow, provided the diameter of the vessel is known. The probe is directed towards the blood vessel; no preparation of the vessel is necessary. This method is clinically attractive. However, since the diameter of the vessel usually is not known, it cannot be calibrated.

Rheoencephalography.

If an alternating voltage (e.g. 20 kHz, 5 V) is applied across the head, an electric current can be measured which is modulated by the pulsatile flow. The applicability of this method is small, because the variation of the impedance is mainly due to extracranial blood flow and total blood volume.

Heat-clearance techniques.

A thermo couple or thermistor is inserted into a vessel or brain tissue. The temperature of the probe is kept constant at a slightly higher level than its environment, by applying an electric current. The

current required to maintain this temperature difference is a measure of the rate of removal of heat by the blood and can be calibrated in terms of blood flow. A disturbing factor is the physiological variation of the blood temperature. The method is invasive and traumatic. In another heat-clearance technique a heat bolus is injected, and a temperature decay is sensed, e.g. by a thermistor which is placed downstream. This technique, however, is inferior to dilution techniques where dyes like cardiogreen are used.

Serial angiography.

In cerebral angiography X-ray pictures are taken while the vessels are filled with an X-ray contrast medium. These pictures yield important information about the anatomy of the vascular system. Cerebral circulation can be studied from angiograms by means of X-ray films of the transit of the contrast medium, which is injected arterially. Though the transit time of the contrast medium is related to blood flow, a reliable measure of c.b.f. cannot be derived from it. For c.b.f. measurement the transit time of a diffusable gas, like Xe-133, is a better measure. Valuable complementary information is gained by the combination of angiography and the Xe-clearance technique, performed in one arterial puncture. Since contrast medium may induce alterations in c.b.f. measurement of c.b.f. should precede angiography.

Radioactive-tracer transit methods.

The transit by blood of a substance through the cerebrum, is related to blood flow. To measure the transit time of the substance, radioactive labels are

used. Two types of tracer substances are used for c.b.f. studies, namely tracers not diffusing outside the vascular system, like I-131-Hippuran or Tc-99m-sodium pertechnetate (radiocirculography) and diffusable tracers like Xe-133 or Kr-85 (clearance technique). In both cases a bolus of tracer is injected into the internal carotid artery and the radioactivity is detected by scintillation detectors placed extracranially. The use of diffusable tracers has replaced radiocirculography, since the latter yields much less quantitative information. Because of the trauma of the carotid puncture, alternative methods of application of the tracer gas are of great interest. In particular, the application of Xe-133 by inhalation is very attractive from clinical point of view, because of its atraumatic nature.

Tracer fractionation methods.

It is assumed that the distribution of a tracer applied arterially, to different tissue regions is in proportion to the distribution of flow to these regions (Sapirstein's principle). Purely experimental methods of c.b.f. measurements have been developed from this principle. The tracer accumulated in different tissue regions is measured on tissue samples from an experimental animal. In this way a pattern of c.b.f. distribution is obtained. The distribution of the radioactivity in the tissue can be studied by means of X-ray films exposed to the tissue (autoradiography), or by counting the activity of the samples with detectors. Diffusable tracers used for autoradiographic studies are I-131-trifluoriodomethane and C-14-antipyrine. To study heterogeneity of c.b.f. vascular bound tracers are also used, i.e. radioactively

labelled microspheres. Microspheres with diameters of about 15 μm are trapped in the capillaries. Metabolizing microspheres are made of albumen. A disadvantage of these microspheres is that they release the label. Stable microspheres are the carbonized microspheres supplied by 3-M Company. They consist of a compound containing 67% carbon and 23% Oxygen. The radioactive nuclide is incorporated in the spheres.

II-DESCRIPTION OF THE CLEARANCE TECHNIQUE OF MEASURING CEREBRAL BLOOD FLOW.

II-1 A review of the development of clearance techniques.

A method for the measurement of cerebral blood flow, in which nitrous oxide is used, was published in 1945 by Kety and Schmidt. Nitrous oxide is a metabolically inert gas and is freely diffusible in tissue. The residence time of this gas is determined by the rate of perfusion of tissue by blood. Since the gas is inert, the law of conservation of substance holds (Fick's principle). If the blood flow through an organ is F and the concentrations of the gas in the arterial and the venous blood of that organ are c_a and c_v respectively, then the rate of tracer accumulation in the organ is, according to the Fick's principle,

$$\frac{dq}{dt} = F (c_a - c_v) \quad (1)$$

where q is the amount of tracer in the tissue.

Further, it is assumed that nitrous oxide diffuses so easily in the tissue that its distribution in the tissue may be taken to be in thermodynamic equilibrium, even during uptake and clearance of the gas by the perfusion of the blood. From theoretical considerations Kety (1951) argues that the concentration of the gas in venous blood is continuously in equilibrium with the mean concentration in the tissue.

According to Henry's law, the concentration of a non-polar gas in a substance is proportional to the partial pressure of the gas in the gas phase with which the substance is in thermodynamic equilibrium. The ratio of the concentration c_t of the dissolved gas in the tissue

and the concentration c_g in the gas phase is the (Ostwald-) solubility coefficient β ,

$$\beta = \frac{c_t}{c_g} \quad (2)$$

For the description of the clearance process we need the equilibrium ratio of the concentrations of the gas in tissue and in blood. This ratio is called the tissue-blood partition coefficient λ and can be obtained from the solubility coefficients by the relation

$$\lambda = \frac{c_t}{c_b} = \frac{c_t / c_g}{c_b / c_g} = \frac{\beta_t}{\beta_b} \quad (3)$$

where c_b is the concentration of the gas in blood. Since Henry's law holds for nitrous oxide, the hypothesis of Kety implies that

$$c_t = \frac{q}{V} = \lambda c_b = \lambda c_v \quad (4)$$

where V is the tissue volume.

Substitution of (4) in (1) gives the differential equation,

$$\frac{dc_t}{dt} + \frac{F}{\lambda V} c_t = \frac{F}{V} c_a \quad (5)$$

By integration we find

$$f = \frac{F}{V} = \lambda \frac{c_v(t_2) - c_v(t_1)}{\int_{t_1}^{t_2} (c_a - c_v) dt} \quad (6)$$

where f is the blood flow. t_1 and t_2 are the times of the beginning and the end of the observation.

The nitrous oxide was administered by inhalation. During uptake, arterial and venous concentrations were measured in blood samples by means of an infra-red

gas analyzer. Blood samples were taken from the carotid artery and the jugular vein. A problem here is that blood samples from the jugular vein yield the concentration of mixed venous blood. The concentration of the gas in jugular venous blood is not equal to λ times the mean concentration in cerebral tissue, unless all parts of the cerebrum are fully equilibrated to the concentration in arterial blood. This equilibrium level is reached when the concentration in cerebral venous blood equals the concentration in arterial blood. Kety and Schmidt (1945) found that the concentration in jugular venous blood had nearly reached the arterial level after an uptake time of 10 minutes. Hence the formula used to calculate blood flow in the original Kety-Schmidt technique is

$$f = \lambda \frac{c_v (10 \text{ min})}{\int_0^{10} (c_a - c_v) dt} \quad (7)$$

In 1965 Lassen and Klee published results of the analyses of uptake curves and the succeeding clearance curves of diffusable inert gas (Kr-85). After an uptake time of 10 minutes the clearance was started by inhalation of fresh air. Formula (6) applies for both the uptake and the clearance phases. It turned out, however, that the calculated blood flow was on average 8.5% higher during uptake than during clearance. At lower flow rates this percentage increased. The cause of this discrepancy is that an uptake time of ten minutes is not sufficient to reach equilibrium between tissue and arterial blood in poorly perfused regions, even though jugular venous concentration may approximate the arterial concentration rather well after ten minutes. Lassen and Klee concluded that the

error in the Kety-Schmidt technique may be counteracted by prolonging the uptake time to 15 or 20 minutes and by extrapolation of the measured concentration curves to infinity, using exponential functions. Another significant modification in the method of Lassen and Klee is the use of the radioactive β -emitter Kr-85 instead of nitrous oxide. This makes the measurement of concentration in blood samples easier and more accurate. As Kr-85 is a radioactive tracer, its amount in the cerebrum can be measured directly by a detector placed over the cranium. To obtain regional information such detection has to be restricted to a part of the cerebrum, by collimation.

Studies of this so-called residue detection method have been described by Lewis et al (1960). Detection of Kr-85 by its β -radiation needs the cranium to be opened, which of course reduces the applicability of the method. Ingvar and Lassen (1962) introduced an important modification of the residue-detection method. They administered Kr-85 by an injection into the internal carotid artery instead of by inhalation. They assumed that the clearance of Kr-85 from blood passing the lungs is highly effective, so that recirculation of the gas is negligible. This implies that $c_a = 0$ during the clearance phase, so that the differential equation (1) combined with (4) becomes,

$$\frac{dc_t}{dt} = - \alpha c_t \quad (8)$$

where

$$\alpha = \frac{F}{\lambda V} \quad (9)$$

If the initial concentration in the tissue at the beginning of the clearance is $c(T)$, the solution (8) is

$$c(t) = c(T)e^{-\alpha(t-T)} \quad (10)$$

From the steepness of the clearance curve, plotted on a semi-logarithmic scale, α can be found and hence the blood flow with the formula

$$f = \lambda\alpha \quad (11)$$

We may expect a mono-exponential clearance curve only if the tissue is homogeneous with respect to α . Such a homogeneously cleared part of tissue is referred to as a compartment. If a bolus, having a total activity q_0 Ci is injected very quickly, so that clearance has not yet started when q_0 is distributed evenly in the tissue, we have,

$$c(T) = \frac{q_0}{V} \quad (12)$$

As will be described in the next section, experimental cerebral clearance curves appear not to be mono-exponential, so that the clearance process is not that of a one-compartment system.

Since 1963 (Glass and Harper) Kr-85 has been replaced by the very attractive soft gamma emitter Xe-133. With this tracer gas the residue-detection method can be performed with intact skull and an acceptable radiation dose. Some relevant characteristics of Xe-133 and Kr-85 are given in Table 1. From the point of view of radiation safety it is important that Xe-133 has a small physical half-lifetime $T_{\frac{1}{2}}$.

isotope	particle emitted	find isotope	$T_{1/2}$	$E_{\max} \beta$ (MeV)	$E \gamma, x$ (MeV)	β_g	β_w
Kr-85	β^-	Rb-85	12.6 y	0.67	0.52 (in 0.4% of emission)	0.055	0.076
Xe-133	β^-	Cs-133	5.3 d	0.35	0.081 and 0.031	0.1	0.2

Table 1.: Some characteristics of the radioactive tracer gases Kr-85 and Xe-133: β_g and β_w are the solubility coefficients of grey and white cerebral tissue respectively.

At present the injection with Xe-133 is the most frequently used method for the measurement of cerebral blood flow in both clinical and physiological studies. An important disadvantage for clinical application of the injection technique however is the necessity of the arterial puncture. For this reason Mallett and Veall (1963) developed a method of Xe-administration by inhalation, similar to the original method of Kety and Schmidt, but combined with the residue-detection method. Although the atraumatic inhalation procedure is clinically attractive, it is afflicted with some serious problems, making this method less attractive from a measurement point of view. It has not yet been decided which of the two methods is preferable under different circumstances. To discuss both methods we must describe in more detail the application of the residue-detection method to the measurement of c.b.f..

II-2 Application of the residue-detection method.

In Fig. 1 the measurement of regional cerebral

blood flow by the injection method is illustrated. This figure also shows a recording of the radioactivity of the expired air, although there is no need for this recording in the injection technique. This expired air activity curve is shown in order to compare it with the curve which is recorded when the inhalation technique is applied. In the inhalation technique this air activity curve is used in order to correct for tracer recirculation.

The 'field of vision' of the extra-cranial radiation detector is defined by the collimator. In this way the clearance from a defined region of the cerebrum is measured. Each detected photon from this region is converted into an electric pulse. Hence, the detected radioactivity is expressed as a pulse rate r . The pulse rate is proportional to the radioactivity in the detector field. As a consequence of the absorption of radiation in the tissue and of the heterogeneity of detection efficiency, the proportionality factor depends on the geometrical distribution of the tracer in the tissue. Since this distribution does not change in a compartment, the proportionality factor is a constant. Thus we define this factor G by

$$r(t) = G \Delta V c(t) \quad (13)$$

where ΔV is the amount of tissue within the detector field.

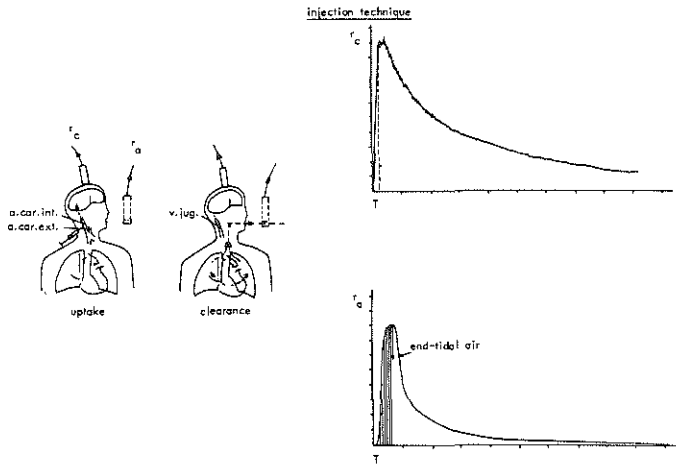


Fig. 1.: Illustration of the measurement of cerebral blood flow according to the injection technique.

If measurements are performed using the injection technique with Xe-133, it turns out that the cerebral clearance curves cannot be described by mono-exponential functions. An example of a semi-logarithmic plot of a clearance curve is shown in Fig. 2. It reveals that a sum of two exponential terms does provide a good fit. The half-value-time $T_{\frac{1}{2}}$ of the slow component is about 5 minutes and of the fast component is about 0.8 minutes. As the ratio of the decay constants is about 6, the two exponential terms can be separated rather well using a simple graphic peeling technique (Perl, 1960).

Two types of tissue can be distinguished in the cerebrum, the cortical grey brain tissue and the more fatty white brain tissue deeper in the brain. The capillary density in the grey tissue is greater than it is in the white tissue and the specific blood flow in the grey tissue is also greater than that in the white tissue. The partition coefficient of Xe in white tissue is greater than it is in grey tissue. The differences between grey and white tissue are illustrated in Fig. 2.

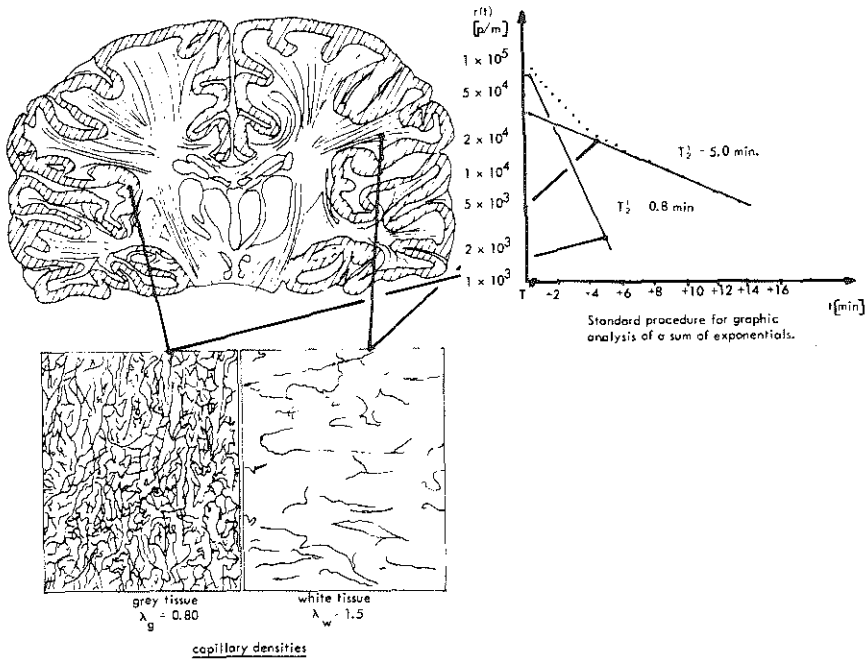


Fig. 2.: Interpretation of the two exponentials fitted to the clearance curve, according to the two-compartmental model.

The usual interpretation of the bi-exponential clearance curve (e.g. Hoedt-Rasmussen et al, 1966) is that the 'fast' exponential term represents the clearance of the grey tissue compartment and the 'slow' exponential term the clearance of the white tissue compartment. Hence the interpretation of the parameters of the fitted mathematical model

$$r(t) = Ae^{-\alpha t} + Be^{-\beta t} \quad (14)$$

is as follows:

$$\alpha = \frac{f_g}{\lambda_g}$$

where f_g is the specific blood flow in grey tissue
 λ_g is the tissue-blood partition coefficient
of grey tissue

$$\beta = \frac{f_w}{\lambda_w}$$

where f_w is the specific blood flow in white tissue
 λ_w is the tissue-blood partition coefficient
of white tissue

A is the initial pulse rate from grey tissue
compartment

B is the initial pulse rate from white tissue
compartment

Following the principle of Sapirstein (1958), it is assumed that the amount of tracer injected into the artery will be distributed to the various regions supplied with blood by this artery in proportion to the blood flow to these regions. Hence the part q_g of the original amount q_0 that enters the grey tissue compartment, and the part q_w that enters the white

tissue compartment are respectively,

$$q_g = \frac{F_g}{F_g + F_w} q_o \quad q_w = \frac{F_w}{F_g + F_w} q_o \quad (15)$$

where F_g and F_w are the values of blood flow of grey and white tissue compartments, so that

$$F = F_g + F_w \quad (16)$$

By using proportionality factors as defined in formula (13), namely G_g for the grey tissue compartment and G_w for the white tissue compartment, we write

$$A = G_g \frac{q_g}{V_g} \Delta V_g \quad \text{and} \quad B = G_w \frac{q_w}{V_w} \Delta V_w \quad (17)$$

Combining the formulas (14), (15), (16) and (17) we find

$$r(t) = \frac{q_o}{F} \left(G_g f_g \Delta V_g e^{-\frac{f_g}{\lambda_g} t} + G_w f_w \Delta V_w e^{-\frac{f_w}{\lambda_w} t} \right) \quad (18)$$

The difference between G_g and G_w will be discussed in section III-3-2. We simplify the situation by taking $G_g = G_w = G$. We may write then

$$r(t) = \frac{q_o G}{F} \left(f_g \Delta V_g e^{-\frac{f_g}{\lambda_g} t} + f_w \Delta V_w e^{-\frac{f_w}{\lambda_w} t} \right) \quad (19)$$

The volumes of grey and white tissue can be calculated, as fractions of the volume of cerebral tissue in the detector field from the coefficients A and B by means

of the formulas

$$W_g = \frac{\Delta V_g}{\Delta V_g + \Delta V_w} = \frac{A/f_g}{A/f_g + B/f_w} \quad (20a)$$

$$W_w = \frac{\Delta V_w}{\Delta V_g + \Delta V_w} = 1 - W_g \quad (20b)$$

These fractions W_g and W_w are referred to as the relative weights of the grey and white tissue compartments respectively. With these relative weights we can calculate the regional mean specific blood flow, using the formula

$$\bar{f} = W_g f_g + W_w f_w \quad (21)$$

Specific blood flow values could be expressed in cm^3 blood per second per cm^3 tissue. It is, however, convention to express it in cm^3 blood per minute per 100 gram tissue. Where we refer to values from literature we will follow the convention. Our results will be expressed in $\text{cm}^3/\text{min}/100 \text{ cm}^3$ tissue. According to Ingvar et al (1965) figures of c.b.f. in man, referred to as normal values are:

$$\begin{aligned} f_g &= 79.7 \pm 10.7 \text{ cm}^3/\text{min}/100 \text{ g tissue} \\ f_w &= 20.9 \pm 2.6 \text{ cm}^3/\text{min}/100 \text{ g tissue} \\ \bar{f} &= 49.8 \pm 3.9 \text{ cm}^3/\text{min}/100 \text{ g tissue} \\ W_g &= 0.492 \pm 0.039 \end{aligned}$$

Since the solubility of Xe is greater in erythrocytes than it is in blood plasma, the partition coefficients depend on the haematocrit of the blood. Fig. 3 shows the dependance of the solubility coefficient of Xe and

Kr in blood on the haematocrit, adopted from measurements of Kitani (1962). In this figure are also shown the partition coefficients, calculated with formula (3). For a haematocrit of about 40% we find, for Xe, $\lambda_g = 0.8$ and $\lambda_w = 1.5$. These values of the partition coefficients are used to calculate the blood flow values f_g and f_w with formula (14).

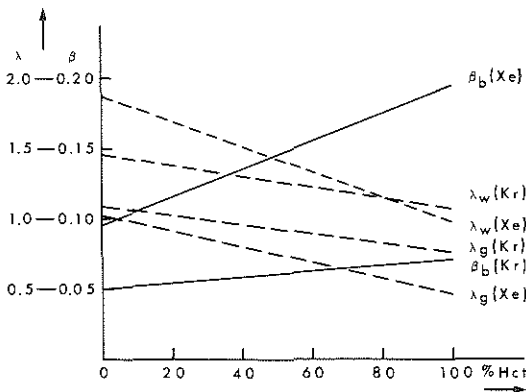


Fig. 3.: Solubility coefficients β_b of Xe and Kr in blood and tissue-blood partition coefficients λ_g and λ_w of grey- and white brain tissue, related to haematocrit.

If the tracer is administered according to an arbitrary infusion function, the radioactivity recorded extra-cranially, depends on the course of that infusion function. According to the theory of linear systems the response of a system to an arbitrary input function equals the convolution of the input function and the pulse response of that system. Therefore we introduce a pulse response function $u(t)$, which is the curve recorded extra-cranially, following the pulsatile infusion of unit amount of tracer. Hence from (19) we derive

$$u(t) = \frac{G}{F} \left(f_g \Delta V_g e^{-\frac{f_g}{\lambda_g} t} + f_w \Delta V_w e^{-\frac{f_w}{\lambda_w} t} \right) \quad (22)$$

For the tracer infusion rate $i(t)$ we write

$$i(t) = F c_a(t) \quad (23)$$

When an arbitrary infusion of tracer is applied, then the extra-cranial recorded curve is,

$$r(t) = \int_0^t i(t') u(t - t') dt' \quad (24)$$

so that,

$$r(t) = G \int_0^t c_a(t') \left(f_g \Delta V_g e^{-\frac{f_g}{\lambda_g} (t - t')} + f_w \Delta V_w e^{-\frac{f_w}{\lambda_w} (t - t')} \right) dt' \quad (25)$$

or using relative weight factors,

$$r(t) = GV \int_0^t c_a(t') \left(f_g W_g e^{-\frac{f_g}{\lambda_g} (t - t')} + f_w W_w e^{-\frac{f_w}{\lambda_w} (t - t')} \right) dt' \quad (26)$$

As mentioned in section II-1, it is assumed that the tracer gas in venous blood from cerebral tissue, leaves the body via perfusion and ventilation in the lungs. This is not strictly correct because a fraction of the gas in the pulmonary capillary blood remains in equilibrium with alveolar air, and contributes to the recirculation of some gas to the cerebrum. Hence, because of the recirculation, the tracer administered as a pulse into the artery is followed by an 'infusion' of recirculated tracer.

The effect of recirculation of Xe or Kr on the measurement of c.b.f. by the injection technique has been studied by Hoedt-Rasmussen et al (1966). The extent of tracer recirculation was evaluated by an intravenous injection of the same amount of radioactivity as employed in the intra-arterial injection. They found that recirculation does not influence the initial height of the clearance curve. When Xe is injected intravenously, the radioactivity of the cerebrum increases after some delay, reaches a maximum value about one minute after the injection and thereafter decreases gradually, showing, after about seven minutes, a steady clearance rate corresponding to a mono-exponential function with $T_{1/2}$ of about the same magnitude as the tail part of the clearance curve after an intra-arterial injection. According to Hoedt-Rasmussen et al, recirculation affects the result of two-compartmental analysis mainly by increasing the coefficient of the 'slow' exponential, thus leading to an underestimation of the relative weight of the grey tissue compartment by about 7%.

If the tracer gas is administered by inhalation, recirculation has more severe consequences for the analysis of the clearance curves. Fig. 4 gives an illustration of the measurement of c.b.f. by the

inhalation technique. In the method described by Mallett and Veall (1965) the Xe-gas is administered by having the patient to breathe from a closed circuit for 5 minutes. After this uptake period, the intake of the circuit is closed to the Xe-supply and opened to room air and at the same time the Xe passes via an outlet tube to the outside air. The clearance onset is then recorded extra-cranially for 20 minutes.

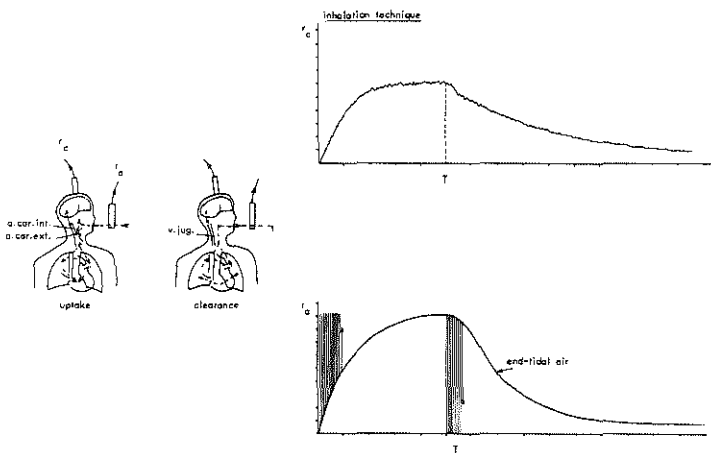


Fig. 4.: Illustration of the measurement of cerebral blood flow, according to the inhalation technique.

They reported that this clearance curve could be fitted by a sum of two exponential terms with $T_{\frac{1}{2}}$ (fast component) = 1.40 ± 0.02 min and $T_{\frac{1}{2}}$ (slow component) = 10.75 ± 0.20 min. Hence the clearance found here is much slower and the ratio of the decay constants greater than in the injection technique. Two causes of these differences have been mentioned in literature, i.e. the recirculation of the tracer and the contribution of extra-cerebral tissue to the clearance curve.

At the end of the uptake period in the inhalation technique, the arterial tracer concentration does not fall immediately to an insignificant level, as is supposed to be the case in the injection technique. Since in the inhalation technique the tracer is accumulated in the whole body during the uptake period, and leaves the body via the lungs during the clearance period, the gas concentration in the lungs during clearance is higher than in the injection technique. This causes a more significant tracer recirculation in the inhalation technique, and consequently a slower decrease of the recorded residue than in the injection technique. In this way the analysis of the clearance curves in the inhalation technique results in an underestimation of c.b.f.. To correct for the recirculation one needs to know the arterial concentration and perform a deconvolution analysis with that concentration function and the recorded clearance curve. The arterial concentration could be measured on blood samples, but in that case the merit of the inhalation method that it is atraumatic, is lost. In a subsequent publication Veall and Mallett (1966) reported a method for correction for recirculation, namely by means of the recorded radioactivity of the expired air. Just as the percentage of carbon dioxide

in the expired air is a measure for the amount of carbon dioxide in the blood, so the radioactivity of the Xe in the expired air is a measure for the arterial Xe concentration. They used the $T_{1/2}$ -value of the radioactivity of the expired air to correct the $T_{1/2}$ -value of the fast component of the clearance curve, according to a simple linear relationship. The mean value of the correction of $T_{1/2}$ for the fast component was 0.44 min. Despite this correction they still found lower blood flow values than are reported for the injection technique.

Veall and Mallett did not derive a figure for the relative weights of the compartments from their measurements. To calculate the mean specific flow they assumed the relative weight W_g of the grey tissue compartment to be 0.6 and thus found $\bar{f} = 40 \text{ cm}^3/\text{min}/100 \text{ g tissue}$.

In a methodological study on patients, Jensen et al (1966) compared the inhalation technique of Malett and Veall with the injection technique. They calculated the clearance curve to be expected with the inhalation technique, by convolution of the recorded radioactivity of the expired air by the inhalation technique, with the clearance curve recorded in the injection technique. This constructed curve was compared to the experimental clearance curve in the inhalation technique. It turned out that the constructed curve differed systematically from the observed curve, in such a way that the observed clearance rate was smaller. They argued that the slower clearance could not be ascribed fully to recirculation, because even after a clearance period of ten minutes, when recirculation was negligible, the discrepancy still existed. They concluded that the extra-cerebral tissue, e.g. skull, scalp and air spaces in the head might cause the significantly slower

clearance when the inhalation technique was applied. To exclude the contribution to the clearance curve of radioactivity originating from scalp, which normally is also filled with Xe in the inhalation technique, Mallett and Veall occluded scalp blood flow by means of a tourniquet. They found that the fast component of the clearance curve was not influenced significantly in this case, but that the $T_{1/2}$ -value of the slow component decreased about 13%.

II-3 Experience with the application of the Xe-133 inhalation technique on patients.

We did some preliminary Xe-inhalation studies with an provisional set-up on patients (van Duyl, 1969), according to the method of Mallett and Veall (1965). Fig. 5 shows the Xe-air breathing circuit used in this study. It consists of a closed and an open circuit, with forced ventilation. The volume of the closed system was kept constant during the uptake by adding oxygen, while the carbon dioxide produced by the patient was absorbed in soda lime. Parallel to the breathing circuit an air-sample circuit to measure continuously the radioactivity of the respired air was provided. The radioactivity of the head was measured with a scintillation detector with a 2-inch NaI-crystal and a multi-hole collimator. Less than 0.5 mCi of Xe-133 was administered per measurement. The order of magnitude of the maximum pulse rate was 400 pulses per second.

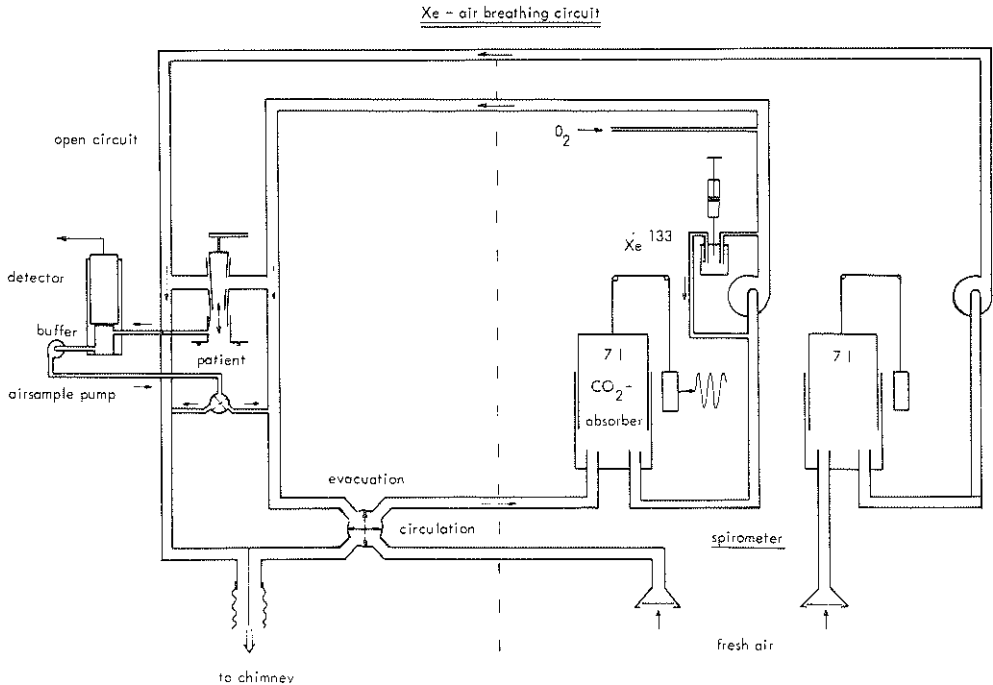


Fig. 5.: Diagram of the provisional set-up of the Xe-inhalation circuit, used for measurements on patients.

Fig. 6 shows a clearance curve, measured on a healthy man, plotted on a semi-logarithmic scale. The uptake period was 5 minutes, as proposed by Mallett and Veall (1965). The curve is analysed in two exponentials, according to the graphic peeling technique. The values of $T_{\frac{1}{2}}$ of the 'fast' and the 'slow' component are in accordance with those published by Mallett and Veall. The value of $T_{\frac{1}{2}}$ of the fast component, corrected for recirculation according to the simple method of Veall and Mallett (1966), is given also in Fig. 6. In contrast

to their observations we never found that cerebral tissue was equilibrated with Xe after an uptake period of 5 minutes. We reached this level after about 15 minutes of inhalation.

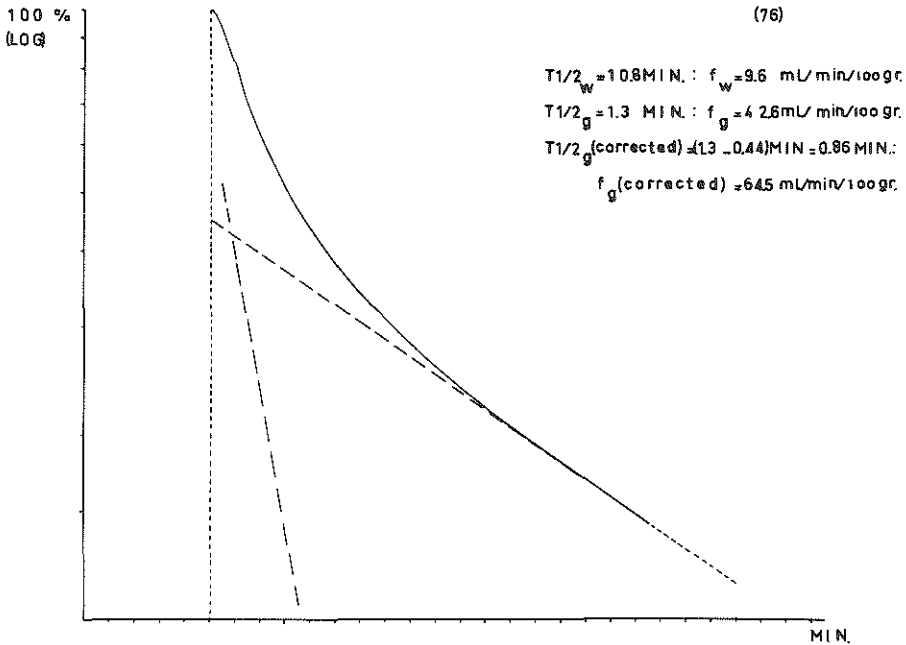


Fig. 6.: Semi-logarithmic plot of a clearance curve, recorded from the head of a normal subject, after 5 minutes inhalation of Xe-133.

In Fig. 7 three normalized clearance curves measured in different patients, after uptake periods of 0.5, 5 and 10 minutes are plotted on a semi-logarithmic scale. The first parts of these curves clearly demonstrate a decrease in the rate of clearance when the uptake period is made longer. The $T_{1/2}$ -values of these curves

are respectively 4.0, 4.3 and 8.2 minutes.
 The increase of the $T_{1/2}$ -value is mainly due to the increasing contribution of the slow component in the clearance curve, when the uptake period is made longer.

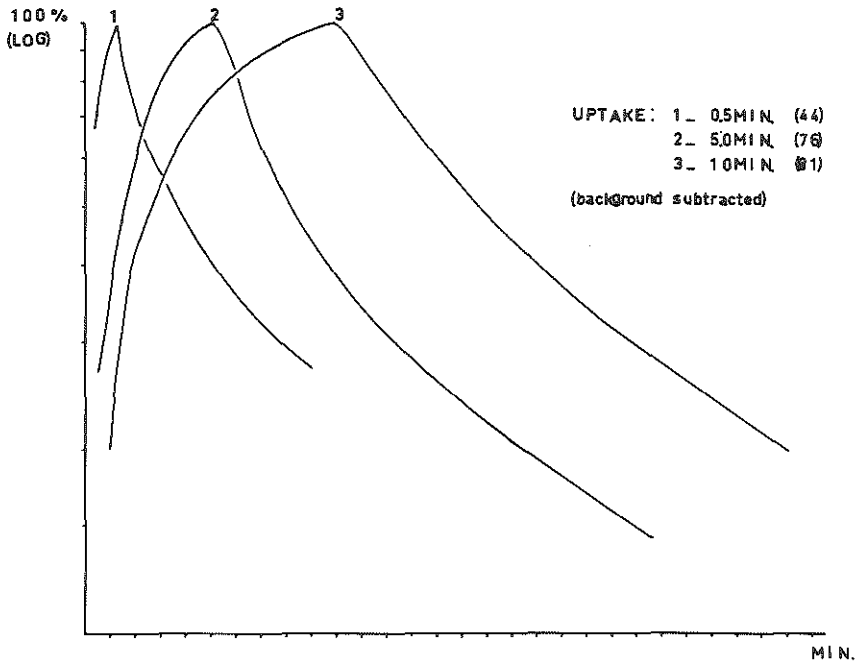


Fig. 7.: Clearance curves, recorded after different periods of inhalation of Xe-133.

In Fig. 8 the upper graph refers to a bi-exponential clearance curve as may be found in a healthy man, after a bolus injection of Xe-133. Taking this clearance curve as a pulse response, the clearance curves to be expected after constant tracer infusions over 1, 5 and 10 minutes have been constructed and are shown as the

lower graphs in the figure. The dotted curves refer to the white tissue compartment, the broken curves to the grey tissue compartment. The thin solid curves represent the sum of the clearance curves of both cerebral tissue compartments. For comparison the normalized clearance curves are also shown (thick solid curves).

The graphs demonstrate three important consequences of increasing the uptake period. Firstly, the initial value at the start of the clearance is higher when the uptake period is longer. Secondly, the contribution of the slow component in the clearance curve increases. And, finally, as a consequence of the increased contribution of the slow component, the $T_{1/2}$ -value increases also.

The relative contribution of the grey tissue compartment to the clearance curve as a function of the uptake period, for the same situation as in Fig. 8, is given in Fig. 9. The other curve in this figure refers to the factor by which the arterial concentration must be increased to reach a certain initial value of the clearance curve, for different uptake periods. The value reached after an uptake period long enough to have both compartments in equilibrium with arterial blood is taken as the reference. This curve is comparable to the strength-duration curve known in neurophysiology. It shows a steep increase in the arterial concentration necessary to reach a certain level of radioactivity. The initial level of radioactivity is important, because it is a factor affecting the accuracy of the analysis of the clearance curves.

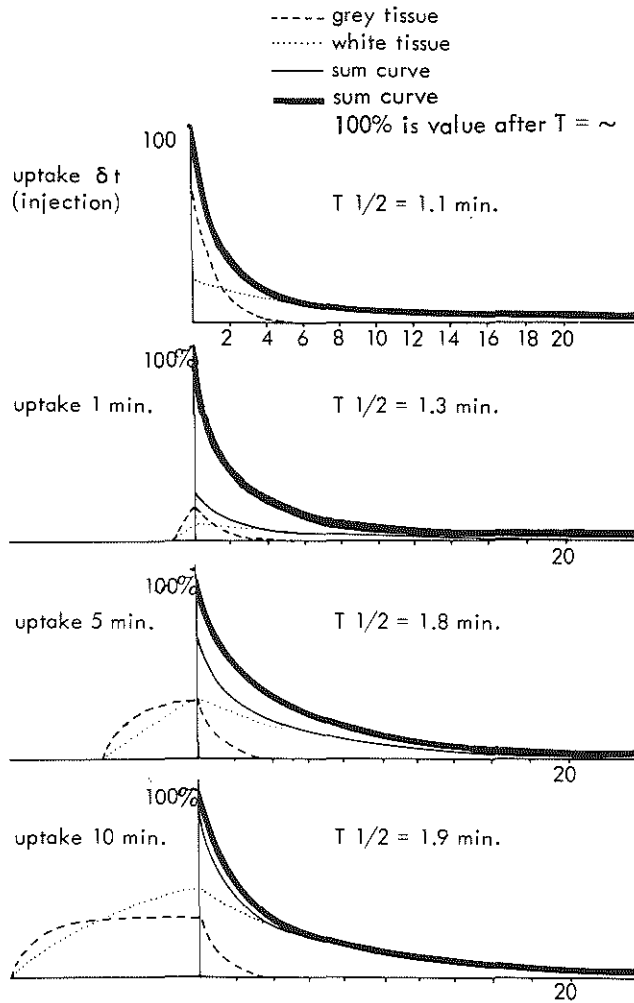


Fig. 8.: Illustration of the theoretical influence of the duration of a constant infusion, on the clearance curves:

Assumed pulse response:

$$u(t) = 75e^{-0.85t} + 25e^{-0.14t}$$

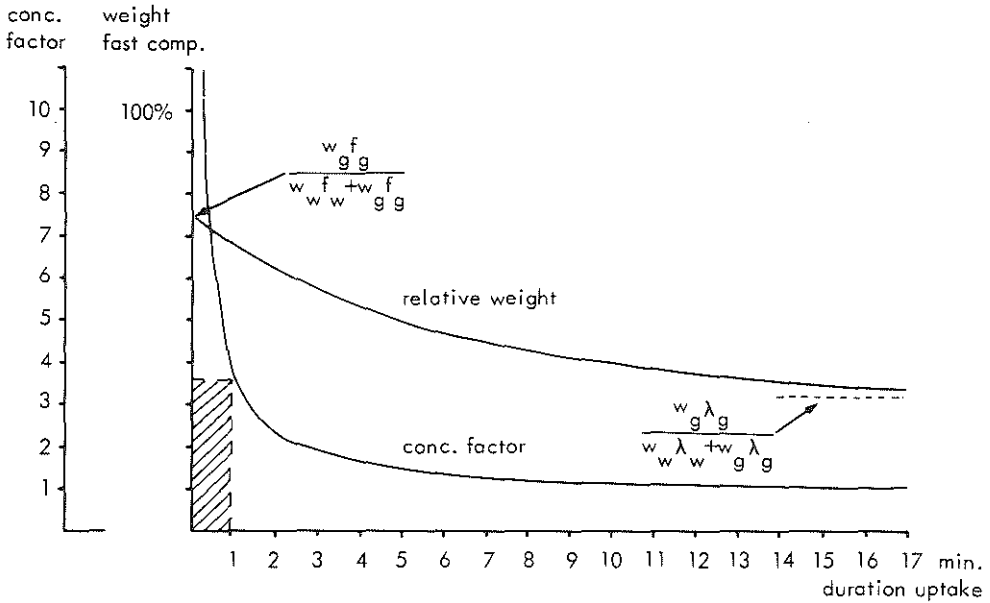


Fig. 9.: Relative weight of the fast component, and the concentration factor for constant initial pulse rate, as a function of duration of infusion (theoretical curves).

The dependence of $T_{1/2}$ on the uptake period, found in the constructed clearance curves is qualitatively in accordance with the experimental results. However, in the experiments the increase of $T_{1/2}$ is considerably greater.

The tracer infusion in the inhalation technique is not a block function as was used to construct the curves of Fig. 8. The upper graphs of Fig. 10 show the radio-activity of the exhaled air and that of the head during the uptake and clearance period in a patient. According to Veall and Mallett (1966), the air-curve is representative of the arterial Xe-concentration. It appears that at the end of the uptake period the air-curve decays rapidly ($T_{\frac{1}{2}}$ is about 25 sec.). The lower two graphs in Fig. 10 refer to the air-curve and the head-curve recorded after an intravenous injection of about 300 μ Ci of Xe-133. The concentration in the respired air has about the same magnitude as measured in the upper graphs. The decaying part is similar to the air-curve after the end of the inhalation uptake period. The head-curve recorded after intravenous injection demonstrates that a considerable amount of tracer passes the lungs and reaches the cerebrum. The air-curve, recorded after the inhalation uptake period, reveals that a considerable amount of tracer recirculates and that this affects the course of the recorded head-curve.

If this head-curve is deconvoluted with the air-curve, we get the pulse response of the tracer transferring system. This pulse response is similar to the clearance curve after a bolus injection, provided that the same regions in the detector field are supplied with Xe. The slower clearance after inhalation cannot fully be ascribed to tracer recirculation, because extra-cerebral, slow components are involved in the inhalation technique, as described in the previous section. This is taken to be a reason for the fact that in the experiments the increase of $T_{\frac{1}{2}}$ with longer uptake periods is greater than it should be by the constructed curves.

The next section will show, however, that slow components

in the clearance process are not only of extra-cerebral origin.

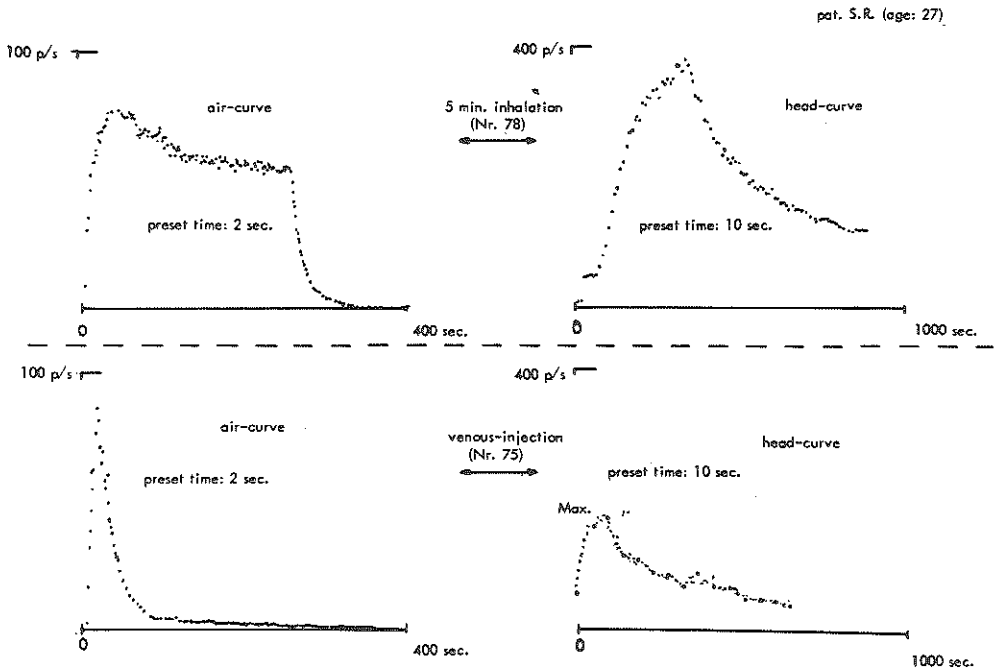


Fig. 10.: upper two curves: recorded pulserate of head and exhaled air after 5 minutes of Xe-inhalation;

lower two curves: curves recorded after intravenous Xe-injection.

II-4 Heterogeneity of cerebral blood flow.

In the two-compartmental analysis of the clearance curve it is assumed that c.b.f. consists mainly of two components, corresponding to the flow through grey and the flow through white tissue. Lassen (1965) measured the clearance curve of Kr-85 by its β -radiation. The absorption of β -radiation is so great that only the β -radiation from brain cortex can be detected extra-cranially. These cortical clearance curves, however, appear to be bi-exponential. This indicates that c.b.f. is more heterogeneous than the two-compartmental model suggests and implies that the clearance of Kr-85 and Xe-133, detected by γ -radiation, must actually be described by at least three exponential terms.

Heterogeneity of cerebral blood flow has been investigated in the cat by Landau et al (1955), using an autoradiographic technique. An inert gas, I-131-trifluoriodomethane, was administered intravenously for one minute. At the end of the infusion the animal was decapitated, the head frozen and cut into coronal sections of about 5 mm thick. Autoradiograms of the sections were developed by the β -radiation of I-131. Some difficulties occurred with the used volatile tracer which was used. The technique has been improved considerably by Reivich et al (1969), by using freely diffusible, non-gaseous C-14-antipyrine as an inert tracer.

It has been assumed that the accumulation of the antipyrine in a tissue region can be described by a compartmental model. Hence the concentration of antipyrine in such a compartment, after a constant infusion for a time T can be derived by the formula,

$$c_i(T) = \int_0^T c_a(t') f_i e^{-\frac{f_i}{\lambda_i} (T-t')} dt' \quad (35)$$

Provided λ_i is known - and it is about 1 for antipyrine throughout the cerebrum -, formula (35) can be solved for f_i , if c_i is known. The distribution of the concentration of antipyrine in the tissue could be derived from the density pattern of the autoradiograms. Fig. 11, adopted from Reivich et al (1969), shows the result of such a study. It appears that there is a wide spectrum of specific flow values, particularly in grey tissue, and further that this distribution can be affected considerably by anaesthetics. In this figure mainly two distribution lobes can be distinguished, which can be identified with grey and white tissue respectively. According to these distribution lobes there is a mean specific blood flow in grey tissue and a mean specific blood flow in white tissue.

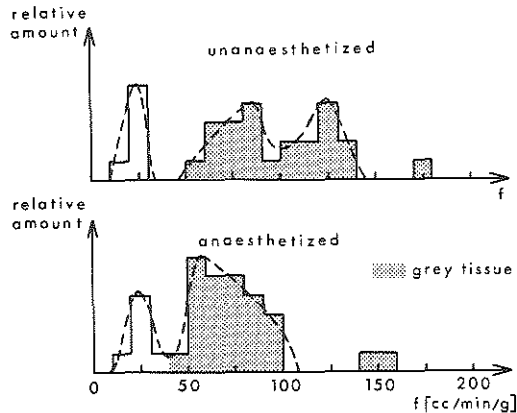


Fig. 11.: Distribution of cerebral blood flow in the anaesthetized and unanaesthetized cat, found with the C-14-antipyrine technique (after Reivich et al, 1969).

Eckman et al (1975) compared autoradiographic studies on conscious cats, using C-14-antipyrine, with studies published by Landau et al (1955) in which I-131-trifluoriodomethane was used. They found that the c.b.f. values were up to 50% lower with C-14-antipyrine. From a computer model study they concluded that the discrepancy could be caused by too low a permeability of the capillary membrane to antipyrine.

For normal perfused grey tissue permeability of the capillary wall does not limit the uptake or clearance rate of a tracer if $PS > 0.12 \text{ cm}^3/\text{sec/g}$, where P is the permeability coefficient of the capillary wall, and S the total area of permeable capillary wall. For normal perfused white tissue the corresponding figure is $PS > 0.035 \text{ cm}^3/\text{sec/g}$.

According to Crone (1965), PS for antipyrine is about $0.020 \text{ cm}^3/\text{sec/g}$. Hence antipyrine appears to be a not entirely satisfactory tracer for the study of heterogeneity of c.b.f., because of the limited capillary permeability in the brain, which makes the compartmental model invalid.

A method for studying the heterogeneity of c.b.f., which is not affected by permeability problems, is made possible by means of the carbonized microspheres, supplied by the 3-M Company. Typical problems involved in the microsphere technique are studied by Edlich et al (1968). Studies with microspheres (Tschetter et al 1968) confirm the great heterogeneity of c.b.f., as described by Reivich et al (1966).

Regional distribution of c.b.f. has also been studied with the clearance technique e.g. by Wilkinson et al (1969) using 16 scintillation detectors placed over one hemisphere. Perfusion of grey tissue was found to be significantly lower in the temporal region (by about 20% of mean) and higher in the precentral region (by

about 15%) than throughout the rest of the hemisphere. The fact that the distribution of blood flow as a function of depth is more heterogeneous than assumed in the two-compartmental model, has been demonstrated by the clearance studies with Kr-85. More evidence of the heterogeneity in clearance rate as a function of depth in cerebral tissue is given by Van Duyl et al (1976). This evidence is based on simultaneous recording of 81-keV and 31-keV radiation of Xe-133 during clearance.

With the knowledge of the heterogeneity of c.b.f., the question arised how the parameters found in fitting a two-exponential model to the clearance curve are related to the distribution pattern of the flow. We may assume that, as a consequence of the heterogeneity, the clearance curve is composed of a distribution of many exponentials, generally represented by

$$r(t) = \sum_{i=1}^n A_i e^{-\alpha_i t} \quad (36)$$

Based on their observations of the flow distribution, Reivich et al (1969) assumed two Gaussian distributions of the decay constants of the clearance curves, one representing the flow distribution divided by the partition coefficient in grey tissue, and the other representing the flow distribution divided by the partition coefficient in white tissue. Fig. 12 is an example of such a distribution. One such a Gaussian distribution can be represented by

$$W(\alpha) = \frac{1}{\sigma\sqrt{2\pi}} e^{-\frac{(\bar{\alpha}-\alpha)^2}{2\sigma^2}} \quad (37)$$

where $W(\alpha)$ is the density function of the relative weight of tissue in this distribution, with decay constant α , and where $\bar{\alpha}$ is the mean decay constant and τ the standard deviation of the distribution.

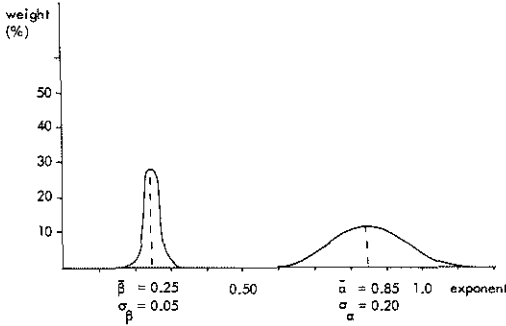


Fig. 12.: Example of a bi-modal Gaussian distribution of exponentials, assumed to constitute a cerebral clearance curve.

The residue-function of a clearance process composed of such a Gaussian distribution of exponentials is

$$H^*(t) = \frac{1}{\sigma\sqrt{2\pi}} \int_0^\infty e^{-\frac{(\bar{\alpha}-\alpha)^2}{2\sigma^2}} e^{-\alpha t} d\alpha \quad (38)$$

This formula can be written in the following form,

$$H^*(t) = e^{-\bar{\alpha}t} e^{\sigma^2 t^2 / 2} \left[1 - \frac{1}{\sqrt{2\pi}} \int_{-\infty}^{(\sigma^2 t - \bar{\alpha}) / \sigma} e^{-\frac{x^2}{2}} dx \right] \quad (39)$$

Reivich (1969) showed that if the integral term is ignored, and a 15-minutes clearance curve generated by the multi-exponential model is fitted by the equation

$$H^*(t) = e^{-\bar{\alpha}t} e^{\sigma^2 t^2 / 2} \quad (40)$$

the fit error is less than 0.05% for $\bar{\alpha} = 0.85$ and $\sigma = 0.20$ or for $\bar{\alpha} = 0.25$ and $\sigma = 0.05$.

Since a distribution of c.b.f. is composed of two lobes, Reivich used this approximate mathematical model twice and fitted to the clearance curves,

$$r(t) = A e^{-\bar{\alpha}t} e^{\sigma_{\alpha}^2 t^2 / 2} + B e^{-\bar{\beta}t} e^{\sigma_{\beta}^2 t^2 / 2} \quad (41)$$

Here $\bar{\alpha}$ and σ_{α} are the mean decay constant and standard deviation related to blood flow in grey tissue, and $\bar{\beta}$ and σ_{β} these in white tissue.

Reivich synthesized clearance curves, composed of 18 exponentials equally spaced along the abscissa and weighted according to the bi-modal distribution. The constructed curves, with different mean values and standard deviations, were fitted with a bi-exponential model. Thus it could be determined under what conditions the two exponentials describe the mean flow rates (decay constants) of the grey and white tissue accurately.

For the situation given in Fig. 12, which is assumed to represent normal flow rate distribution approximately, it appeared that the difference between α and $\bar{\alpha}$ and between β and $\bar{\beta}$ were less than 15%. It appeared that a variation of the standard deviation of the distribution of the slow exponentials had a larger effect on the error than an equal variation of the standard deviation of the distribution of the fast exponentials.

Reivich concluded from his study that the two-compartmental model in cases of normal flow rates may fail to reflect accurately at the average values of flow and of relative weight for white and grey tissue. If, on the other hand, the approximate mathematical model of formula (41) is fitted, he found that the clearance rate

was slightly overestimated with less than 0.5%. Hence it is concluded that the model of Reivich is a better fit than the two-exponential model to the bi-modally distributed multi-exponential clearance curves.

To what extent this conclusion has value for experimental clearance curves depends on the correspondence of the real distribution of exponentials constituting the clearance curves to the theoretical distribution assumed in the model study. This question has not yet been answered.

It must be noted that, since Reivich's model consists of 6 independent parameters, a comparison of that model with a three-exponential model, which is also defined by 6 parameters, is more appropriate than one with a two-exponential model, which is defined by only 4 parameters. The three-exponential model may result in a fit error, which is comparable to that with the Reivich's model. In so far as the heterogeneity of c.b.f. evokes a bi-modal distribution of exponentials constituting the clearance curve where each mode corresponds to a tissue type, a merit of Reivich's model is that it yields an estimation of the standard deviations of the modes.

II-5 Improvements to the Xe-inhalation technique.

In section II-3 it has been concluded that extra-cerebral slow components contribute to the clearance curves. To take account of this contribution, Obrist et al (1967) prolonged the observations time of the clearance curves to 50 minutes. The head-curve was deconvoluted with the recording of the radioactivity of the expired air. The obtained curve was fitted with a three-exponential model. They ascribed the slowest exponential to the clearance of extra-cerebral tissue. The other two exponentials were ascribed to grey and white tissue compartments.

Their results are in a rather good agreement with those found with the injection technique in normal subjects. Disadvantages of their method are the complexity of the analysis, the necessity of a high radioactivity level to obtain reliable results, and the long observation time. Because of the non-orthogonality of exponentials, separation into a series of exponential components may be ambiguous, (Worsley, 1964 ; Van Duyl, 1974), section III-3-1. In connection to this Obrist et al speak of unstable solutions. Therefore the fitting of a three-exponential model to a decay curve is a precarious affair.

The source of the extra-cerebral contributions is not fully clear. The assumption that extra-cerebral tissue only contributes to the third exponential may be erroneous, because Mallett and Veall (1965) have shown that the $T_{1/2}$ of the fast component of scalp clearance curves is close to the $T_{1/2}$ of the slow component of the cerebral clearance curves found by the injection technique.

For excluding extra-cerebral contributions Crawley and Veall (1970) published a gamma spectrum technique.

This technique is based on the difference between the absorptions in tissue of the 81-keV and 31-keV radiations of Xe-133, which enables a depth discrimination of radiation sources. Yet, it did not turn out to improve the results of the inhalation technique. The relative weights of the exponential components, constituting the clearance curve after a tracer infusion, depend on the decay constants and the duration of the infusion in the way explained in II-3.

Since the flow in grey tissue is of main interest, one can take advantage of the reduction in the contribution of the slow components which occurs when the infusion time is shortened. Obrist et al (1975) studied the validity of the inhalation technique with the uptake period reduced to 1 minute, an observation time of 10 minutes and with a two-exponential approach. Since the cerebral clearance curves have a multi-exponential character instead of being composed of two or three exponentials, Obrist et al (1975) evaluated their method of analysis on synthesized multi-exponential clearance curves. They analyzed clearance curves synthesized from a tri-modal Gaussian distribution of exponentials, and fitted by two- and three-exponential models. The first two models correspond to those assumed also by Reivich et al (1969). The mean value of the slowest, third mode was based on a three-compartmental analysis of inhalation data, while its standard deviation was chosen in such a way that the distribution would include the heterogeneous clearance rates of skin and muscle tissue.

They studied the relation between the fitted fast decay constant α and the mean value $\bar{\alpha}$ of the corresponding distribution at high, normal and low perfusion rates. It appeared that the difference between α and $\bar{\alpha}$ depended on the length of the fitted curve. From this study it

was decided that a good fit was obtained if about 11 minutes of the clearance curve was fitted by a two-exponential model. Three-exponential analyses of 40-minute experimental clearance curves, and two-exponential analyses of 10-minute parts of these curves, yielded approximately equal values for the fast component. In the simplified analyses by a two-exponential model it is assumed that the fast component represents the grey tissue. The second component is less meaningful because of extra-cerebral contamination. As a consequence, the flow for the white tissue cannot be calculated. Furthermore, because the partition coefficient to be used in the slow component is not known, neither can the relative weights of the compartments be calculated.

On the other hand, from his approach Obrist et al (1975) could calculate the ratio of the absolute blood flow in the grey tissue compartment to the total absolute blood flow in the tissue under observation, i.e. F_g/F . Although this fraction is not equivalent to relative tissue weight, it nevertheless provides information about the relative contribution of the first compartment.

To reach a radioactivity level after a 1-minute uptake, which is high enough for a reliable analysis, a high Xe-concentration of inhaled air is necessary (Fig. 9). Obrist et al used a concentration of about 2mCi/liter. With such a high concentration the radioactivity of the air passages however, does contaminate the clearance curves. Therefore they proposed to fit the clearance curve about 0.6 minutes after the cessation of Xe-inhalation, because then the contamination is considerably reduced.

Recently Reivich et al (1976) published the results of a comparison between the injection technique and the inhalation technique according to the approach of Obrist

et al. They found a linear regression equation between the regional fast flow for inhalation and injection:

$$f_g \text{ (injection)} = 0.87 f_g \text{ (inhalation)} + 10 \text{ cm}^3/\text{min}/100 \text{ g} \quad (42)$$

There is a good correlation between the results of the two techniques, although there is still a systematic difference. The inhalation technique is applied more frequently since Obrist et al (1975) introduced improved methods of analysis for this technique.

II-6 Alternative methods of analysis of the clearance curves.

When the clearance curves are analysed in terms of a two-compartmental model, the mean blood flow can be calculated by (21). If one is only interested, however, in the mean specific blood flow, an alternative analysis is appropriate. This alternative analysis, sometimes erroneously called the stochastic analysis, is based on less structural assumptions of tracer transfer than the compartmental analysis. It is part of a theory of tracer kinetics based on moments of distribution functions, as used in the theory of statistics. A simplified description of this theory taken from Meier and Zierler (1954) will be given here. The particles of an injected tracer will pass through an organ along different paths. Any path can be characterized by the transit time needed for particles to traverse it. We define a function $h(t)$, such that $h(t)dt$ is the fraction of particles entering the organ at $t = 0$, which leave the organ between the times t and $t + dt$. This

function is called the distribution of transit times or the tracer transfer function. Because all particles entering the organ eventually leave it

$$\int_0^{\infty} h(t) dt = 1 \quad (43)$$

We assume for the moment that a tracer substance is injected, which is constrained to pass through the organ in the same way as the blood particles. Then the concentration of the tracer in blood at the venous outlet is,

$$c_v(t) = \frac{q_0 h(t)}{F} \quad (44)$$

The volume through which the tracer is distributed in the organ can be conceived to be divided into subvolumes according to the different transit times of tracer particles or blood particles. An elementary vascular subvolume $dV_v(t)$ contains blood with transit times between t and $t + dt$. The amount of blood with transit times between t and $t + dt$, which enters the organ during dt , is $Fh(t)dt$. Between 0 and t , $dV_v(t)$ is filled so that $dV_v = thF(t)dt$. Hence the total volume of the vascular system is,

$$V_v = F \int_0^{\infty} th(t) dt = F\bar{t} \quad (45)$$

where \bar{t} is the mean transit time.

The amount of tracer that has left the organ during the interval $(0, t)$ after a bolus injection is,

$$\Delta q(t) = q_0 \int_0^t h(t') dt' \quad (46)$$

so that the amount of tracer that remains in the organ at the moment t is,

$$q(t) = q_0 \left[1 - \int_0^t h(t') dt' \right] \quad (47)$$

We define the residue function as

$$H^*(t) = 1 - \int_0^t h(t') dt' \quad (48)$$

so that,

$$q(t) = q_0 H^*(t) \quad (49)$$

Because of (43) and (48) we find that

$$H^*(0) = 1 \quad (50)$$

and

$$\int_0^{\infty} H^*(t) dt = \bar{t} \quad (51)$$

If clearance is supposed not to be started before the uptake of the tracer in the tissue is finished, the maximum pulse rate r_0 is proportional to the injected amount q_0 . With this assumption, and (51) and (49), we find that,

$$\frac{1}{r_0} \int_0^{\infty} r(t) dt = \bar{t} = \frac{V_v}{F} \quad (52)$$

According to this relation the ratio of the vascular volume in the detector field to the absolute blood flow

through this volume is equal to the mean transit time of the intravascular tracer and also to the ratio of the area under the recorded pulse rate curve to the maximum pulse rate.

If a diffusable tracer is used, the volume in which the tracer is distributed is mainly determined by the tissue volume, instead of the vascular volume. Hence, then V_v must be replaced by an equivalent blood volume, which would contain the same amount of tracer as the tissue under equilibrium conditions. This equivalent volume is λV where V is the tissue volume, so that the mean transit time for a diffusable tracer is given by

$$\bar{t} = \frac{\lambda V}{F} \quad (53)$$

With the same conditions leading to (52) we thus find that for a diffusable tracer,

$$\frac{1}{r_0} \int_0^{\infty} r(t) dt = \bar{t} = \frac{\lambda V}{F} \quad (54)$$

If the tissue is heterogeneous with respect to λ and F , and if it is composed of tissue regions i with λ_i and F_i , the mean transit time of the tissue is

$$\bar{t} = \frac{1}{F} \sum_{i=1}^n F_i \frac{\lambda_i V_i}{F_i} = \frac{1}{F} \sum_{i=1}^n \lambda_i V_i \quad (55)$$

If we introduce the mean partition coefficient defined, as

$$\bar{\lambda} = \frac{\sum_{i=1}^n \lambda_i V_i}{V} \quad (56)$$

we can write

$$\bar{t} = \frac{\bar{\lambda} V}{F} = \bar{\lambda} \bar{f} \quad (57)$$

where \bar{f} is the mean specific blood flow in the tissue. Hence we finally can derive the interesting relation,

$$\frac{1}{r_0} \int_0^{\infty} r(t) dt = \frac{\bar{\lambda}}{\bar{f}} \quad (58)$$

According to this relation the mean blood flow can be determined from the ratio of the maximum height of the clearance curve and the area under the clearance curve, provided that the mean partition coefficient is known. This method for the determination of the mean blood flow was proposed by Meier and Zierler (1954) and is referred to in the literature as the 'height-over-area' method. When an exponential model is fitted to the clearance data, so that

$$r(t) = \sum_{i=1}^n A_i e^{-\alpha_i t}$$

then the mean transit time can be calculated by (52) as follows

$$\begin{aligned} \bar{t} &= \frac{1}{r_0} \int_0^{\infty} r(t) dt = \frac{\int_0^{\infty} \sum_{i=1}^n A_i e^{-\alpha_i t} dt}{\sum_{i=1}^n A_i} = \\ &= \frac{\sum_{i=1}^n A_i \tau_i}{\sum_{i=1}^n A_i} = \bar{\tau}. \end{aligned} \quad (59)$$

where

$$\alpha_i = \frac{1}{\tau_i} \quad (60)$$

Hence, the mean transit time \bar{t} is equal to the mean time constant $\bar{\tau}$ of the fitted exponential model. Relation (58) is more general than it was originally supposed to be. Roberts et al (1973) theoretically showed that for this relation to be valid it is not necessary that the diffusing tracer is in equilibrium within a tissue region, as is assumed in the compartmental model. A sufficient condition is that the tracer is in equilibrium at the boundaries between the phases only. This condition applies both to the tissue phases and to the blood phase. In other words the mean transit time, given by (57), is independent of the diffusion coefficients of the tracer within the different phases. A rationalization of this somewhat paradoxical conclusion is that the diffusion coefficient and the average depth of penetration of tracer into the tissue phase are coupled. In other words the average penetration depth will be small if the diffusion coefficient is low, whereas if the diffusion coefficient is high, the penetration depth will be large. The time required for a tracer to enter and then to be cleared from the tissue is, however, the same in both cases because the faster diffusing tracer has to travel correspondingly longer distances. This aspect of the mean transit time will be referred to discussions in chapter V .

Though very simple in theory, there are practical complications in the 'height-over-area' method. Firstly, one must be sure that no significant clearance has taken place before the uptake is finished. For this reason this method cannot be applied in the case of the inhalation technique.

Secondly, for the determination of the area under the clearance curve it must be extrapolated to infinity. Because of the multi-exponential character of the clearance curve, such an extrapolation is difficult to perform accurately.

The extrapolation problem is also involved in the N_2O -inhalation technique of Kety and Schmidt (1945). They assumed, however, that equilibrium is reached after an uptake period of 10 minutes.

Based on the same assumption a simplified 'height-over-area' method has been proposed (Lassen and Hoedt-Rasmussen, 1966). In this method the difference between the maximum value of $r(t)$ and the value of $r(t)$ after 10 minutes is taken as the 'height', while the area under the clearance curve during the first 10 minutes, $A(10)$ is taken as the 'area'. Thus the extrapolation problems are avoided.

As described in section II-2, Lassen and Klee (1965) found that at least 15 minutes were necessary to reach equilibrium, and they estimated that with Kety-Schmidt technique the mean blood flow was about 10% overestimated. As a consequence, an error of the same magnitude is involved in this simplified 'height-over-area' method of Lassen and Hoedt-Rasmussen.

Hoedt-Rasmussen et al (1966) calculated the mean blood flow by applying an extrapolation to determine the area. The area was estimated by the formula: $A = A(15) + r(15) \cdot T_{1/2} / 0.693$.

Here $r(15)$ is the pulse rate after 15 minutes and $T_{1/2}$ is the half-value-time of the apparently mono-exponential function which described the slowly decaying tail of the curve observed after about 7 minutes.

Another complication in the analysis by the 'height-over-area' method is caused by the recirculation of the tracer. The area associated with the recirculated amount of tracer must be subtracted, in order to calculate the

mean transit time of the tracer through the tissue. By performing an intravenous injection of a dose equal to that administered intra-arterially, Hoedt-Rasmussen et al (1966) estimated the contribution of recirculation to the area. They found that the contribution, relative to that dose, is about 10%.

When their extrapolation method and their correction for recirculation are applied, the figure obtained for the mean blood flow is similar to that found with the compartmental analysis.

When multi-probe instrumentation came into use, there was a need for a quick and simple analysis of clearance curves. Paulson et al (1969) determined the initial slope of the clearance curves as a measure of the clearance rate of the fastest component. Their approach is based on the assumption of a mono-exponential decay during the first two minutes. The exponent of the fitted exponential function is called the initial-slope-index (I.S.I.). The validity of the mono-exponential description of the first part of the curve, even though the curve essentially is composed of at least two exponentials, is discussed in section V-1-2.

Sveinsdottir et al (1971) made a comparison between regional c.b.f. values calculated by the I.S.I. method and by the 'height-over-area' method. They concluded that the two-minute I.S.I., though theoretically erroneous, contained in practice the same information as that obtained from the more laborious one, but theoretically more correct, 'height-over-area' method. It was even found that the reproducibility of the I.S.I. method was slightly better than that of the 'height-over-area' method, which is more strongly affected by recirculation, errors in extrapolation and eventually remaining radioactivity from previous measurements. Kanno and Uemura (1975) evaluated the I.S.I. method on

synthetized two-exponential curves. They confirmed that the I.S.I. is a suitable measure to evaluate the change of the fast component.

Doyle et al (1975) affirmed the good linear correlation between the I.S.I. and the mean c.b.f. given by compartmental analysis of hydrogen clearance curves.

The good correlation between the I.S.I. method and the more complicated analyses of experimental curves is surprising, as noted by the authors quoted.

An important advantage of the I.S.I. method for clinical use is of course the short observation time of the clearance.

Risberg et al (1975) evaluated the I.S.I. method for the Xe-inhalation technique. They adopted the procedure published by Obrist et al (1975), described in section II-5. The I.S.I. was calculated from the deconvoluted head-curve between 1 and 2 minutes after cessation of the inhalation period.

Because the I.S.I. is mainly determined by the fast components in the clearance, this index is only slightly affected by slowly perfused extra-cerebral tissue. This technique combines the advantage of the short observation needed for the I.S.I. determination and with that of an atraumatic Xe-administration. Thus a series of c.b.f. measurements can be performed on normal subjects.

An important extra advantage of the inhalation technique is that both hemispheres can be mutually compared in one measurement. We conclude that the inhalation technique according to Obrist et al (1975) combined with the use of the I.S.I. method seems to have a future in the comparative flow studies, both clinical and physiological.

III-METHODS AND MATERIALS FOR THE MEASUREMENT OF CEREBRAL BLOOD FLOW IN THE PIG.

III-1_Surgery

III-1-1 Anatomy of cerebral vessels in the pig.

In order to apply the Xe-injection technique to the pig, it is necessary to know the position of the internal carotid artery and its significance in the cerebral blood supply. The branching pattern of the arteries in the neck is different for different species (Batson, 1944). As described in section I-2 the human brain is supplied with blood via two pairs of arteries, the right and left internal carotid arteries and the right and left vertebral arteries. In other animals the external carotid and occipital arteries may contribute significantly to brain blood supply. The uncertainties about the presence or absence of the four paired arteries and their interconnections constitute the major problem in studying blood flow on the arterial side. Furthermore, some animals have a peculiar elaboration of vessels, known as a rete mirabile, in addition. In many species this network provides intra- and extra-cranial junctions between the brain vessels and the external carotid arteries.

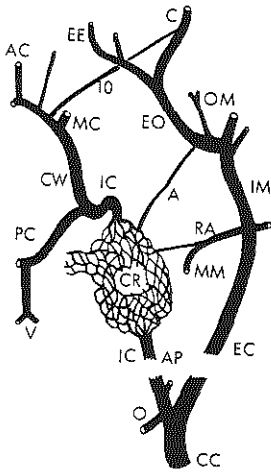
Fig. 13 is a scheme of the afferent brain vessels of the pig, taken from Daniel et al (1953). It shows that the pig has a rete mirabile. However, as an exception to the general rule, this rete does not constitute a significant anastomosis between internal and external carotid systems. The anastomosis seems to be even smaller than in the dog, while the dog has no rete mirabile. The rete is divided into two parts, situated

extra-durally on either side of the basisphenoid and more or less within the cranial cavity. The only significant connection between the extra-cranial arterial supply and the intra-dural internal carotid is realized in the rete (Boulay and Verity, 1973), namely from the internal maxillary via an anastomotic artery and an anastomotic ramus.

Concerning the name and significance of the branch from the common carotid artery to the rete, different views are to be found in the literature. Referring to the classic description of Ellenberger and Baum (1943), Boulay and Verity state that by the time a foetus is at full term or shortly after birth the internal carotid artery, which developed in an orthodox fashion, has usually shrunk to a narrow channel in its intra-osseous portion and has entirely disappeared in the neck. Not infrequently, however, the ascending pharyngeal artery is large and has connections with the intra-cranial rete, which pass through the floor of the skull.

Daniel et al (1953) state explicitly that the rete derives almost its entire blood supply from the ascending pharyngeal artery. This artery is a large vessel which, shortly after arising from the common carotid artery, branches off from the occipital artery. Furthermore they found that the rete received insignificant contributions from the internal maxillary artery. Hence the major contribution to the circle of Willis would appear to be derived from the ascending pharyngeal artery through the carotid artery.

Flechsigs and Zintsch (1969) prefer to use the name internal carotid artery instead of the ascending pharyngeal artery. One reason for this is to stress its significance as an afferent vessel for the brain of a pig. For that reason we shall refer to this artery with the name internal carotid artery.



- A arteria anastomotica
 AC anterior cerebral artery
 AP ascending pharyngeal artery
 C ciliary artery
 CC common carotid artery
 CR carotid rete
 CW circle of Willis
 EC external carotid artery
 EE external ethmoidal artery
 EO external ophthalmic artery
 IC internal carotid artery
 IM internal maxillary artery
 IO internal ophthalmic artery
 MC middle cerebral artery
 MM middle meningeal artery
 O occipital artery
 OM arteries of extrinsic ocular muscle
 PC posterior communicating artery
 RA ramus anastomoticus
 V vertebral artery

Fig. 13.: Survey of arterial vessels in the brain of a pig (after Daniel et al, 1953).

The occipital artery branches off from the internal carotid artery at the glomus caroticum and connects the internal carotid to the vertebral system.

In man the occipital artery is a branch of the external carotid artery and does not contribute significantly to brain blood supply. Another notable anatomic difference between man and pig is that the common carotid artery originates from a bifurcation of a bi-carotid trunk, which branches off from the brachio-cephalic trunk in

the pig.

To explore the anatomy of the blood supply to the brain of a pig we made a series of angiographs, with Conray-60^o as a contrast medium. The pig was anaesthetized by a combination of azaperone and metomidate administered by infusion into the jugular vein, section III-1-2.

The pig was intubated with a cuffed rubber tube.

Figs. 14 a, b and 15 a, b are selected from the series of radiographs. Figs. 14 a and 15 a are radiographs in a ventro-dorsal projection. Figs. 14 b and 15 b are radiographs in a lateral projection. In order to make the vessels more easily distinguishable in the lateral projections, the method of subtraction has been used, that is, they show the difference between two radiographs, one of which was made with and one without contrast medium in the vessels.

Both the catheter for anaesthesia and the respiration tube can be seen in the radiographs.

The contrast medium was injected mechanically, via a catheter placed in the common carotid artery. In order to obtain pictures of the regions supplied by different branches of the common carotid artery, the catheter tip was placed in different positions. In Figs. 14 a and b the catheter tip is placed just upstream of the branching point of the internal carotid artery. Figs. 15 a and b show the situation when the catheter tip is moved into the internal carotid artery. Comparison of the two situations gives a good impression of the difference between the regions supplied by the external and internal carotid arteries.

Fig. 15 b clearly shows that the occipital artery is connected to the vertebral artery. The vertebral artery is filled here by backflow of contrast medium.

It is noted from other angiographs that the occipital and internal carotid arteries are filled well, when the

catheter is placed in the vertebral artery. Hence it seems that the occipital artery forms a significant anastomosis between the vertebral and internal carotid systems.

Measurements made by means of an electromagnetic flow probe placed around the common carotid artery showed that, when the external carotid artery is tied off, the flow is reduced to about $1/3$ of its original value, which implies that about $1/3$ of the blood flow in the common carotid artery is supplied to cerebral tissue, section IV-5.

We conclude from our studies that, in order to administer Xe in cerebral tissue, it must be introduced into the internal carotid artery. If, however, the catheter tip is placed in the internal carotid artery, it constitutes a considerable resistance to blood flow in this artery. Therefore it is preferred to place the tip about half-way along the common carotid artery, while the external carotid artery is tied off. If the external carotid artery is not ligated, the greater fraction of the injected Xe would be transported to extra-cerebral tissue. This wasted Xe-133 would contribute to background radiation. Since it would also contribute to a high concentration in the lungs, it would increase the amount of tracer recirculation.



Fig. 14 a: Cerebral angiogram in ventro-dorsal projection:
catheter tip just upstream of the branching point of the internal carotid artery (IC).

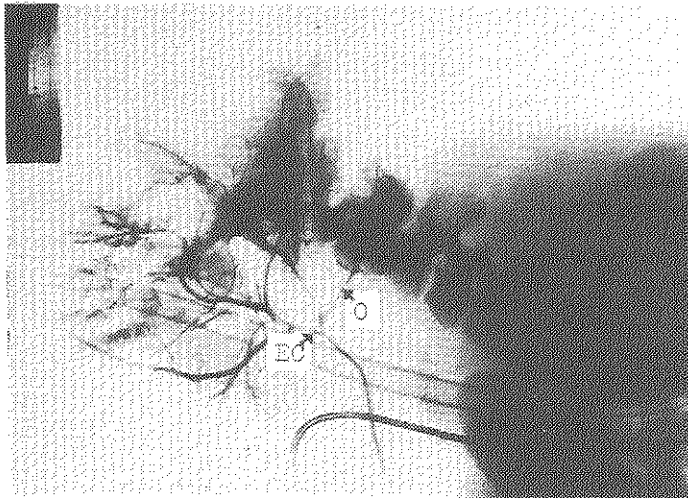


Fig. 14 b: Same situation as in Fig. 14 a; lateral projection (subtraction technique).

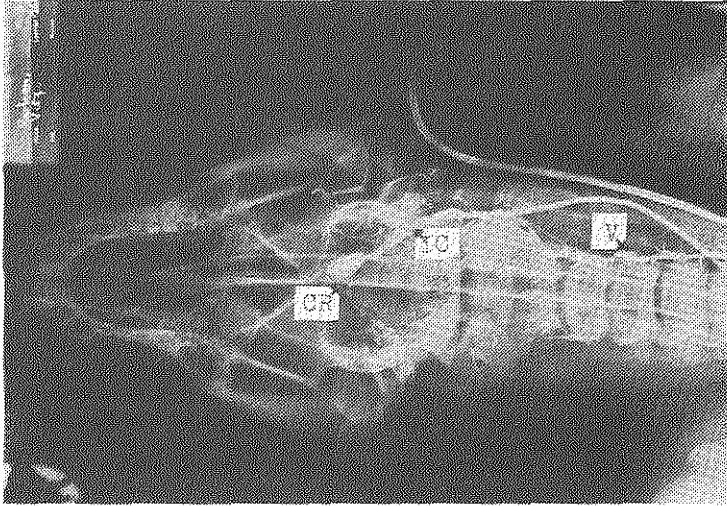


Fig. 15 a: Cerebral angiogram in ventro-dorsal projection:
catheter tip in the internal carotid artery (IC).

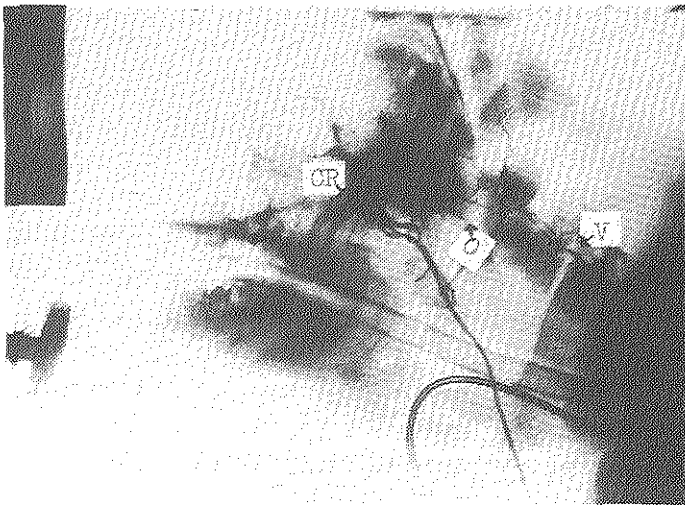


Fig. 15 b: Same situation as in Fig. 15 a, lateral
projection (subtraction technique).

III-1-2 Preparation of the animal.

During the initial period of our experiments we used Yorkshire piglets weighing 20 to 35 kg and aged 10 to 15 weeks. It is stated in the literature that c.b.f. in man decreases with age, more rapidly during childhood and then slowly later on (Purves, 1972). In order to obtain a more homogeneous set of results we preferred to do our experiments on adult pigs. Adult Yorkshire pigs, however, are not easy to handle in the experiments.

We used for anaesthesia a schedule developed by Lagerwey (1973), based on a combination of azaperone (Stresnil®) and metomidate (Hypnodil®) both marketed by Janssen Pharmaceuticals of Beerse in Belgium. The pig was sedated, by an intra-muscular injection azaperone (2mg/kg body weight) and atropine (0.012mg/kg). After 15 minutes the animal was supposed to be quiet enough to introduce the anaesthesia by means of an injection of metomidate (4mg/kg body weight) into a vein of the ear. This method appeared not always to work successfully. We introduced the anaesthesia by an intra-peritoneal injection of metomidate (10mg/kg), which was much easier to perform. Since we had abandoned the injection into the ear veins, we could also proceed with the experiments with another race of the pig, in which the ear veins are not visible, the so-called mini-pig.

An advantage of this race is that in the range of body weight mentioned above, these pigs are almost mature (15-30 weeks). In this thesis the measurements on these mini-pigs only will be reported.

About 15 minutes after the intra-peritoneal injection, the pig was under general anaesthesia. Then the pig was intubated (accomplished with some xylocaine spray) with an endo-tracheal tube (Rüsch, 10.7 mm diameter, 32 cm

long) provided with a cuff.

To exclude the exhaled air from contributing radio-activity to the clearance curves, the tube was covered inside with a sheet of lead about 0.5 mm thick.

The pigs were mechanically ventilated by means of a Bennett anaesthesia ventilator (type BA-4). With this ventilator a negative expiration pressure can be applied. A negative expiration pressure of about 10 cm water turned out to be important in maintaining blood pressure at a normal level during the experiments. Cummings et al (1972) remarked that respiration in a pig, whether spontaneous, assisted or mechanically controlled, is accomplished almost complete by diaphragmatic movement and that the thorax remains quite rigid. Anaesthetics, which inhibit the diaphragmatic musculature, allow movement of the organs in the thoracic and abdominal cavities, resulting in an increased pressure on the vena cava, This seriously can impair the venous return, and may result in heart failure. For this reason Cummings et al prefer a lateral recumbency during anaesthesia instead of a dorsal recumbency.

To facilitate surgery we did our experiments with the pigs in dorsal position. However, the fact that maintenance of physiological conditions was improved when a negative respiration phase was applied may indicate that the negative pressure compensates the effects mentioned by Cummings et al.

We aimed to measure c.b.f. in conditions which approached the normal physiology as closely as possible. It is difficult, however, to reach a physiological steady state under anaesthesia and to maintain it during experiments that last 4 to 8 hours.

The effect of anaesthesia on c.b.f. is an important topic in medical research. Depending on the applied anaesthetic agents applied and the amount administered,

the c.b.f. may be increased or reduced, (Sokoloff, 1959). The aim of Lagerwey's research was to develop a steady-state anaesthesia for the pig for use during cardiovascular experiments lasting about 6 hours. After considering of several types of anaesthesia described in the literature, Lagerwey decided to apply the combination of two agents, the neuroleptic azaperone (Stresnil[®]) and the analgetic metomidate (Hypnodil[®]). In fact metomidate alone is a weak analgetic, but when it is combined with azaperone good general anaesthesia can be attained.

Our first group of experiments (section IV-2) long-term anaesthesia was performed by infusion of a solution in saline of azaperone and metomidate via a double-lumen catheter (Ch.8), brought into the left internal jugular vein. This catheter was connected to an infusion pump (Braun Unita I), which infused metomidate (8mg/kg body weight/hr.) into the central lumen and azaperone (2mg/kg body weight/hr.) with atropine (0.012mg/kg/hr.) into the peripheral lumen of the catheter. The concentration of the pharmacological agents in saline was adjusted as to deliver the required amount of drugs in a total volume of 2 ml/kg/hr.

Since the effect of these anaesthetic agents on c.b.f. had never been studied, in relation to c.b.f., we did some experiments with the better known anaesthetic nitrous oxide, section IV-3. Nitrous oxide was mixed with oxygen in a ratio of 2:1.

Nitrous oxide is a good analgetic but a weak hypnotic. Therefore the use of nitrous oxide alone does not guarantee good anaesthesia (Lagerwey, personal communication). If, on the other hand, the combination of the anaesthetic agents azaperone and metomidate was used some animals did react to surgery. Hence, following

Lagerwey again, we finally anaesthetized the pig by the infusion of azaperone and metomidate plus nitrous oxide combined with oxygen in a ratio of 2:1, section IV-4 and 5. The amount of oxygen administered here is high enough to prevent hypoxia.

The pigs were ventilated with this gas mixture at a tidal volume of 400-600 cm³ at a frequency of 8-16 strokes per minute. To reduce atelectasis it was preferred to combine a high tidal volume with a low respiration frequency.

In Fig. 16 the experimental set-up is illustrated.

During the Xe-clearance period, the respiration circuit is half opened via a three-way cock, so that expired air is removed via the ventilation system of the Isotope Laboratories.

During the clearance the expiration of the pig is sustained by negative pressure in the ventilation system. By means of the ventilation system of the Isotope Laboratories the Xe-133 is rarefied in an air stream of 4000 m³/hr. Each clearance experiment lasts about one hour. In that period about 2 mCi Xe-133 must be evacuated. Hence the mean concentration of Xe-133 in the air leaving the Isotope Laboratories during a clearance experiment is about 0.5 μ Ci/m³.

The arterial pressure of carbon dioxide can be experimentally increased by hypoventilation, and decreased by hyperventilation.

To realize high levels of carbon dioxide, extra carbon dioxide was added to the respiration gas. Spontaneous respiration during hypercapnia could be prevented by administering the muscle relaxant, alloferine (1 ml/hr). In contrast to the concentration of carbon dioxide the arterial concentration of oxygen and the pH have only a minor influence on c.b.f., section I-2. In some experiments the concentrations of the blood gases in arterial blood samples were determined according to the

Astrup method (Stortenbeek, 1970). In later experiments, when a capnograph was available, we confined ourselves to monitoring the percentage carbon dioxide, P_{CO_2} .

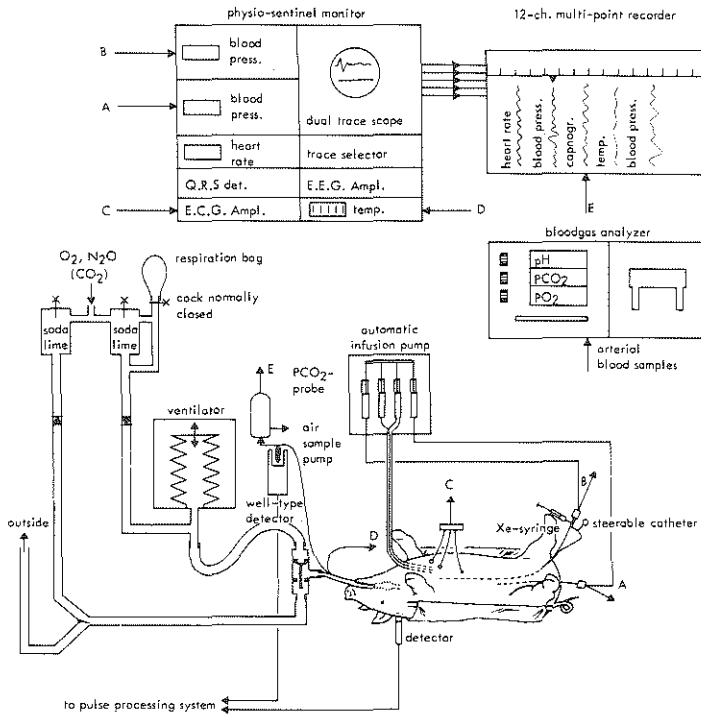


Fig. 16.: Survey of the set-up for the measurement of the cerebral blood flow of the pig according to the Xe-133 clearance technique.

The capnograph is based on a continuous infra-red gas analyzer. The capnograph used (Godart MO-1) has the special feature of a low sample-flow-rate (approx. 65 cm³/min), so that it does not disturb the ventilation of the animal. The maximum value of the percentage of carbon

dioxide in the expired air was taken as a measure for the arterial concentration of carbon dioxide (Smalhout, 1967). Smalhout found that a plateau value of the P_{CO_2} of 5 to 5.5% in healthy subjects corresponds to an alveolar and arterial pressure of carbon dioxide of 35 to 40 mmHg. The capnograph is slightly sensitive to O_2 and N_2O . Fig. 17 shows the relationship between P_{CO_2} and P_aCO_2 which we found in our experiments.

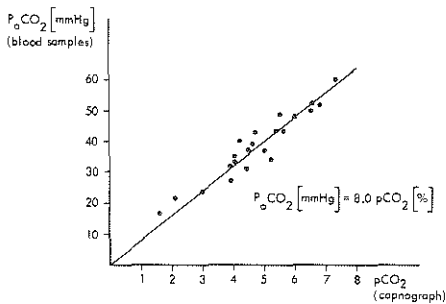


Fig. 17.: Experimentally established relationship between the arterial pressure of CO_2 (P_aCO_2) and the percentage CO_2 (P_{CO_2}) measured in the expired air.

In order to measure the radioactivity of the respired air, a helical glass tube could be interposed into the sampling-air stream to the capnograph. This helical tube fits into a well-type scintillation crystal (Wenzel, M.P.A.-10).

The electrocardiogram was obtained, using Van Einthoven's standard lead II (Winsor, 1968), by means of subcutaneous electrodes. It was monitored on a Physio-Sentinel Monitor (Mennen-Greatbach).

Furthermore, the heart frequency derived from the cardiogram, was measured and recorded continuously. The temperature was monitored continuously via a thermo-probe, placed beside the respiration tube. The pig was kept at a temperature of about $37^{\circ}C$ by means of an electrically heated blanket.

In order to measure blood pressure a short catheter (Ch.6)

was introduced into the abdominal aorta via the right femoral artery. The catheter was connected to a pressure transducer (Statham, P23), which was continuously flushed with saline, by an infusion pump, in order to prevent blood from entering the catheter. Systolic, diastolic and mean blood pressure could be read from the Physio-Sentinel Monitor. Systolic and diastolic pressure were recorded continuously.

All the physiological variables which were monitored were recorded on a 12-channel multi-point recorder (Philips, PR-3500). Normal values of several physiological parameters, taken from Lagerwey (1973), are given in Table 2.

		mean	st. dev.
haemoglobine	%	10.4	0.942
haematocrit	%	32.0	3.17
pH art.		7.413	0.0378
$P_a \text{ CO}_2$	mmHg	43.8	3.81
base excess	maeq l ⁻¹	+2.9	
st. bicarb.	maeq l ⁻¹	26.4	2.38
$P_a \text{ O}_2$	mmHg	86.7	5.88
heart frequency	min ⁻¹	95.6	9.08
syst. blood press.	mmHg	98.2	10.4
diast. blood press	mmHg	67.4	8.2
respiration freq.	min ⁻¹	12-18	

*Table 2.: Normal values
of some physiological
parameters of the pig
(Lagerwey, 1973).*

The next step in surgery was the preparation of the branching point where the internal carotid artery branches off from the left common carotid artery. Except in a few experiments (section IV-4), the external carotid artery was ligated during c.b.f. measurements. This ligation, however, was postponed until all other preparations were finished. Care was taken that the carotid plexus was not clamped. When the external carotid artery was tied off, no significant physiological change was observed.

Head skin was removed by means of a high frequency

coagulation knife (Mark, Electrotome 120).

A round 'window' was then milled in the skull, above the left hemisphere, just large enough to fit the collimator of the detector. To avoid loss of cerebrospinal fluid, and hence fall in intra-cranial pressure, a sheet of about 2 mm of scalp bone was left intact. Fig. 18 gives an impression of the positioning of the collimator.

Injection of Xe-133 into the common carotid artery via a puncture, a method often applied in man, turned out often to cause a local vasoconstriction or a bleeding of the tunica intima.

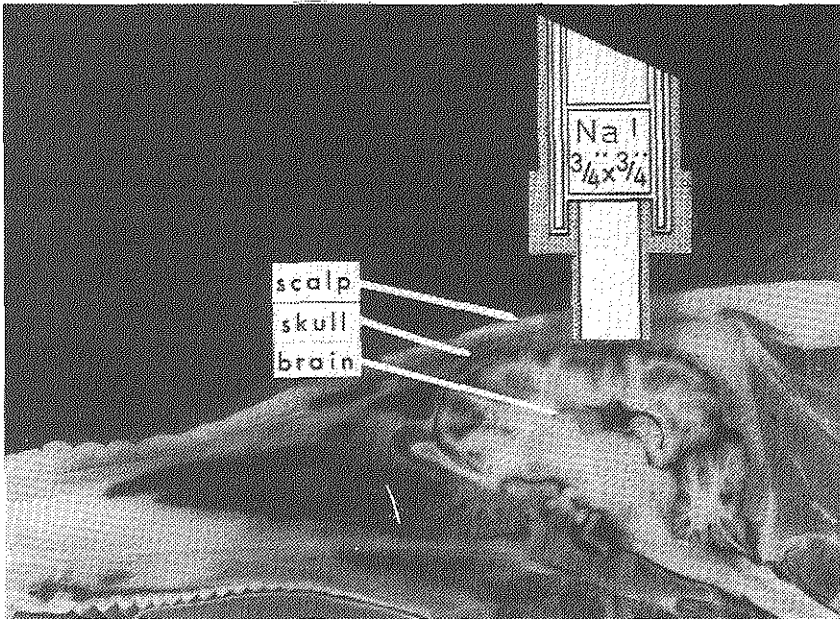


Fig. 18.: Arrangement of scintillation detector over cerebrum of pig.

After trying several methods of catheterization we found that the best method was the introduction of the catheter into the common carotid artery via the left femoral artery. We used an X-ray opaque catheter, with a tip that could

be controlled by a joystick (Meditech, 85 cm long, diameter 1.5 mm). Under X-ray fluoroscopy, the catheter tip was manipulated through the aortic arch and the bi-carotid trunk into the left common carotid artery. The catheter tip was placed about half-way along the common carotid artery. In order to measure the blood pressure in the common carotid, the catheter was connected to a pressure transducer (Statham, P23).

The ligation of the external carotid artery concluded the preparation of the animal. In the first series of experiments we checked the situation by angiography. Later we avoided angiography since the contrast medium may affect the cerebral circulation (Brown and Donaldson, 1970; Van Duyl et al, 1975). When all physiological parameters had become stable, Xe-133 was injected. In the initial period of our experiments we obtained Xe-133 from the Radiochemical Centre at Amersham (multi-dose syringe cartridges of 10 mCi in 3 cm³ saline). Later we obtained it from I.R.E. in Belgium (multi-dose syringe cartridges of 12.5 mCi in 2.5 cm³ saline). About 2 mCi Xe-133, dissolved in about 1 cm³ saline, was injected within 1 second. The Xe-133 bolus was flushed out of the catheter by a rapid injection of saline. The clearance was recorded during either 45 or 20 minutes. Measurements were performed at different P_{co₂} levels. When the clearance was recorded for 45 minutes at least one hour elapsed between successive injections, so that the residual radioactivity remaining from the one experiment was negligible in the next. When the clearance was recorded for 20 minutes, in order to perform a sequence of successive c.b.f. measurements at different P_{co₂} levels, the interval between two injections was about 40 minutes.

III-2 Equipment for the measurement of the clearance curves.

III-2-1 The scintillation detector.

Cerebral radioactivity was measured by means of a small scintillation detector. The detector consists of a NaI crystal, activated by Thallium, with a diameter of $\frac{3}{4}$ inch and a thickness of $\frac{3}{4}$ inch. The crystal is fixed to the top of a photomultiplier tube (Philips, XP 1110) with some grease in between. The scintillation detector, together with a high-voltage divider circuit, is put in an aluminium tube. To exclude radiation from outside the view of the probe it was enveloped in a lead sheet of thickness 2 mm and a pipe collimator of lead was fixed on top of the probe, Fig. 19.

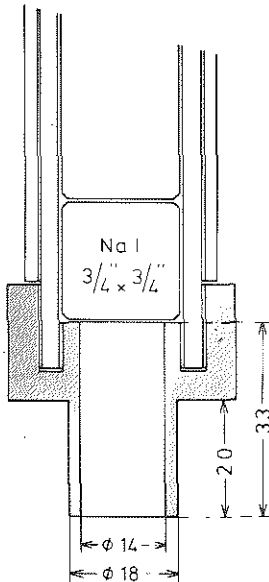


Fig. 19.: Dimensions of the collimator of the scintillation detector.

Via a coaxial cable the detector is connected to the high-voltage supply unit of a 4-channel gamma spectrometer (Meditronic, Mod. H.A.4).

In this device the pulses are separated from the high-voltage and fed into a pre-amplifier with a capacitive input impedance. The pre-amplified pulses are then passed to the main pulse amplifier. In order to select the pulse heights within a certain range the pulses are processed by single-channel pulse-height discriminators (Wenzel, N.E.D.-10).

The pulse-height spectrum of Xe-133 measured with our equipment is given in Fig. 20. The spectrum consists of two well separated peaks, one due to 81-keV gamma rays and one due to 31-keV X-rays, which are produced by internal conversion (Table 1). The 'width at half maximum', W.H.M., expressed as a fraction of the position of the maximum of the peak is about 0.22 for the 81-keV peak and about 0.40 for the 31-keV peak. Because of the contributions from scattered radiation, the peaks are only symmetrical within a pulse-height window that is smaller than 1.5 W.H.M.. The symmetrical parts of the peaks are approximately Gaussian, with standard deviations σ , which are theoretically proportional to the square root of the energy of the radiation (Haskins, 1957), i.e.

$$\sigma \text{ (81-keV)} : \sigma \text{ (31-keV)} = \sqrt{81} : \sqrt{31} \quad (61)$$

Further these standard deviations are proportional to the gain of the photomultiplier.

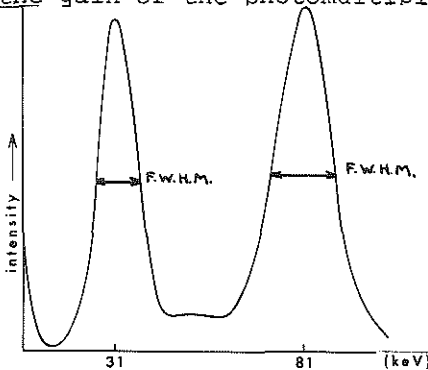


Fig. 20.: Energy spectrum of Xe-133, measured with the equipment described in text.

Clearance curves are usually recorded by the detection of the 81-keV radiation. In our experiments, however, radiation at both energies, 81 keV and 31 keV, was selected simultaneously by means of two pulse-height discriminators in parallel.

Following Wagner (1968), we used discriminator windows with a width of 1.25 W.H.M.. This width expressed in the standard deviation of a Gaussian peak is equal to 2.95σ . The lower and upper levels of the window were set symmetrically around a peak in order to reduce changes in the pulse rate due to small variations in the gain of the photomultiplier tube.

For the used window we calculated the variation in pulse rate caused by a variation in gain. It appears that when the location of the mean value of a Gaussian peak is shifted relative to its original location half-way the window, by a distance shorter than 20% of the standard deviation of the peak, then the pulse rate is reduced by less than 1%.

For the 81-keV peak the standard deviation divided by the mean value equals about 0.10. Hence a shift of the pulse-height spectrum, of the 81-keV radiation, expressed as a fraction of the mean pulse height, equals 0.10 times the value of that shift expressed as a fraction of the standard deviation of the spectrum. For the 31-keV radiation the corresponding figure equals about 0.17. Consequently a change in the gain of 2% causes a shift of the 81-keV peak of 20% of the standard deviation of that peak and thus a reduction in pulse rate of less than 1%. For the 31-keV peak 2% change in gain causes a shift of about 11.5% and consequently a reduction in pulse rate of less than 0.3%. Therefore the ratio of pulse rates for the two types of radiations, r_{31}/r_{81} , will increase if the gain increases or decreases with respect to the situation in which the apparatus was

originally adjusted. We then find that, approximately:

$$\frac{\Delta (r_{31}/r_{81})}{r_{31}/r_{81}} (\%) = \Delta r_{81}(\%) - \Delta r_{31}(\%) \quad (62)$$

We conclude that a change in the gain of 2% results in changes of about 1% in the '81-keV' pulse rate and about 0.35% in the '31-keV' pulse rate, and about 0.65% in r_{31}/r_{81} .

Provided that the high-voltage supply is stable to within 0.1%, the photomultiplier tubes usually meet this requirement for gain stability. According to its specification, the high-voltage supply which we used has a stability that is better than 0.01% for a 10% change of mains voltage. Hence we did not expect instability problems. The photomultipliers initially used, however, were more unstable than expected.

We studied the instability of the type of photomultiplier tube that we used (Philips, XP 1110) in more detail (Van Duyl and Brenninkmeijer, 1975). The location of the energy peak of Cs-137 was measured by means of a multi-channel analyzer (Philips, 111500). Two kinds of gain instability could be distinguished; a stationary instability or drift, found at a constant radioactivity level, and a dynamic instability (shift), caused by an alteration of radioactivity. The shift consists of an almost instantaneous part, followed by a more slowly changing part. It appears that in the tests the response to an increase in the pulse rate from the background level takes more than four hours to become stable and that the shift of the peaks in the spectrum relative to its original location may be more than 10%. The tubes were in operation at background radiation level for more than 24 hours before the tests were performed. The dynamic

shift, after a stepwise increase of pulse rate, may be more than 16%. Because of these unacceptable instabilities, we from then on used only tubes that were, at our request, selected by Philips, according to selection criterion 08 (Philips data handbook, part 6, electron tubes, Jan. 1974). The measuring conditions for this selection are as follows. A Cs-137 source is placed in front of the tube, so that the pulse rate is 1000 pulses per second. The location of the energy peak at this pulse rate is measured. Then the pulse rate is changed in one step from 1000 to 10,000 pulses per second. After ten minutes the location of the energy peak is measured at the new pulse rate. According to selection criterion 08 the obtained shift of the peak must be less than 1%.

These selected tubes met our requirements for stability, i.e. better than 1%. In our opinion, however, the selection criterion 08 of the manufacturer is not adequate to guarantee that our requirements are met. In the injection technique the scintillation detector is exposed to a large stepwise increase in radioactivity. As explained in sections II-5 and 6 the first two to ten minutes provide crucially important parts of the recorded clearance curves. Since according to the selection criterion, the shift must be less than 1%, ten minutes after the stepwise increase of the pulse rate, it is not warranted that the shift is less than 1% in the first ten minutes also.

In most of our observations the instantaneous shift was greater than that after 10 minutes, although less than 1%. The characteristics of the collimator for the 81-keV and 31-keV radiation are described in appendix I.

III-2-2_Pulse_processing

The pulses, selected by the pulse-height analysers, were recorded on an analog magnetic tape recorder (Philips, Analog 7). However, we did not feed these pulses directly into the recorder, because then a considerable number of pulses would not be recorded. This is a consequence of the unfavourable statistical distribution of intervals between the pulses, which is described by a negative-exponential probability function (Rainwater, 1947). About 63% of the intervals are shorter than $1/r$; r is the mean pulse rate.

In order to record separately detectable pulses on magnetic tape, there should be a minimum interval between the pulses. We found that with a tape speed of 15 inches per second (according to the specification the bandwidth of the recorder then is 50 kHz), pulses with a duration of 5 μ sec. and a minimum interval of 40 μ sec. between them would be detected adequately. When the mean pulse rate is 10^4 per second, about 33% of the intervals are smaller than 40 μ sec.. Hence we had to adapt the interval statistics to the limitations of the recorder.

This problem has been studied in more detail by Kerkhoff (1970). We solved it by constructing a derandomizer based on a queuing system.

The derandomizer consists of an array of 5 memory locations. Each input pulse is fed into the first location and then shifted rapidly forward to the most distant empty place in the queue. The front position of the queue is read out and recorded on the magnetic tape, at a frequency adapted to the recorder, namely 25 kHz. (i.e. an interval of 40 μ sec.). The dead time of the derandomizer, which is determined by the clock frequency for shifting the pulse, is less than 1 μ sec.. This is smaller than the dead time of the pulse-height analyzer,

which is 3 μ sec..

From a computer simulation of this derandomizer, it was concluded that if the mean pulse rate is 10^4 pulses per second, while the read-out frequency is 25,000 pulses per second, less than 0.3% of the pulses would be lost, due to the occupation of the 5 memory locations. Results of a test of real derandomizers are in agreement with the theoretical expectations.

Pulse rates higher than 10^4 pulses per second have been avoided, because piling-up of the pulses may then occur and an error in the measurement may be introduced. Because of the statistical nature of radioactivity the pulse rate detected, from a radioactive source is subjected to variation. The probable error in the pulse rate depends on the number of pulses counted, and can be calculated from the formula

$$\frac{0.67}{\sqrt{r \cdot T}} \quad (63)$$

where T is the counting time (Price, 1964). With a pulse rate in the range from 10^4 to 10^2 pulses per second and the 4-second counting time which we used, the probable error varies from 0.3 to 3.4%. Hence the error introduced by the derandomizer is of the same order of magnitude as this statistical error for the highest pulse rate.

The pulses were recorded via the derandomizers during 20 or 45 minutes of clearance. The recordings were monitored by means of an oscilloscope, as shown in Fig. 9. Via a multiplexer, an analogue pulse rate meter (Philips PW 4242) and a paper recorder (Servogor, RE-511) any channel could be recorded on paper chart during the clearance.

Since only one digital read-out channel was at our disposal, we had to replay all the recordings one after

another via a multiplexer, as shown in Fig. 21. The selected channel of the multiplexer is connected to two scalars (Philips, PW 4232). During the preset counting time of 4 sec., selected on the timer (Philips, PW 4261), one of the scalars counts the pulses. A pulse at the preset time stops that scalar and simultaneously starts the other scalar. Then the first scalar is read out via the printer-control (Philips, PW 4209) and the output can be printed (Victor printer). Via a puncher interface the data are punched (Facit) on paper tape in I.B.M.-8 code.

When the scalar has been read out, it is reset and is started again when the preset time has been elapsed. In order to prevent a time shift between the replay of the tracks on the tape recorder, the start of the recording is marked on a separate channel of the tape recorder, Fig. 22. The marker consists of a sine wave of 2 kHz lasting one second. The sine wave passes a band filter during replay, and is then integrated so that it finally initiates a start pulse. The start pulse resets the timer and commands the multiplexer to switch to the next channel. Data processing then starts again. The end of the recording is also marked by a sine wave. This sine wave, at the end of the tape, acts as a pulse which stops data processing. Some minutes later the tape recorder stops and rewinds automatically. Because the speed of rewinding is higher than the speed of replay, the sine waves do not pass the band filter and hence no control pulses are generated during rewinding. When rewinding is finished the replay starts automatically and the first control pulse, initiated by the sine wave, connects the next channel to the read-out system. Thus the read-out of the recorder tracks is automatically performed successively.

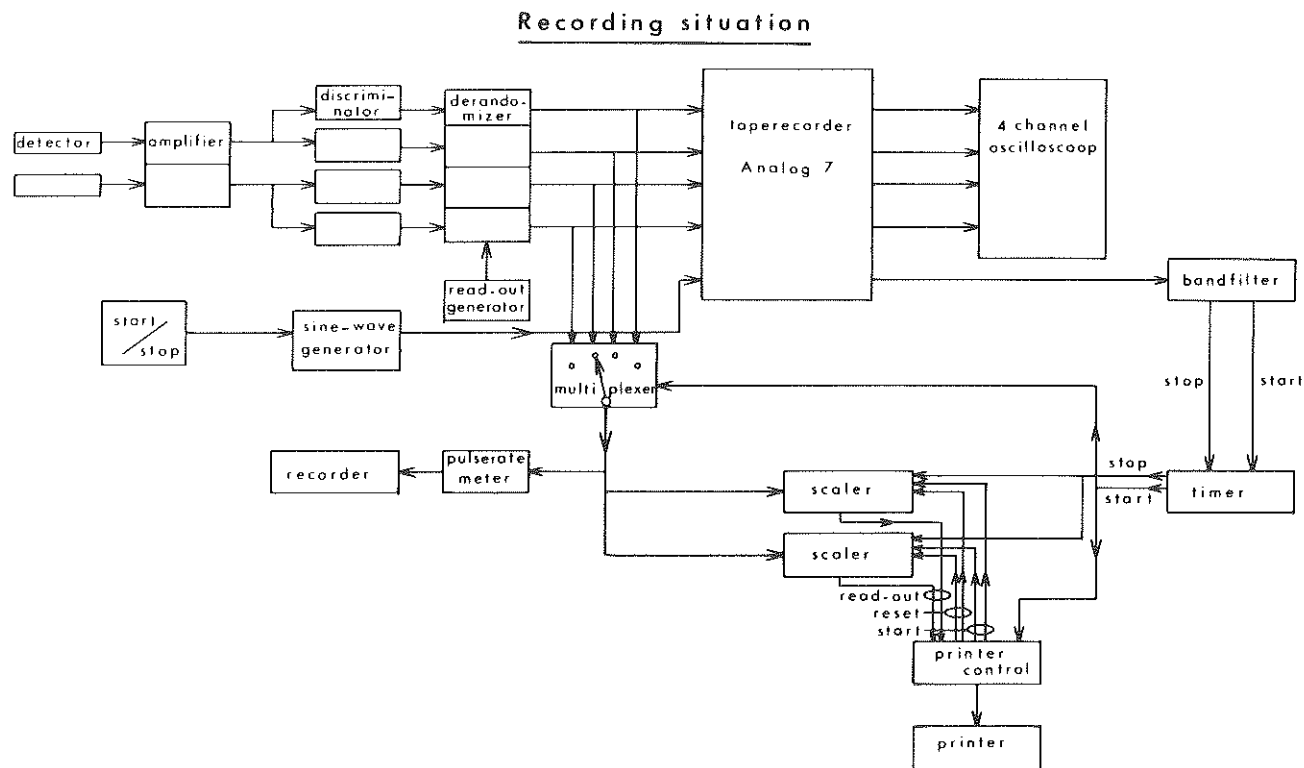


Fig. 21.: Scheme of the electronic equipment for the recording of the clearance curves.

Replay situation

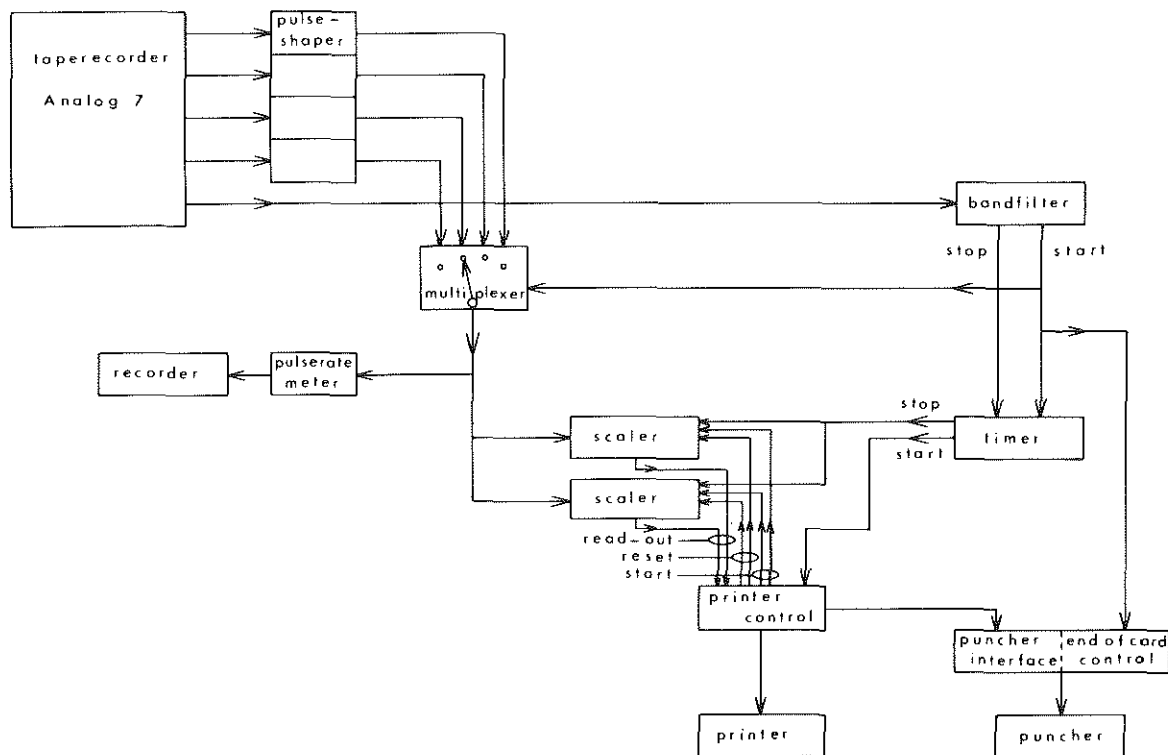


Fig. 22.: Scheme of the electronic equipment for the replay of the clearance data, recorded on magnetic tape.

The paper tape had to be converted into punch cards which could be fed into a computer terminal. To facilitate this conversion an end-of-card code was generated whenever 80 characters have been punched.

In some experiments the radioactivity is measured in the right hemisphere also. In that case four clearance curves were recorded, namely '81-keV' and '31-keV' clearance curves from each hemisphere.

If the radioactivity of the expired air was measured, it too was recorded on the tape recorder. The radioactivity curve of the expired air was recorded via an analogue pulse rate-meter, on a pen recorder (Servogor). Because of the quick changes in this radioactivity, as explained in section II-2, the time constant of the rate meter was here made small, 0.1 sec..

For quick analysis of the cerebral clearance curves during the experiments an electronic device has been developed (Van der Zwart, 1974, Van Duyl et al, 1976), Fig.23.

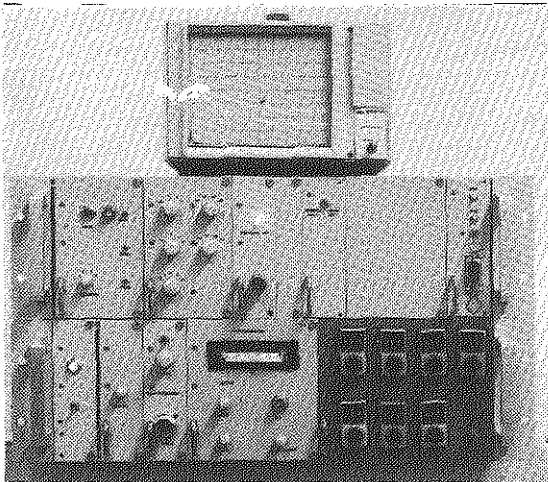


Fig. 23.: Picture of the curve-simulator (prototype) for the analysis of exponential decay curves.

This analysis is based on simulation of the measured curve by an electronic model. The measured curve is fed into a memory and represented on a monitor. On this monitor a second curve can be fitted to the measured

clearance curve by adjusting the 'coefficient'- and 'exponent'-knobs of the model. Comparison of both curves can be accomplished by eye or by minimizing the inclination of a meter that indicates the area between both curves. The parameters fitted to the curve that is being analysed, can be read off from the potentiometer settings. This device has not yet been fully evaluated.

III-3 COMPUTER PROGRAM FOR THE ANALYSIS OF THE CLEARANCE CURVES

III-3-1 Digital fitting procedure

According to the compartmental model of the clearance process, the clearance data can be fitted by a multi-exponential model, i.e.:

$$r(t) = K + \sum_{i=1}^n A_i e^{-\alpha_i t} \quad (64)$$

In this mathematical model the constant K is primarily included to account for background radiation. This model has been fitted to the data, by means of a digital computer, by the method of minimizing the sum of squares of the deviations between measured data and the model. The weighted sum of least squares is denoted by:

$$\phi = \sum_{j=1}^m \frac{1}{r_j^*} (r_j^* - r_j)^2 \quad (65)$$

where m is the total number of data points, r_j^* the observed pulse rate and r_j the pulse rate according to the mathematical model.

The factor $1/r_j^*$ in (65) is a weighting factor, introduced to ensure that the observations subjected to larger variances will have smaller influence on the fitting procedure. The data of the clearance curves are subject to variations which follow a Poisson distribution, so that the variance in the observed value of the pulse rate is about equal to that value (Price, 1964). Therefore the weighting factors are chosen to be equal to the reciprocal value of the observed pulse rates.

The minimum sum of the squares, obtained by the adjustment of the parameters K , A_1 and α_1 , is due to noise in the observed data. However, if the model used does not describe the data adequately, the lack of fit will also contribute to the residual sum of squares. As a consequence of the applied weighting factors and the Poisson statistics, the residual weighted sum of squares is a statistical quantity distributed according to a χ^2 -distribution with $(m - k)$ degrees of freedom, where m is the total number of the data points and k the number of parameters to be fitted (Draper and Smith, 1967).

Because the number of the degrees of freedom is greater than 100, the χ^2 -distribution is practically identical to the Gaussian distribution with $(m - k)$ as the mean value and $\sqrt{2(m - k)}$ as the standard deviation (Abramowitz and Stegun, 1964). The eccentricity of the residual sum of squares, defined by:

$$\xi = \frac{\phi - (m - k)}{\sqrt{2(m - k)}} \quad (66)$$

is therefore a measure for the probability that the sum of squares is due to noise only.

An error in the fit of the model will always cause the sum of squares to increase. If a residual sum of squares has an eccentricity $\xi = 2$, the chance that this is only due to noise alone is 2.3%. We used this eccentricity parameter to judge the quality of the fit of an exponential model to the clearance curves.

The way in which a lack of fit influences the result of a fitting procedure depends on the applied weighting factors. In our situation a fit error in the high pulse rate range, i.e. at the beginning of the clearance curve,

contributes less to the sum of squares than an equal fit error in the data points in the low pulse rate range in the tail of the curve.

When ϕ is the minimum of the weighted sum of squares, the derivatives of ϕ with respect to the parameters must be zero. To satisfy this condition a set of non-linear equations has to be solved. Because of the non-linearity it can be done only by an iterative procedure.

Two types of frequently applied iterative procedure are the gradient-method and the Gauss-Newton method (De Wilde, 1964). According to the gradient-method the iterative steps in the parameter space are taken in the direction of the negative gradient of ϕ (steepest descent). This method is always convergent. In the exponential model, however, the minimum is situated in a flat region and consequently the convergence of the procedure is very slow.

In the Gauss-Newton method the steps are based on the linear term of a Taylor series expansion. This method is faster, although not always convergent.

The computer program used for the analysis of the clearance curves was taken from Kirkegaard (1970). In this program both types of iteration procedures are combined in a manner proposed by Marquardt (1959). Starting with initial estimates of the decay constants, the iteration steps are mainly taken according to the gradient-method. After each iteration, that yields a decrease in the sum of squares, the steps are taken more and more in a direction according to the Gauss-Newton method. The iteration stops when the relative change in the exponents is less than about 3×10^{-5} . The program is used in double precision as recommended by Kirkegaard.

III-3-2 Reliability of the parameters of a fitted exponential model

Separation of an experimental curve into exponentials can give very unreliable results. This is caused by the lack of sensitivity of the sum of squares to certain variations in the parameter set, so that quite different sets of parameters may fit one set of data equally well.

If $r^*(t; p_1, \dots, p_k)$ is the actual function of the process that generates the experimental data, determined by the parameter vector $\underline{p}^* = (p_1, \dots, p_k)$, then the aim of the fitting procedure is to find \underline{p}^* . Let an estimated parameter vector be $\underline{p} = (p_1, \dots, p_k)$. Then the sum of squares is:

$$\phi(\underline{h}) = \int_0^t \left(r^*(t'; \underline{p}^*) - r(t'; \underline{p}) \right)^2 dt' \quad (67)$$

where $\underline{h} = \underline{p} - \underline{p}^*$ is the error vector.

When \underline{p} is assumed to be in the neighbourhood of \underline{p}^* , then ϕ can be approximated by the first three terms of a Taylor-series expansion:

$$\phi(\underline{h}) = \phi(\underline{h})_{\underline{p}^*} + \underline{h}^T \left(\frac{\delta \phi}{\delta \underline{p}} \right)_{\underline{p}^*} + \frac{1}{2} \underline{h}^T \left(\frac{\delta^2 \phi}{\delta \underline{p}^2} \right)_{\underline{p}^*} \underline{h} \quad (68)$$

It is evident from (67) that $\phi(\underline{h})_{\underline{p}^*} = 0$. The sum of squares has a minimum at \underline{p}^* , hence $\left(\frac{\delta \phi}{\delta \underline{p}} \right)_{\underline{p}^*} = 0$ also. Thus we may write:

$$\phi(\underline{h}) = \frac{1}{2} \underline{h}^T \left(\frac{\delta^2 \phi}{\delta \underline{p}^2} \right)_{\underline{p}^*} \underline{h} \quad (69)$$

Here $\frac{1}{2} \left(\frac{\delta^2 \phi}{\delta \underline{p}^2} \right)_{\underline{p}}$ is a symmetric matrix that converts the square of the distance between \underline{p} and \underline{p}^* in the parameter space to the sum of the squares of the deviations between $r(t; \underline{p})$ and $r^*(t; \underline{p}^*)$.

If the error vector \underline{h} is expressed on a vector base, composed of the eigenvectors of matrix $\frac{1}{2} \left(\frac{\delta^2 \phi}{\delta \underline{p}^2} \right)_{\underline{p}^*}$, then an equivalent transformation matrix, working on \underline{h} , is a diagonal matrix with the eigenvalues of the original matrix, along the diagonal (Bijl and Salet, 1964). Thus the following simple relationship is found:

$$\phi(\underline{h}) = \sum_{i=1}^k \zeta_i c_i^2 \quad (70)$$

where ζ_i are the eigenvalues and c_i the components of \underline{h} , along the eigenvectors.

Julius (1972) used this theory to determine the sensitivity of ϕ to a change of the parameters in the neighbourhood of \underline{p} . He defined the following sensitivity parameter:

$$S = \frac{\sum_{i=1}^k \zeta_i c_i^2}{\sum_{i=1}^k c_i^2} \quad (71)$$

Here $\sum_{i=1}^k c_i^2$ is equal to the distance between \underline{p} and \underline{p}^* . S depends on the direction of \underline{h} but not on its magnitude. We write S in the following form:

$$S = \zeta_1 + \frac{(\zeta_2 - \zeta_1) c_2^2 + (\zeta_3 - \zeta_1) c_3^2 + \dots + (\zeta_k - \zeta_1) c_k^2}{c_1^2 + c_2^2 + \dots + c_k^2} \quad (72)$$

If we assume that ζ_1 is the smallest eigenvalue, then the fraction in (72) is positive. This implies that $c_2 = c_3 = \dots = c_k = 0$ for the minimum value S . In other words ϕ is least sensitive to a small excursion along $\underline{h} = \underline{c}_1$. This minimum S is equal to ζ_1 . Similarly we find that ϕ is maximally sensitive to a small excursion along $\underline{h} = \underline{c}_k$, if \underline{c}_k is chosen to correspond with the greatest eigenvalue. This maximum S equals ζ_k . The least sensitive direction and the most sensitive direction are perpendicular to each other. For the function $f(t) = 3e^{-t} + 2e^{-2t} + 1e^{-3t}$ Julius (1972) found that the minimum S was 0.6321×10^{-12} , while the maximum S was 11.79. Hence, a small change in the squared length of the parameter vector will at most result in a change in ϕ which is 11.79 times larger, while it may result in a change in ϕ which is 10^{-12} times smaller. This great difference in the sensitivity to perpendicular excursions in the parameter space indicates that the minimum ϕ is situated in a trough. If the iteration path follows the bottom of the trough, the procedure may stop at a point far from the minimum. The situation of the stopping point depends on the initial starting point of the iteration process, the method that is being applied and, last but not least, on the noise in the experimental data. Noise causes statistical variation in the value of the minimum ϕ . Different results may be obtained from a regression analysis, depending on the noise and the computer program used. If the analysis is performed repeatedly on the same program and the same initial estimates of the parameters, the results will all be the same. If another program is used to fit parameters to the same data another set of parameters may be found (Ianczos, 1956).

Marquardt's method of iteration used in Kirkegaard's program was especially developed to find a minimum in long curved troughs in the parameter space (Marquardt, 1963). The shape of the trough, and as consequence the difficulty of separating of exponentials, depends on the ratio of the coefficients and the decay constants. In many practical situations a reliable separation into two exponentials can be performed. The separation into three or more exponentials, however, may encounter insurmountable difficulties, because excessive accuracy of the data may be required (Lanczos, 1956; Myhill, 1967, 1968).

To study the reliability of the separation into three exponentials by our program, we analysed decay curves which were synthetized by a computer (Sparreboom, personal communication). The data were generated according to the function

$$f(t) = 9000e^{0.9t} + 3000e^{0.3t} + 1000e^{0.1t},$$

to which was added Gaussian noise with a mean value zero and a standard deviation equal to the square root of the value of the function.

Figure 24 shows histograms of the deviations of the fitted parameters from the parameter values of the synthetized function for 30 generated curves. In this figure the mean values of the fitted parameters are shown also. These histograms reveal a wide variation in the fitted parameters, indicating the great influence of noise in the data.

In Fig. 25 only one decay curve can be distinguished, though in fact two curves are recorded over each other, namely the original synthetized curve and a curve generated from three exponentials with parameters found to fit to the original curve (i.e. one of the 30 analyses). Both curves are generated here without added noise.

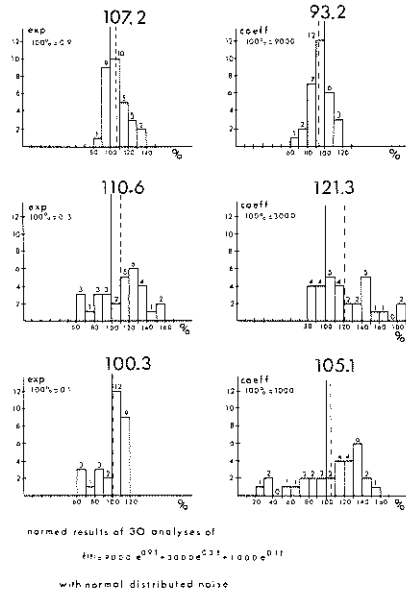


Fig. 24.: Histograms of results of a series of analyses on a sum of three given exponentials.

It appears that the curves are practically identical although the difference in the parameters is great. This illustrates the lack of uniqueness and the difficulty of separation into exponentials, even without added noise.

Referring to the function $f_1(t) = 3e^{-t} + 2e^{-2t} + e^{-3t}$ cited above, Julius (1972) found that an excursion from the minimum ϕ , in the least sensitive direction in the parameter space, the following functions have values differing by less than 5% from those of the original function:

$$f_2(t) = 3.156e^{-1.012t} + 2.875e^{-2.301t}$$

$$f_3(t) = 3.824e^{-1.064t} + 6.632e^{-3.592t} - 4.296e^{-6.360t}$$

In other words even a two-exponential model fits a three-exponential function within 5%.

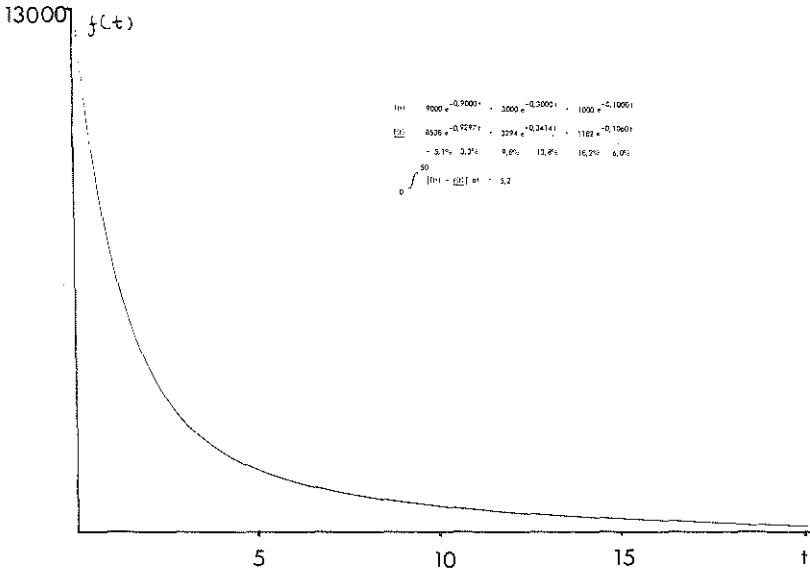


Fig. 25.: Recordings of two curves generated by two different sets of parameters defining a sum of three exponentials.

We conclude that, because of the serious problems encountered in separation into exponentials, it is useful to evaluate the reliability of the results by comparing them to an analysis of synthetized curves having parameters with similar values.

III-4 Features of a compartmental model in relation to the '81-keV' and '31-keV' clearance curves

In the series of preliminary studies on patients, described in section II-3, we determined 4 pulse-height spectra from the radiation, detected extra-cranially during clearance by means of a multi-channel analyzer. It was found that the shape of this spectrum changed during clearance. It was decided to study the features of the spectrum in relation to a two-compartmental model (Hengst, 1971; De Bruin, 1972).

In the experiments with pigs we measured the 81-keV and the 31-keV radiation, selected by means of two pulse-height analyzers, as described in section III-3.

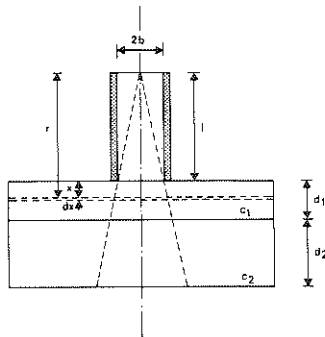


Fig. 26.:

Two-compartmental model, combined with the collimator of a radiation detector.

Figure 26 shows a two-compartmental model combined with a pipe-collimator. Both compartments are filled with water containing Xe-133, which is distributed homogeneously. If we assume that the response from a plane source can be approximated by (4A) and (5A), as derived in Appendix I, the response from the upper

compartment can be calculated by integration of these formulas between the boundaries $x = 0$ and $x = d_1$, so that,

$$r_{81} = \int_0^{d_1} g_{81} c_1 e^{-\mu_{81}' x} dx = g_{81} \frac{(1 - e^{-\mu_{81}' d_1})}{\mu_{81}'} c_1 \quad (73a)$$

$$r_{31} = \int_0^{d_1} g_{31} c_1 e^{-\mu_{31}' x} dx = g_{31} \frac{(1 - e^{-\mu_{31}' d_1})}{\mu_{31}'} c_1 \quad (73b)$$

The response from the lower compartment is found by integration between the boundaries $x = d_1$ and $x = d_1 + d_2$, thus:

$$\begin{aligned} r_{81} &= \int_{d_1}^{d_1+d_2} g_{81} c_2 e^{-\mu_{81}' x} dx = \\ &= g_{81} \frac{e^{-\mu_{81}' d_1}}{\mu_{81}'} (1 - e^{-\mu_{81}' d_2}) c_2 \end{aligned} \quad (74a)$$

$$\begin{aligned} r_{31} &= \int_{d_1}^{d_1+d_2} g_{31} c_2 e^{-\mu_{31}' x} dx = \\ &= g_{31} \frac{e^{-\mu_{31}' d_1}}{\mu_{31}'} (1 - e^{-\mu_{31}' d_2}) c_2 \end{aligned} \quad (74b)$$

According to the theory in section II-2 the cerebral clearance process by this model can be represented by:

$$c_1 = \frac{q_0}{F} f_g e^{-\frac{f_g}{\lambda} t} \quad (75a)$$

$$c_2 = \frac{q_o}{F} f_w e^{-\frac{f_w}{\lambda_w} t} \quad (75b)$$

Hence, according to the two-compartmental model, the '81-keV' and '31-keV' clearance curves can be described by the formulas:

$$r_{81} = \frac{q_o g_{81}}{F \mu_{81}} \left[(1 - e^{-\mu_{81}' d_1}) f_g e^{-\frac{f_g}{\lambda_g} t} + e^{-\mu_{81}' d_1} (1 - e^{-\mu_{81}' d_2}) f_w e^{-\frac{f_w}{\lambda_w} t} \right] \quad (76a)$$

$$r_{31} = \frac{q_o g_{31}}{F \mu_{31}} \left[(1 - e^{-\mu_{31}' d_1}) f_g e^{-\frac{f_g}{\lambda_g} t} + e^{-\mu_{31}' d_1} (1 - e^{-\mu_{31}' d_2}) f_w e^{-\frac{f_w}{\lambda_w} t} \right] \quad (76b)$$

A comparison of these formulas with (14) and (18) of section II-2 reveals that:

$$A_{81} = \frac{q_o g_{81}}{F \mu_{81}} (1 - e^{-\mu_{81}' d_1}) f_g \quad (77a)$$

$$B_{81} = \frac{q_o g_{81}}{F \mu_{81}} e^{-\mu_{81}' d_1} (1 - e^{-\mu_{81}' d_2}) f_w \quad (77b)$$

$$A_{31} = \frac{q_o g_{31}}{F \mu_{31}} (1 - e^{-\mu_{31}' d_1}) f_g \quad (77c)$$

$$B_{31} = \frac{q_0 g_{31}}{F \mu_{31}} e^{-\mu_{31}' d_1} (1 - e^{-\mu_{31}' d_2}) f_w \quad (77d)$$

Hence, the ratios of the coefficients of the exponentials of the '81-keV' and '31-keV' clearance curves are:

$$\frac{A_{31}}{A_{81}} = \frac{g_{31}}{g_{81}} \frac{\mu_{81}' (1 - e^{-\mu_{31}' d_1})}{\mu_{31}' (1 - e^{-\mu_{81}' d_1})} \quad (78a)$$

$$\frac{B_{31}}{B_{81}} = \frac{g_{31}}{g_{81}} e^{-(\mu_{31}' - \mu_{81}') d_1} \frac{\mu_{81}' (1 - e^{-\mu_{31}' d_2})}{\mu_{31}' (1 - e^{-\mu_{81}' d_2})} \quad (78b)$$

If g_{31}/g_{81} is known, we can use these formulas to calculate d_1 and d_2 in the model from the two exponentials fitted to the clearance data.

Because the decay constants of the corresponding exponentials are equal, the ratio r_{31}/r_{81} associated with each compartment, is a constant during clearance. This constant is equal to the ratio of the coefficients. The radiation from the lower compartment has to pass the upper compartment before reaching the detector. Consequently the ratio r_{31}/r_{81} from the lower compartment is smaller than the ratio r_{31}/r_{81} associated with the upper compartment, i.e.:

$$\frac{A_{31}}{A_{81}} > \frac{B_{31}}{B_{81}} \quad (79)$$

The ratio r_{31}/r_{81} for the entire cerebrum, however, is a combination of the ratios for the separate compartments

in such a way that the contribution of the 'fast' component decreases during clearance.

If the two-compartmental model gives an adequate description for the cerebral clearance process, the clearance studies should yield a decreasing ratio r_{31}/r_{81} , falling eventually to a constant value when the clearance has become mono-exponential. The features of the two-compartmental model, firstly that the corresponding decay constants of the '81-keV' and '31-keV' clearance curves are equal, and secondly that the ratio r_{31}/r_{81} decreases during clearance eventually to a constant value, have been used to test the validity of the two-compartmental model to describe the cerebral clearance process.

With the collimator as used in our experiments it has been found (Appendix I) that $\mu_{81}' = 0.15 \text{ cm}^{-1}$ and $\mu_{31}' = 0.27 \text{ cm}^{-1}$. From these figures the factor:

$$\frac{\mu_{81}'(1-e^{-\mu_{31}'d})}{\mu_{31}'(1-e^{-\mu_{81}'d})}$$

has been determined as a function of d . This relationship is plotted on a semi-logarithmic scale in Fig. 27. It turns out that:

$$\frac{\mu_{81}'(1-e^{-\mu_{31}'d})}{\mu_{31}'(1-e^{-\mu_{81}'d})} \approx e^{-0.055d} \quad (80)$$

This function multiplied by g_{31}/g_{81} yields the value of r_{31}/r_{81} associated with the upper compartment. It appears that a change in thickness of 0.18 cm of the

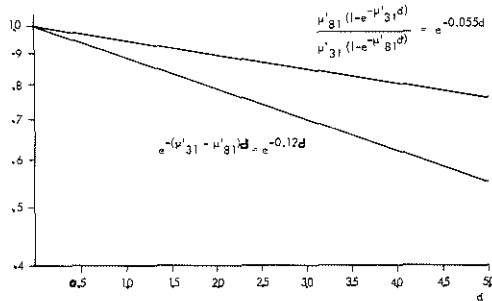


Fig. 27.: Semi-logarithmic plot of $\frac{\mu'_{81} (1 - e^{-\mu'_{31}d})}{\mu'_{31} (1 - e^{-\mu'_{81}d})}$ as a function of d .

upper compartment implies a change of only 1% in the value of r_{31}/r_{81} . The same approximation can be used to determine the value of r_{31}/r_{81} associated with the lower compartment, however, combined with an extra factor $e^{-0.12d}$, also shown in Fig. 27. Finally we find that:

$$\frac{A_{31}/B_{31}}{A_{81}/B_{81}} = e^{-0.055d_1 + 0.12d_1 + 0.055d_2} > e^{0.065d_1} \quad (81)$$

This lower boundary value is a consequence of the fact that the bordering of both compartments is at $x = d_1$. The features of a two-compartmental clearance model are tested on an in-vitro model, consisting of two individually well-stirred perfused compartments. In the measurements in-vivo we found large values of the constant K_{81} and K_{31} . To account for this finding we adapted the in-vitro model by adding the constant plane source. The intensity of the plane source was such, that in periods of 4 seconds on the average 424 '81-keV' pulses were detected and 372 '31-keV' pulses. The ratio

r_{31}/r_{81} measured from this plane source is a little larger than the corresponding value described in Appendix I, because here the windows of the discriminators are broader than $5/4$ W.H.M. The Xe-133 was injected into a tube that supplies water to both compartments.

The Xe-concentrations in the compartments were homogenized by means of motor driven fans. Magnetic stirrers could not be applied because the magnetic field of such stirrers would disturb the gain of the photomultiplier tube. The water in the compartments was continuously refreshed by means of a constant-flow pump. Figure 27 shows the results of the computer analysis of the '81-keV' and '31-keV' clearance curves. The eccentricity of the residual sum of squares of the '81-keV' data was $\xi_{81} = 3.5$ and of the '31-keV' data $\xi_{31} = 2.1$. According to section III-3-1 these values of ξ can indicate that there is a slight lack of fit. This can be ascribed to irregularities in the clearance curves caused by the fans. The decay constants of the fitted corresponding exponentials of the '31-keV' and '81-keV' clearance curves are equal, within the experimental error (Fig. 28). The values of the constants K_{81} and K_{31} are also close to the values of the plane source given above.

In Fig. 27 the ratio of the measured '81-keV' pulse rate and '31-keV' pulse rate is plotted as a function of time. If the fitted value K_{81} is subtracted from r_{81} and K_{31} from r_{31} , the second graph is obtained, denoted by r_{31}'/r_{81}' . The ratio r_{31}'/r_{81}' as a function of time has the theoretically expected course for a two-compartmental model. We conclude that the in-vitro measurement demonstrates the features of a two-compartmental model discussed above.

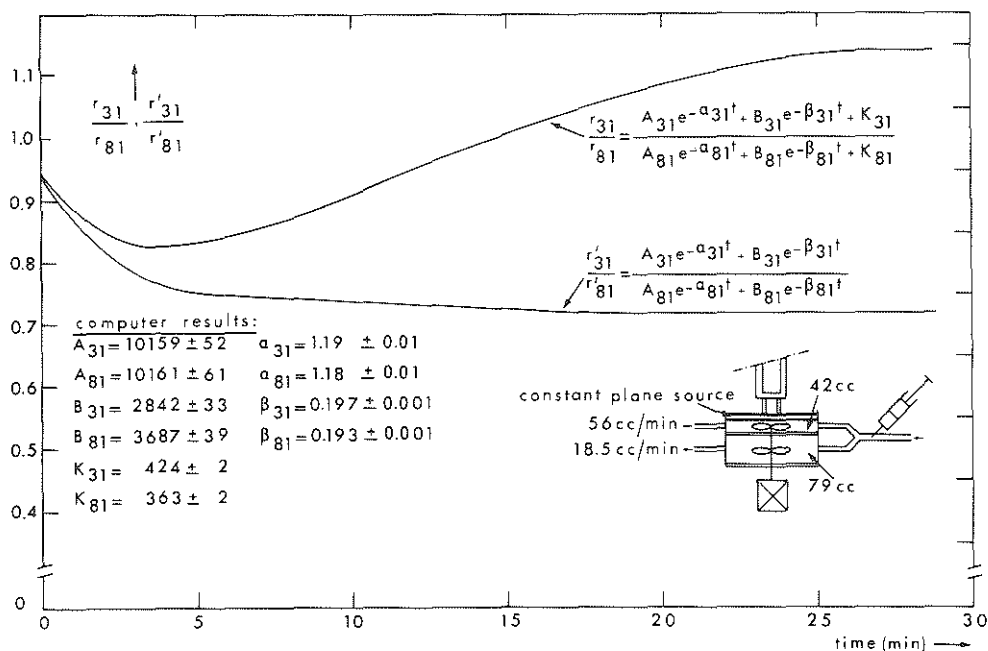


Fig. 28.: Results of computer analysis of clearance of in-vitro model consisting of two well-stirred compartments and constant plane.

Though these features have been demonstrated for a particular, simple shape of the two compartments in the model, it must be noted that they actually are independent of the geometry of the compartments. Hence, if the cerebral clearance process can be described by a two-compartmental model, we expect that the decay constants of the corresponding exponentials, fitted to the '81-keV' and '31-keV' data are equal, and that r'_{31}/r'_{81} decreases eventually to a constant value, despite the capricious shape of the grey and white tissue compartments.

IV-RESULTS OF THE EXPERIMENTS IN VIVO.

IV-1 Introduction.

From 1971 until 1976 cerebral blood flow studies were performed on about a hundred pigs. The results with the Xe-133-injection technique in the pig did not correspond to the results reported for other animals. We devoted a large portion of these studies to the evaluation of the injection technique.

The main problem that has arisen is that with the Xe-133-injection technique considerably lower cerebral blood flow values are found for the pig than those reported for other animals. In this chapter the results of various series of experiments are given, arranged in five groups. Each successive group is characterized by some modifications in the experiments. The modifications were made in an attempt to obtain higher values for the c.b.f. values.

The pigs were prepared and anaesthetized according to schedule described in section III-1-2. Variants of that schedule, used in each group of experiments, are described in the sections.

At the end of this chapter the results of the experiments are summarized. In chapter V some additional experiments are described, the results of which will be discussed in combination with the observations described in this chapter.

IV-2 First group of experiments:

(azaperone - metomidate; open skull; external carotid artery tied off).

Pigs, weighing 20 to 30 kg, were anaesthetized

by an infusion of azaperone and metomidate. The pigs were mechanically ventilated with room air. The scalp was removed and a window was made in the skull.

In Table 3 some physiological parameters, measured in this series are shown. The meaning of the used symbols in the Table is given in the list of abbreviations and symbols.

The systolic blood pressure measured in the common carotid artery via the Xe-injection catheter, was about 10 mm Hg lower than measured in the abdominal aorta (section III-1-2). Blood gases were determined from arterial blood samples, obtained immediately after the injection of Xe-133. A capnograph was not available during this series.

The clearance data were recorded for about 45 minutes and were analysed according to a sum of two exponentials and a constant by computer.

Figs 29 a and 29 b show the experimental data and the fitted curves for the 81-keV and 31-keV radiation, respectively, obtained in exp. nr. 43-I. These figures show both the statistical fluctuations in the data and how well the data is fitted by the model. Judged by eye, generally quite a good fit is obtained, although some lack of fit is seen at the beginning of the curves. In section III-3-1 the eccentricity of the residual sum of squares, ξ , is proposed as a measure for the goodness of fit. It turns out that for the '81-keV' clearance curve $\xi_{81} = 21$ and for the '31-keV' clearance curve $\xi_{31} = 5$. Both eccentricities are higher than 2, indicating that there is a significant lack of fit.

It turns out also that α_{31} is greater than α_{81} and that β_{31} is greater than β_{81} . We shall express these differences as a percentage of that of the decay constants of the fitted '81-keV' clearance curve. Then α_{31} is about 11% greater than α_{81} and β_{31} is about 17% greater than β_{81} .

exp.nr.	sex (m/f) age (w) weight (kg)	bloodpress. S/D (mm Hg)	heart freq. (min ⁻¹)	temp. (°C)	P _a CO ₂ (mm Hg)	pH
40-I	m/-/20	-	120	39.0	-	-
41-I	f/-/20	100/70	80	36.8	53.0	7.32
II	-	110/70	105	36.8	-	-
42-I	f/-/22	100/60	80	38.0	41.0	7.38
II	-	80/45	100	38.0	45.0	7.36
43-I	f/-/21	80/50	75	36.8	52.0	7.22
II	-	80/45	80	36.6	58.0	7.30
44-I	f/-/24	80/40	80	36.2	54.0	7.31
II	-	70/30	120	36.5	55.5	7.35

Table 3.: First group of experiments.

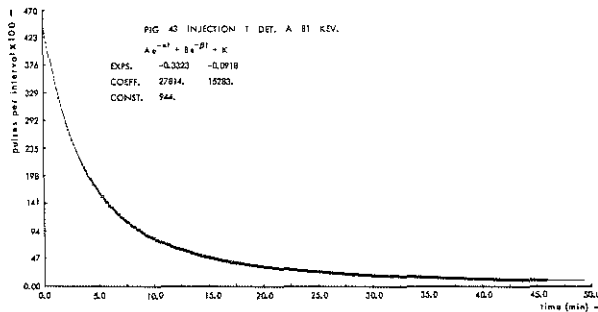


Fig. 29 a: Recorded and fitted data of the '81-keV'-clearance curve in exp. nr. 43-I.

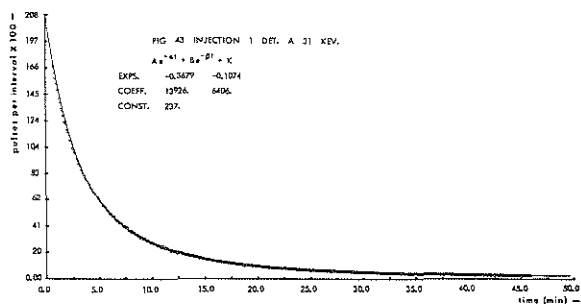


Fig. 29 b: Recorded and fitted data of the '31-keV'-clearance curve in the same experiment as in Fig. 29 a.

In section III-4 it has been shown that the corresponding decay constants of the '81-keV' and '31-keV' clearance curves are equal in a two-compartmental clearance model. Hence the differences found here conflict with the two-compartment theory.

If we assume a haematocrit of 32% (Table 1), we find that, according to the graphs in Fig. 3, the partition coefficients are $\lambda_g = 0.85$ and $\lambda_w = 1.6$. Hence, according to (14) the blood flow values are $f_g = 28 \text{ cm}^3/\text{min}/100 \text{ cm}^3$ grey tissue, and $f_w = 14.7 \text{ cm}^3/\text{min}/100 \text{ cm}^3$ white tissue. When compared to those referred to as normal values in man (section II-2), we note that the values we find here are extremely low. Also the ratio $f_g/f_w = 1.9$ is smaller than the ratio of about 3.8 which is assumed to be normal in man.

The relative weight of the grey tissue compartment, calculated from (20) in this experiment is $W_g = 0.49$, which is within the normal range.

From the parameters fitted to the '31-keV' clearance curve we find that $W_g = 0.54$, i.e. larger than found from the '81-keV' clearance curve. Since, according to the two-compartmental model, the slower cleared compartment is situated under the faster cleared compartment, the radiation from the slower cleared compartment is reduced by absorption in the upper tissue compartment. This reduction is larger for the 31-keV radiation than it is for the 81-keV radiation. This is reflected in the larger value of W_g found with the 31-keV clearance curve. Hence this finding is in agreement with the two-compartmental clearance model.

In section III-3-2 we discussed the equivocality in the parameters obtained by fitting exponential models. In order to check the sensitivity of the fitted parameters to noise in the experimental data, the function fitted to the '81-keV' clearance curve was synthesized by computer. The synthesized function was sampled at intervals of 4 seconds while Gaussian noise was added. In order to simulate the Poisson noise on the clearance data, the mean value of the added Gaussian noise was zero and its standard deviation was taken equal to the square root of the values of the samples. The function which was generated ten times is given in Table 4.

In this Table s is the spread of a parameter as calculated from the ten values found, while $\bar{\sigma}$ is the mean of the ten values of the standard deviations of a parameter which are produced by the computer analyses. The values of the fitted parameters to each generated curve are all within the range determined by these mean standard deviations. The probable error, defined by a deviation of $0.67 \bar{\sigma}$, appears to be less than 1% for all the parameters. The maximum value of ξ obtained in these ten analyses was 1.4, so that in all these analyses a good fit was obtained,

From the analyses of the synthesized curves we conclude that the found eccentricities ξ_{81} and ξ_{31} , obtained in exp. nr. 43-I indicate a lack of fit, which is a consequence of the fact that the two-exponential model does not describe the clearance curves adequately. Furthermore we conclude that the differences in the corresponding decay constants found with the fitted '81-keV' and '31-keV' clearance curves are too large to be due to the statistical nature of the clearance data.

Calculated from the values of the standard deviations, which are produced by the computer analysis for each fitted parameter, the probable error of the coefficients of the fitted clearance curve is less than 1%.

From the fitted clearance curves we find the following ratios: $A_{31}/A_{81} = 0.50$, $B_{31}/B_{81} = 0.42$ and $K_{31}/K_{81} = 0.25$. The fact that $A_{31}/A_{81} > B_{31}/B_{81}$ is in agreement with the two-compartmental clearance model, (79). It is remarkable that the ratio K_{31}/K_{81} is considerably smaller than the ratios A_{31}/A_{81} and B_{31}/B_{81} .

If we interpret these ratios in terms of the dimensions of the two-compartmental model, using the simple geometry of Fig. 26 we obtain information about the geometry of the two tissue compartments.

However, we have first to correct for the absorption of radiation by the intact layer of skull. In a separate measurement we found that, per mm thickness of skull, the transmitted radiation ratio r_{31}/r_{81} is reduced by a factor 0.87. Estimating the thickness of the sheet of skull as 3 mm, the ratio r_{31}/r_{81} should be reduced by a factor 0.66. Hence the corrected ratios of the coefficients are found by dividing by 0.66, and are then equal to 0.76, 0.64 and 0.38 respectively.

The thickness d_1 of the upper compartment of the in-vitro model can be estimated by means of the graphs of Fig. 27.

generated	results of analyses			prob. err. (%)
A = 27814	$\bar{A} = 27785$	$s(A) = 104$	$\sigma(A) = 139$	0.3
B = 15283	$\bar{B} = 15308$	$s(B) = 96$	$\sigma(B) = 148$	0.7
K = 944	$\bar{K} = 945$	$s(K) = 5$	$\sigma(K) = 8$	0.6
$\alpha = 0.3324$	$\bar{\alpha} = 0.3326$	$s(\alpha) = 0.00178$	$\sigma(\alpha) = 0.00209$	0.4
$\beta = 0.0918$	$\bar{\beta} = 0.0919$	$s(\beta) = 0.00037$	$\sigma(\beta) = 0.00061$	0.5

Table 4.: Results of the analysis of the generated function

$$Ae^{-\alpha t} + Be^{-\beta t} + K$$

with values of the coefficients and decay constants corresponding to the fitted 81-keV clearance curve of exp. nr. 43-I (675 samples), (Table 5).

We find that d_1 is about 50 mm. This value is similar to the thickness of the brain tissue under the collimator. If the boundary between this compartment and the more slowly cleared compartment is at a depth of 50 mm, then according to (81):

$$(A_{31}/A_{81})/(B_{31}/B_{81}) > e^{0.065 \times 5.0} = 1.38.$$

Because $A_{31}/A_{81} = 0.66$, this means that B_{31}/B_{81} should be less than $0.66/1.38 = 0.48$. Since $B_{31}/B_{81} = 0.76$, the second compartment must partly overlap the first one. In other words it can be concluded that at a certain distance

from the collimator there is a region where fastly and slowly cleared compartments are intermixed. The constants K_{81} and K_{31} are about 2% of the initial values of the clearance curves. These values are too high to ascribe simply to background radiation. The ratio $K_{31}/K_{81} = 0.25$ corresponds to a plane source in water at a distance of about 8 cm from the collimator.

Because K_{31}/K_{81} is considerably smaller than B_{31}/B_{81} we note that if the values of the constants are ascribed entirely to a Xe-source in the cerebrum, this source must be located in deep brain regions.

The in-vitro model, with its dimensions calculated from the fitted coefficients of the cerebral clearance curves, does not correspond to a compartmental model for the cerebral clearance, as will be shown in chapter V. Nevertheless the conclusions, that the more slowly cleared compartment is situated at a greater distance from the collimator than the more quickly cleared compartment, and that there is an overlap of both compartments, are in agreement with the distribution of grey and white tissue as seen in the cross section of the cerebrum, Fig. 18.

Table 5 shows the results of a series of 7 experiments. The conclusions drawn from the results of exp. nr. 43-I, concerning a) the low c.b.f. values, b) the lack of fit of the two-exponential model, c) the difference between the corresponding decay constants of the '81-keV' and '31-keV' clearance curves, d) values of the relative weights W_g from the '81-keV' and '31-keV' clearance curves and e) the ratio of the coefficients, apply for all these experiments.

A second scintillation detector was placed above the right hemisphere. Also on that side skin was removed and a window in the skull was made. The right external carotid artery, however, was not tied off. It appears that

exp.nr.	A	a	$\sigma(a)$	%	B	β	$\sigma(\beta)$	%	K	ξ	K_{31}/K_{81}	A_{31}/A_{81}	B_{31}/B_{81}	W_g
40-I	29468	0.336	0.002	10	9200	0.077	0.001	16	881	14	0.25	0.52	0.37	0.64
	15405	0.369	0.002		3396	0.089	0.001		221	3				0.67
41-I	35644	0.389	0.003	12	13634	0.100	0.001	16	934	18	0.27	0.57	0.48	0.56
	20235	0.435	0.003		6572	0.119	0.001		252	6				0.61
41-II	32503	0.322	0.002	8	23096	0.092	0.001	10	1252	5	0.25	0.60	0.44	0.44
	19423	0.350	0.003		10158	0.100	0.001		314	0.05				0.39
42-I	30846	0.387	0.003	13	12303	0.107	0.001	15	577	17	0.22	0.48	0.42	0.56
	14664	0.438	0.003		5193	0.123	0.001		128	3				0.60
42-II	42786	0.369	0.002	17	9768	0.095	0.001	31	884	11	0.20	0.45	0.41	0.47
	19456	0.430	0.003		4052	0.124	0.001		172	4				0.72
43-I	27815	0.332	0.003	11	15284	0.092	0.001	17	945	21	0.25	0.50	0.42	0.49
	13927	0.368	0.003		6406	0.107	0.001		237	5				0.54
43-II	34115	0.346	0.003	13	14892	0.086	0.001	22	1284	23	0.22	0.45	0.37	0.53
	15279	0.390	0.003		5476	0.105	0.001		288	7				0.58
44-I	27689	0.333	0.002	14	11484	0.069	0.001	30	1387	13	0.23	0.40	0.29	0.49
	10961	0.381	0.003		3368	0.091	0.001		322	2				0.60
44-II	31534	0.372	0.002	12	10089	0.070	0.001	37	1932	15	0.20	0.37	0.28	0.52
	11672	0.413	0.003		2776	0.096	0.002		388	4				0.65

Table 5.: Results of two-exponential analyses of the first group of experiments.

the initial values of the pulse rates measured with the second detector is 20 to 40% of the initial pulse rates measured with the first detector. Care was taken that in the field of vision of the second detector the amount of tissue of the left hemisphere was as small as possible, so that the main fraction of the measured radioactivity originates from the right hemisphere. Obviously the Xe-133 is transported to the right hemisphere by means of the collateral circulation. The decay constants, found with a two-exponential model were in the same range as those obtained from the clearance curves of the left hemisphere.

We subtracted from the data of the clearance curves the values of the fitted constants K_{81} and K_{31} and calculated the ratio of the pulse rates thus obtained, denoted by r'_{31}/r'_{81} . Fig. 30 shows the course of r'_{31}/r'_{81} obtained in exp. nr. 41-II. The continuous curve in this plot is derived from the fitted clearance curves, again after subtraction of the fitted constants. These curves appear to decrease continuously instead of levelling to a constant value, as we found in Fig. 28. Plots of r'_{31}/r'_{81} for the other experiments in this series follow similar courses. These decreasing courses are directly connected with the differences noted already between the corresponding decay constants of the fitted '81-keV' and '31-keV' clearance curves and between the ratios of the coefficients. These plots show, however, that the xenon becomes relatively more and more concentrated in deeper brain tissue during the clearance, although not in accordance with a two-compartmental model.

Because the two-exponential model does not fit the data exactly, the parameters of this model do not characterize the clearance process exactly. We therefore extended the mathematical model to include of three exponentials and a constant.

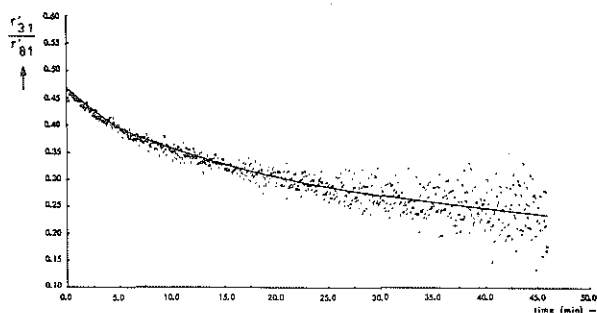


Fig. 30.: Fitted and experimental data of r'_{31}/r'_{81} during clearance in exp. nr. 41-II.

The results of fitting this model to the clearance data are shown in Table 6. The values of the eccentricities of the residual sum of squares, compared to those in Table 5, indicate that the fit is now considerably improved. We note that the decay constants α are greater and spread over a larger range than the values α in Table 5. The decay constants β in Table 6 appear to be of similar magnitude to the values of α in Table 5, although they are slightly smaller. In a similar way the decay constants γ correspond to the values of β in Table 5. Hence the first exponential in the three exponential model appears to represent a strong variable extra component in the clearance curves.

The difference between α_{81} and α_{31} is in most cases much greater than that found with the two-exponential model and does not have a constant sign. If we ascribe the first exponential to the clearance of the grey tissue compartment the blood flow in this tissue varies between

exp.nr.	A	a	$\sigma(a)$	B	β	$\sigma(\beta)$	C	γ	$\sigma(\gamma)$	K	ξ	$\bar{\tau}$
40-I	3939	4.305	0.384	29231	0.316	0.002	8406	0.072	0.009	822	0.98	5.04
	1275	5.797	1.165	15293	0.359	0.002	3224	0.086	0.001	214	0.63	4.06
41-I	22627	0.536	0.015	22236	0.207	0.009	5707	0.058	0.004	606	1.58	4.89
	15538	0.523	0.038	9082	0.213	0.047	2597	0.079	0.019	192	0.99	3.86
41-II	2257	12.750	3.210	32623	0.316	0.002	22677	0.091	0.001	1238	2.29	6.10
	5429	0.649	0.007	16650	0.273	0.012	8038	0.089	0.002	274	0.08	5.30
42-I	12377	0.687	0.036	24768	0.264	0.009	7271	0.081	0.003	453	2.06	4.53
	8326	0.681	0.040	8992	0.272	0.022	2955	0.096	0.005	100	-1.84	3.81
42-II	4305	2.879	0.254	42268	0.348	0.002	8617	0.087	0.001	841	0.69	4.02
	2086	1.586	0.236	18760	0.396	0.005	3403	0.114	0.002	163	0.55	3.24
43-I	6398	1.115	0.073	27696	0.257	0.004	11005	0.075	0.001	788	2.63	5.75
	5831	0.613	0.056	11179	0.246	0.017	3802	0.084	0.004	189	-0.51	4.81
43-II	9081	0.883	0.053	31599	0.261	0.005	10358	0.066	0.002	1003	3.47	5.62
	8049	0.570	0.044	10188	0.245	0.022	2983	0.076	0.006	220	1.87	4.47
44-I	8368	0.703	0.048	23523	0.248	0.007	8722	0.053	0.002	1047	1.18	6.67
	5947	0.545	0.090	6699	0.242	0.049	2017	0.064	0.011	258	-1.64	4.77
44-II	10651	0.706	0.048	24754	0.276	0.009	7722	0.052	0.002	1552	2.54	5.85
	5573	0.613	0.058	7452	0.287	0.025	1762	0.071	0.005	339	0.55	4.05

Table 6.: Results of three-exponential analyses of the first group of experiments.

45 and 1084 $\text{cm}^3/\text{min}/100 \text{ cm}^3$ in this series, while these values are not correlated with the $P_a\text{CO}_2$.

In order to calculate the relative weight of this compartment, we must know the blood values associated with the other exponentials. The question then arises, which values of the partition coefficients should be used to calculate these flow values from the decay constants. For an estimate of the relative weight of the fast compartment we assume $\lambda = 1$. We then find that W_g varies in this series between 0.005 and 0.2, which is a remarkably broad range. All values of the ratio A_{31}/A_{81} , with the exception of exp. nr. 41-II, are in the range 0.48 - 0.91. This means that not in all cases the first exponential can be ascribed to a cortical Xe-source. In exp. nr. 41-II, $A_{31}/A_{81} = 2.4$. This value is too large to be ascribed to any plane source.

In section II-4 it was noted that Lassen (1965), based on clearance of Kr-85, concluded that the clearance curves of the cerebral cortex were two-exponential rather than one-exponential. This is in agreement with our observation that a three-exponential model describes the Xe-clearance curves more adequately than a two-exponential model. The values of the fitted parameters, however, do not justify an interpretation of these exponentials in terms of three separate compartments.

In order to investigate the effect of noise in the data on the reliability of the fitted parameters, we performed a series of analyses on synthesized three-exponential clearance curves, just as we did for the two-exponential model. We synthesized the curve which was found in the analysis of the '81-keV' clearance curve of exp. nr. 43-I, Table 7.

The maximum value of ξ in these ten analyses was 1.7, so that a good fit was obtained in all cases. Although the probable errors in the fitted parameters are larger than

those of the two-exponential model in Table 4, these errors are much smaller than the differences between the corresponding decay constants obtained by fitting the '81-keV' and '31-keV' clearance curves with a three-exponential model. Hence the conclusion drawn previously, that each fitted exponential cannot be ascribed the clearance of a separate compartment, is not merely a consequence of noise in the clearance data.

The three-exponential model reveals an exponential term with a large decay constant. We decided to ignore the first 70 seconds of the clearance curves and to analyse the remaining part of the curves according to a two-exponential model. Results of these analyses are shown in Table 8.

It appears that the values of ξ are considerably smaller than those given in Table 4, indicating that a significantly better fit is obtained. Nevertheless, we find significant differences between the corresponding decay constants of the '81-keV' and '31-keV' clearance curves, of about the same magnitude as differences in Table 5.

Because in a two-compartmental clearance model the corresponding decay constants of the '81-keV' and '31-keV' clearance curves are equal, we conclude that the two-compartmental model is not valid for this truncated part of the in-vivo clearance curves either, even though a reasonable fit may be obtained with a two-exponential model.

In section II-6 it has been shown that the mean transit time \bar{t} of the Xe-133 is a measure for the mean blood flow, irrespective of the validity of a compartmental model. Furthermore it has been shown that, if a multi-exponential model is fitted to the clearance curve, the mean transit time is equal to the mean time constant $\bar{\tau}$ of that model. From the fitted three-exponential model we calculated the mean time constants. The values are given in Table 6.

generated	results of analyses			prob. error (%)
A = 6398	$\bar{A} = 6435$	s(A) = 178	(A) = 315	3
B = 27695	$\bar{B} = 27787$	s(B) = 120	(B) = 212	0.5
C = 11004	$\bar{C} = 10922$	s(C) = 233	(C) = 303	2
$\alpha = 1.1148$	$\bar{\alpha} = 1.1217$	s(α) = 0.06131	$\bar{\sigma}(\alpha) = 0.06704$	4
$\beta = 0.2572$	$\bar{\beta} = 0.2568$	s(β) = 0.00306	$\bar{\sigma}(\beta) = 0.00418$	1
$\gamma = 0.0764$	$\bar{\gamma} = 0.0747$	s(γ) = 0.00106	$\bar{\sigma}(\gamma) = 0.00142$	1

Table 7.: Results of the analysis of the generated function $Ae^{-\alpha t} + Be^{-\beta t} + Ce^{-\gamma t} + K$ with values of the coefficients and decay constants corresponding to the fitted curve of exp. nr. 43-I (Table 6).

It turns out that in all cases $\bar{\tau}_{31} > \bar{\tau}_{81}$. The value of the mean time constant is determined by the relative values of the coefficients of the exponentials, which are affected by the absorption of the radiation in the tissue. Hence this systematic difference between the mean time constants of the '81-keV' and '31-keV' clearance curves shows again that Xe is washed out faster from cortical cerebral tissue, than from deeper brain tissue. The values of $\bar{\tau}_{81}$ are in the range 4.02 to 6.67 min. According to (57) we can derive the value of the mean blood flow if the value of the mean partition coefficient is known. If we assume $\bar{\lambda} = 1$, then the range of $\bar{\tau}_{81}$ corresponds to mean blood flow in the range 24.9 to 15.0 $\text{cm}^3/\text{min}/100 \text{ cm}^3$ tissue.

exp.nr.	A	a	$\sigma(a)$	%	B	β	$\sigma(\beta)$	%	K	ξ	K_{31}/K_{81}	A_{31}/A_{81}	B_{31}/B_{81}
40-I	21306 10673	0.316 0.359	0.002 0.003	14	7805 2951	0.071 0.086	0.001 0.001	21	820 214	1.0 0.4	0.26	0.50	0.38
41-I	24558 13148	0.358 0.412	0.003 0.004	15	11132 5446	0.115 0.091	0.001 0.001	22	891 245	10 4	0.27	0.54	0.49
41-II	23762 13924	0.316 0.331	0.003 0.003	5	20730 8666	0.091 0.097	0.001 0.001	7	1239 302	2.3 1.0	0.24	0.59	0.42
42-I	21003 9070	0.350 0.404	0.003 0.004	15	9628 4091	0.099 0.117	0.001 0.001	18	541 121	6 0.2	0.22	0.43	0.42
42-II	29182 12401	0.349 0.405	0.002 0.003	14	7886 3136	0.088 0.116	0.001 0.002	32	843 165	0.7 0.6	0.20	0.42	0.40
44-I	19732 7361	0.305 0.357	0.002 0.004	17	9786 2800	0.064 0.085	0.001 0.001	33	1278 309	3.6 0.03	0.24	0.37	0.29
44-II	21367 7548	0.343 0.391	0.002 0.004	14	8617 2296	0.064 0.090	0.001 0.002	41	1816 378	5.0 0.8	0.21	0.35	0.27

Table 8.: Results of two-exponential analyses of the first group of experiments
(first 70-seconds of the clearance curves ignored).

Compared to the mean blood flow found in other animals, which are all about $50 \text{ cm}^3/\text{min}/100 \text{ g.}$, the value found in this study is very small.

If we assume a specific gravity of cerebral tissue equal to 1 we need to assume $\bar{\lambda} = 2.5$ to obtain $\bar{f} = 50 \text{ cm}^3/\text{min}/100\text{g}$, if $\bar{\tau}_{81} = 5 \text{ min.}$ This value of the mean partition coefficient, however, is even larger than that published for white brain tissue.

The results of these experiments were discussed at the sixth international C.B.F. symposium at Philadelphia, (Van Duyl et al, 1975). The criticisms concentrated on the low c.b.f. values found in these experiments.

IV-3 Second group of experiments:

($\text{N}_2\text{O}-\text{O}_2$; skull intact; external carotid artery tied off.)

Because anaesthetics affect cerebral blood flow, it was decided to perform a series of experiments with the better known agent nitrous oxide, which had already been used in c.b.f. studies (Sokoloff, 1959), section III-1-2. This series of experiments was performed on mini pigs of about 28 weeks old, weighing 28 to 36 kg. Details of the applied anaesthesia are given in section III-1-2.

Table 9 shows the physiological parameters observed. The values of P_aCO_2 were varied over a larger range than in the first series of experiments. In this series we avoided the trauma of opening the skull. Head skin alone was removed from where the detector was to be placed. Table 10 shows the results of fitting a two-exponential model. The values of ξ_{81} and ξ_{31} indicate that a good fit is not obtained. If we compare the decay constants in this table with those given in Table 5, we note that, except in exp. nrs. 62-I, II and 64-II, they are in the same range. There were no special reasons to expect the higher values in the other three experiments.

exp.nr.	sex (m/f) age (w) weight (kg)	bloodpress. S/D (mm Hg)	heart freq. (min ⁻¹)	temp. (°C)	P _{co2} (%)	P _a CO ₂ (mm Hg)	pH
62-I	m/27/35	65/40	200	37.5	4.4	31.3	7.44
II	-	75/50	190	37.6	4.8	-	7.41
63-I	m/28/35	85/30	210	37.3	6.0	48.0	7.28
64-I	m/28/35	135/70	205	37.8	3.9	26.7	7.45
II	-	125/70	215	37.7	5.2	33.7	7.38
65-I	m/28/28	90/60	95	35.6	4.6	39.0	7.42
II	-	85/60	140	35.8	4.0	35.0	7.42
III	-	85/60	140	36.2	5.6	43.0	7.33
66-I	m/29/28	110/90	110	36.5	4.5	48.0	7.38
II	-	115/95	110	35.8	6.8	52.0	-

Table 9.: Second group of experiments.

Again we find considerable differences between the decay constants of the '81-keV' and '31-keV' clearance curves. The ratios A_{31}/A_{81} and B_{31}/B_{81} are much smaller than those given in Table 5. This is a consequence of the absorption of the radiation by the skull. It appears, however, that the ratio K_{31}/K_{81} is not smaller than those in Table 5. This indicates that the skull contains Xe-133 that contributes to the constants.

Analyses with a three-exponential model, and analyses of the clearance curves where the first 70 seconds are

exp.nr.	A	a	$\sigma(a)$	%	B	β	$\sigma(\beta)$	%	K	ξ	K_{31}/K_{81}	A_{31}/A_{81}	B_{31}/B_{81}
62-I	9327	0.492	0.006	19	3544	0.101	0.002	16	530	18	0.21	0.20	0.21
	1907	0.589	0.001		748	0.117	0.003		110	3			
62-II	11279	0.523	0.005	17	2845	0.086	0.001	19	695	10	0.24	0.22	0.21
	2516	0.613	0.010		599	0.102	0.003		170	4			
63-I	17769	0.345	0.002	10	3762	0.045	0.001	36	404	12	0.38	0.20	0.15
	3468	0.379	0.005		571	0.061	0.003		153	7			
64-I	2803	0.372	0.009	63	2274	0.063	0.002	22	440	5	0.24	0.16	0.17
	441	0.608	0.033		396	0.077	0.003		105	0.4			
64-II	17318	0.592	0.004	13	2363	0.071	0.001	25	723	18	0.20	0.24	0.19
	4150	0.667	0.007		440	0.089	0.003		144	7			
65-I	8604	0.293	0.006	50	8870	0.087	0.001	20	679	11	0.32	0.28	0.34
	2431	0.441	0.016		3023	0.104	0.001		217	14			
65-II	5733	0.363	0.017	144	9435	0.105	0.003	31	1260	14	0.32	0.28	0.36
	1618	0.885	0.051		3359	0.137	0.002		408	10			
65-III	10599	0.349	0.006	19	6656	0.091	0.002	29	1192	5	0.31	0.25	0.30
	2605	0.415	0.015		1989	0.117	0.004		369	3			
66-I	18048	0.269	0.005	37	10621	0.081	0.002	35	1014	29	0.26	0.18	0.30
	3250	0.369	0.012		3184	0.109	0.002		259	7			
66-II	40625	0.408	0.002	8	9820	0.075	0.001	29	1062	19	0.25	0.22	0.23
	9046	0.442	0.004		2220	0.097	0.002		270	9			

Table 10.: Results of two-exponential analyses of the second group of experiments.

ignored, as were applied to the first group of experiments, have been performed in this series also. The conclusions from these modified analyses are similar to those drawn from the first series. Therefore the conclusions drawn from the results of the first group of experiments are not peculiar to anaesthesia with azaperone and metomidate. Further, the trauma of the removal of the skull is not the cause of the low c.b.f. values, which we obtain.

IV-4 Third group of experiments.

(N₂O-O₂-azaperone-metomidate; open or closed skull; external carotid artery open or tied off; effect of the length of the clearance curves).

In this group of experiments the pigs were anaesthetized following a schedule in which a mixture of N₂O and O₂ was inhaled, and a mixture of azaperone and metomidate infused (section III-1-2). Table 11 shows the physiological parameters in a selection of experiments performed under various conditions. Reported results of c.b.f. measurements according to the injection technique, are based on clearance curves of 20 minutes or shorter. In order to compare our results to those reported, we also fitted the two-exponential model to 20-minute clearance curves of the pig. Clearance curves observed for 20 minutes will be referred to as short (s) clearance curves. Clearance curves observed for 45 minutes will be referred to as long (l) clearance curves.

In exp. nrs. 67-I, II, III and 82-I, the skull was opened and the external carotid artery was tied off. Results of the fit of a two-exponential model to the short clearance curves are given in Table 12. There is a lack of fit, however smaller than found with the long clearance curves (Tables 5 and 8).

exp.nr.	sex (m/f) age (w) weight (kg)	bloodpress. S/D (mm Hg)	heart freq. (min ⁻¹)	temp. (°C)	P _{co2} (%)	skull	a.car.ext.
67-I	f/-/27	100/60	125	36.8	4.5	c	c
II	-	80/55	130	37.0	5.6	c	c
III	-	85/50	145	36.9	7.3	c	c
72-I	m/35/49	90/75	80	33.6	4.4	c	o
73-I	f/51/31	105/75	90	35.6	5.0	o	o
II	-	100/70	80	36.0	6.8	o	o
III	-	140/95	135	36.3	6.0	o	o
IV	-	110/75	125	36.5	5.8	o	c
74-I	m/37/51	-	140	36.2	4.4	o	c/o
II	-	-	150	36.5	4.4	o	o
82-I	m/26/30	90/65	95	35.9	4.3	o	c

Table 11.: Third group of experiments:

o - open c - closed

If we compare the decay constants found in these four experiments with those given in Table 5, we note that they are larger. The differences between the decay constants of the '81-keV' and '31-keV' clearance curves are larger too. Hence, higher c.b.f. values are obtained from the short clearance curves. The fitted parameters, however, do not identify parameters of a two-compartmental model. In order to study the effect of the length of the clearance curves on the parameters, we fitted a two-exponential model to the '81-keV' and '31-keV' clearance data of exp. nr. 82-I over different periods of observation. We calculated from the fitted parameter values, for both the '81-keV'

s - short, l - long

exp.nr.	A	a	$\sigma(a)$	%	B	β	$\sigma(\beta)$	%	K	ξ	clearance (min)	$\bar{\tau}$ (min)	$\frac{K_{31}}{K_{81}}$	$\frac{A_{31}}{A_{81}}$	$\frac{B_{31}}{B_{81}}$
67-I	1487	0.680	0.074	23	5934	0.145	0.004	33.1	1188	2.8	s	5.8	0.24	0.52	0.25
	777	2.247	0.203		1477	0.193	0.003		286	3.9		3.5			
67-II	7505	0.381	0.009	60	3658	0.076	0.006	114.4	1296	1.3	s	6.1	0.28	0.19	0.34
	1447	0.611	0.034		1235	0.163	0.007		358	0.9		3.7			
67-III	10171	0.587	0.008	12.9	3140	0.105	0.004	44.7	1608	3.1	s	3.5	0.23	0.24	0.25
	2476	0.663	0.018		778	0.152	0.009		366	0.8		2.7			
72-I	2603	0.355	0.015	91.5	3666	0.080	0.002	21.2	811	11.2	l	8.5	0.25	0.24	0.21
	628	0.680	0.043		753	0.097	0.002		203	6.9		6.3			
73-I	4202	0.288	0.006	98.9	1733	0.075	0.003	108.0	451	4.3	l	6.4	0.44	0.27	0.95
	1134	0.573	0.034		1644	0.156	0.003		197	2.7		4.5			
73-II	13188	0.408	0.002	-3.2	1177	0.045	0.002	-48.8	561	-0.2	l	4.1	0.35	0.48	0.17
	6295	0.395	0.002		204	0.023	0.008		194	0.9		3.8			
73-III	5473	0.369	0.005	14.4	2278	0.064	0.002	53.1	632	3.1	l	6.5	0.47	0.46	0.40
	2492	0.422	0.009		904	0.098	0.003		300	2.4		4.4			
73-IV	1016	1.255	0.090	21.8	1198	0.137	0.005	51.1	817	4.3	s	4.3	0.42	0.45	0.46
	459	1.528	0.162		555	0.207	0.008		347	1.2		2.9			
74-I	3117	0.454	0.023	134.8	6858	0.089	0.002	25.8	1251	6.8	s	8.4	0.25	0.36	0.34
	1132	1.066	0.065		2339	0.112	0.002		314	5.4		6.3			
74-II	5743	0.415	0.012	45.3	7802	0.071	0.001	29.6	2700	21.3	l	9.1	0.23	0.27	0.32
	1542	0.603	0.027		2513	0.092	0.001		616	6.5		7.4			
82-I	1599	1.427	0.090	5	3380	0.142	0.003	13	1002	3.2	s	5.0	0.22	0.30	0.39
	486	1.355	0.152		1317	0.161	0.004		224	0.3		4.7			

Table 12.: Results of two-exponential analyses of the third group of experiments.

and the '31-keV' clearance data, the blood flow values f_g and f_w and the value of the relative weight of the grey tissue compartment W_g . These values are plotted in Fig. 31. We also plotted the reciprocal values of the mean time constants, $1/\bar{\tau}_{81}$ and $1/\bar{\tau}_{31}$, the values of the constants K_{31} and K_{81} , and the eccentricities of the residual weighted sum of squares ξ_{81} and ξ_{31} .

The graphs show that the longer the clearance curves, the lower are the calculated values of blood flow in grey and white tissue, and the lower are the values of $1/\bar{\tau}_{81}$ and $1/\bar{\tau}_{31}$ which are measures of mean c.b.f., section II-6. The relative weight W_g , however, increases with the length of the clearance curves.

Further the graphs reveal that the fitted values of K_{81} and K_{31} do not correspond to a constant radioactive source, but to a very slowly decreasing component in the clearance process. For the short clearance curves the values of the constants K_{81} and K_{31} are about twice the values found for the long clearance curves.

Also the values of ξ_{81} and ξ_{31} increase with increasing length of the clearance curves. This indicates that the fit of the two-exponential model becomes worse if fitted to longer clearance curves.

We conclude that the parameters derived are seriously affected by the length of the observed clearance curves. Therefore, if we wish to make comparisons between the values of the parameters obtained by fitting clearance curves measured under different physiological conditions, it is necessary to use clearance curves of a standard length.

In other experiments of this series (Table 11) the external carotid artery was not occluded. The analyses, given in Table 12, are based on long clearance curves. If we compare the decay constants found in exp. nrs. 72-I, 73-I, II, III and 74-II with those given in Table 5, we

note that the values of α_{81} are in the same range. The mean time constants found in these experiments are no smaller than in the experiments with closed external carotid artery.

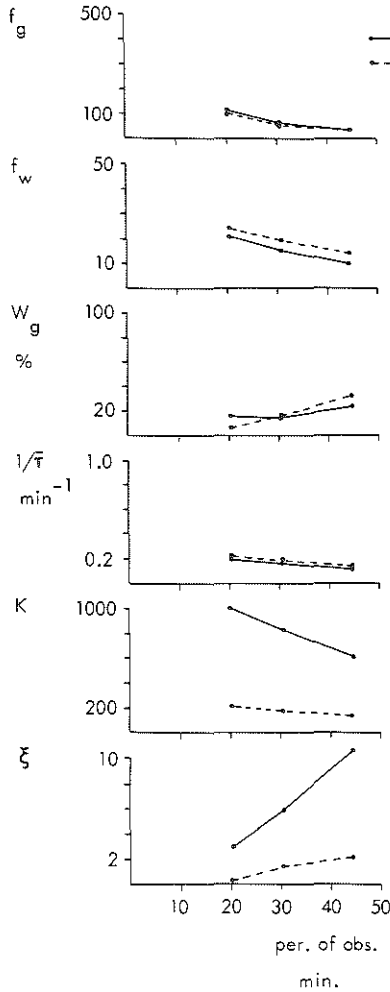


Fig. 31.: Effect of the length of the clearance curves in exp. nr. 82-I on the fitted parameters of a two-compartmental model.

The results of exp. nr. 73-IV are based on the analysis of short clearance curves. Here large decay constants are found like we found for the other short clearance curves.

In exp. nr. 74-I, Xe-133 was injected while the external carotid artery was occluded, but that artery was opened again immediately after the injection.

The c.b.f. is not significantly altered, whether the external carotid artery is tied off or not. However, because of the wide range of the values of the fitted parameters, we cannot conclude that the occlusion of the external carotid has no effect at all on the cerebral clearance curves. The fact, however, that no significant larger c.b.f. values are found is in accordance with the finding that no larger c.b.f. values are measured in the right hemisphere (section IV-2), where the external carotid artery was not tied off either.

IV-5 Fourth group of experiments.

(N₂O-O₂-azaperone-metomidate; open skull; external carotid artery tied off; effect of P_{CO₂}; 20-minute clearance curves).

We investigated the relation between P_{CO₂} and the values of the parameters in a two-compartmental cerebral clearance model. We shall report the results of Xe-clearance measurements performed on two pigs. The analyses are based on short clearance curves. The Xe-injection was carried out when a stable P_{CO₂} level was obtained. The physiological parameters of the experiments are given in Table 13.

Both the '81-keV' and '31-keV' clearance curves are analysed according to a two-exponential model. Except in exp. nrs. 94-VIII and 94-IX, the eccentricities ξ_{81} and

exp.nr.	sex (m/f) age (w) weight (kg)	bloodpress. S/D (mm Hg)	heart freq. (min ⁻¹)	temp. (°C)	P _{co2} (%)	P _a CO ₂ (mm Hg)
87-I	m/-/30	110/80	75	34.0	3.6	-
II	-	100/70	65	33.7	5.5	-
III	-	100/60	65	33.7	7.2	-
IV	-	90/50	110	34.5	9.0	-
V	-	80/50	120	34.6	4.4	-
94-I	m/-/20	100/75	65	37.0	3.7	26.2
II	-	95/70	60	37.0	5.4	41.0
III	-	95/70	70	37.0	7.0	45.1
IV	-	105/80	90	37.2	8.4	48.0
V	-	100/80	80	37.2	3.0	24.9
VI	-	100/80	80	37.8	6.8	52.0
VII	-	100/80	80	37.9	5.8	44.5
VIII	-	95/70	90	38.0	7.1	49.0
IX	-	95/65	90	37.8	5.9	47.2
X	-	90/60	80	37.6	4.5	37.2
XI	-	80/55	80	37.2	2.5	22.7

Table 13.: Fourth group of experiments.

ξ_{31} were less than 6 and 3, respectively.

We used (14) and (20) to express the fitted parameters in terms of the two-compartmental model, taking $\lambda_g = 0.85$ and $\lambda_w = 1.6$. The results of exp. nrs. 87-I to V, are shown in Fig. 32. This figure shows that the parameter values obtained from the '81-keV' and '31-keV' clearance curves are different. Their dependence on P_{CO_2} , however, is roughly similar in both cases.

Remarkable is that at low P_{CO_2} levels, relative high values of f_g are obtained, and that, with increasing P_{CO_2} , f_g first decreases, but then increases for P_{CO_2} higher than 7%. The observation of a decrease in c.b.f. in grey tissue when P_{CO_2} increases, is not in agreement with the physiology of cerebral circulation described in section I-2.

The value of the relative weight W_g is smaller than 5% for $P_{CO_2} < 5\%$. Such small values of W_g are not in agreement with the interpretation of W_g as the relative weight of grey tissue under the radiation detector.

Furthermore, a condition for the validity of this interpretation is, that W_g is a constant if the place of the detector is not changed.

The values of W_g found in section IV-2, which are based on the analyses of long clearance curves, are in the range 0.44 - 0.64, and are closer to the actual relative weight of grey tissue. Hence, although larger values of f_g are obtained with the analyses of short clearance curves than with the long clearance curves, this is accompanied with smaller values of W_g .

In section II-6 it has been pointed out that the reciprocal value of the mean transit time of the Xe is proportional to the mean c.b.f.; $1/\bar{t} = \bar{f}/\bar{\lambda}$. If we assume that the two-exponential model fits the clearance data, then $1/\bar{t} = 1/\bar{\tau}$, where $\bar{\tau}$ is the mean time constant of the fitted model.

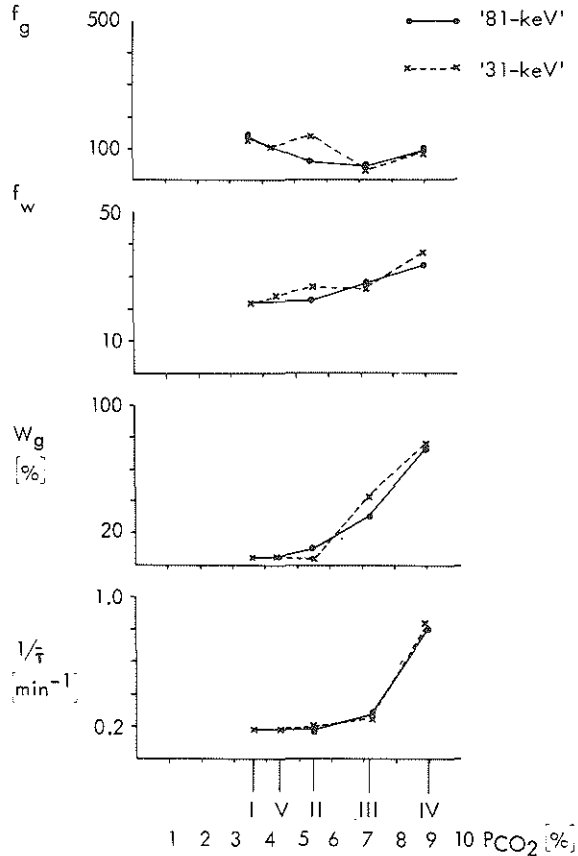


Fig. 32.: Cerebral blood flow values obtained at different P_{CO_2} levels in one pig, analysed according to the two-compartmental model. (exp. nrs. 87-I to V).

The dependence of $1/\bar{\tau}$ on P_{CO_2} is also shown in Fig. 32. It appears that $1/\bar{\tau}$ increases slowly with increasing P_{CO_2} up to 7%, and more steeply for $P_{CO_2} > 7\%$. In other

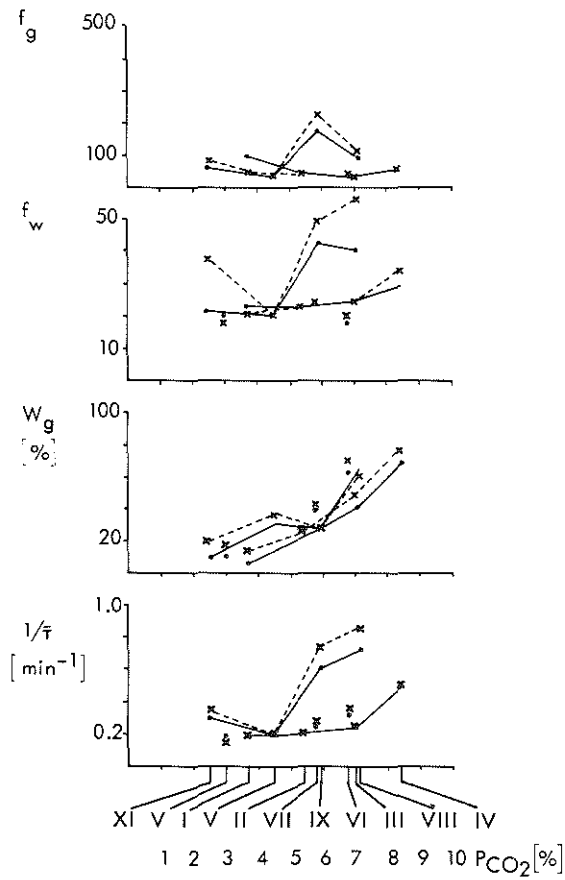
animals a more gradual increase of \bar{f} is found, section I-2.

For $P_{\text{CO}_2} < 7\%$, $1/\bar{\tau}$ is about 0.2 min.^{-1} . If we take $\bar{\lambda} = 1$, we thus find that \bar{f} is about $20 \text{ cm}^3/\text{min}/100 \text{ cm}^3$. A value of about $40 \text{ cm}^3/\text{min}/100 \text{ cm}^3$ is obtained when $P_{\text{CO}_2} > 8\%$. In man too the inhalation of 8% carbon dioxide causes the value of \bar{f} to double, in this case, however, \bar{f} is about $100 \text{ cm}^3/\text{min}/100 \text{ g}$, section I-2.

In Fig. 33 the results of a second series of similar experiments are shown. Exp. nrs. 94-I, II, III and IV concern measurements at successively higher P_{CO_2} levels. These graphs are very similar to those in Fig. 32. The exp. nrs. 94-V, VI and VII were performed at alternating P_{CO_2} levels. The points of these results are not connected in the graphs. The exp. nrs. 94-VIII-IX-X and XI concern measurements at successively lower P_{CO_2} levels. The results with the alternating and decreasing P_{CO_2} levels show the same tendency in relation P_{CO_2} as those with increasing P_{CO_2} levels, though the behaviour is more complicated. Also the differences between the results with the '81-keV' and '31-keV' clearance curves are larger. It is remarkable that, after P_{CO_2} has been reduced to a certain level, higher values of $1/\bar{\tau}$ are obtained than, if it is increased to the same level. This indicates that a hysteresis effect is involved in this physiological control mechanism.

During the measurements of the clearance curves at different values of P_{CO_2} , the position of the detector was not changed. Therefore, no change is to be expected in so far as the values of the ratios K_{31}/K_{81} , A_{31}/A_{81} and B_{31}/B_{81} are determined by the geometry of brain tissue. The mean values and spread of the found ratios are:

	A_{31}/A_{81}	B_{31}/B_{81}	K_{31}/K_{81}
exp. nrs. 87-I to V	0.42 ± 0.09	0.47 ± 0.07	0.35 ± 0.03
exp. nrs. 94-I to XI	0.57 ± 0.04	0.49 ± 0.09	0.28 ± 0.02



I-II-III-IV : increasing P_{CO}₂
V-VI-VII : alternating P_{CO}₂
VIII-IX-X-XI : decreasing P_{CO}₂

Fig. 33.: Cerebral blood flow values obtained at different P_{co}₂ levels in one pig. (exp. nrs. 94-I to XI).

The ranges of A_{31}/A_{81} and B_{31}/B_{81} appear to overlap each other. In exp. nrs. 87-I to V we even find that the mean value of A_{31}/A_{81} is smaller than that of B_{31}/B_{81} . Because the standard deviation in the coefficients obtained by fitting the short clearance curves are up to about 10%, the wide range of the ratios can be ascribed to the inaccuracy of the coefficients. In section III-4 it has been shown that 1% uncertainty in the value of the ratio corresponds to an uncertainty in the thickness of a water compartment of 0.18 cm. Therefore, considering the ranges over which the ratios vary, we cannot derive from it reliable values for the thicknesses of compartments. In our opinion the graphs of Figs 32 and 33 do not refer to independent variables of the two-compartmental model because of the non-validity of that model, (chapter V). Consequently the physiological interpretation of our observations, which are based on the two-compartmental clearance model, may be incorrect.

In one experiment we measured the relation between c.b.f. and P_{CO_2} by means of an electromagnetic flow probe system (Transflow 600). A perivascular probe (P4-571), with an inner diameter of 4.0 mm was placed around the common carotid artery. The zero-flow reference was checked repeatedly by occluding the carotid artery for a short time.

The flow probe was calibrated at the end of the experiment as follows. A small cannula was inserted into the carotid artery. Via this cannula blood could stream freely into a measuring-glass. The flow was calculated from the amount of blood in the glass after 15 seconds. The value was related to the flow probe signal, and thus the calibration factor was obtained. This calibration factor was used to calculate the blood flow from the flow probe recordings during the experiment.

With the external carotid artery open we measured at

$P_{\text{CO}_2} = 5.4\%$, $F = 140 - 150 \text{ cm}^3/\text{min}$. When the external carotid artery was then tied off, the flow was reduced to $48 \text{ cm}^3/\text{min}$.

In Fig. 34 the flow measured with occluded external carotid artery, is plotted against P_{CO_2} . The different P_{CO_2} values are obtained in the same way as in the Xe-clearance experiments. The graph is constructed by means of sample values taken from the F and P_{CO_2} recordings, at intervals of 1 minute. Thus the time variable has been eliminated. The original recordings of F and P_{CO_2} lasted about two hours. The arrows in the graph indicate the direction of the path followed in the phase plane. The beginning and the end of the graph are connected by a broken line.

The graph shows hysteresis; in the descending limb, $P_{\text{CO}_2} = 3 - 7\%$, the blood flow is roughly twice the value in the rising limb. For P_{CO_2} lower than 3% both limbs show a remarkable peak in the flow. This dependence of blood flow on P_{CO_2} in the low P_{CO_2} range corresponds with the observation, made by the ^{13}Xe -clearance technique, that in the low P_{CO_2} range f_g decreases when P_{CO_2} increases. The hysteresis phenomenon also is observed in the clearance measurements.

Hence there is a similarity between the relation of P_{CO_2} and F , measured with electromagnetic flow probe, on the one hand and the relation between P_{CO_2} and \bar{f} , measured with the Xe-clearance technique, on the other. Purves (1972) describes a dependence of cerebral blood flow on $P_a\text{CO}_2$ for $P_a\text{CO}_2 < 20 \text{ mm Hg}$, which is similar to our observations. The behaviour appear to be connected with a protection mechanism which prevents hypoxia.

Concerning the observed hysteresis, no references are found. This phenomenon is an illustration for the fact that c.b.f. measurements do not fully evaluate the physiological adaptation in tissue to assure adequate gas

transport (section I-2).

In order to determine the mean c.b.f. from the measurements with the flow probe, we need to know the weight of the cerebrum. This was 110 g, so that one hemisphere weighed 55 g. Each hemisphere is supplied with blood via the vertebral artery to a minor extent. Hence it follows from the flow measurements on the carotid artery that the mean specific blood flow was more than $F/55 \times 100 \text{ cm}^3/\text{min}/100 \text{ g}$, where F is the measured carotid flow.

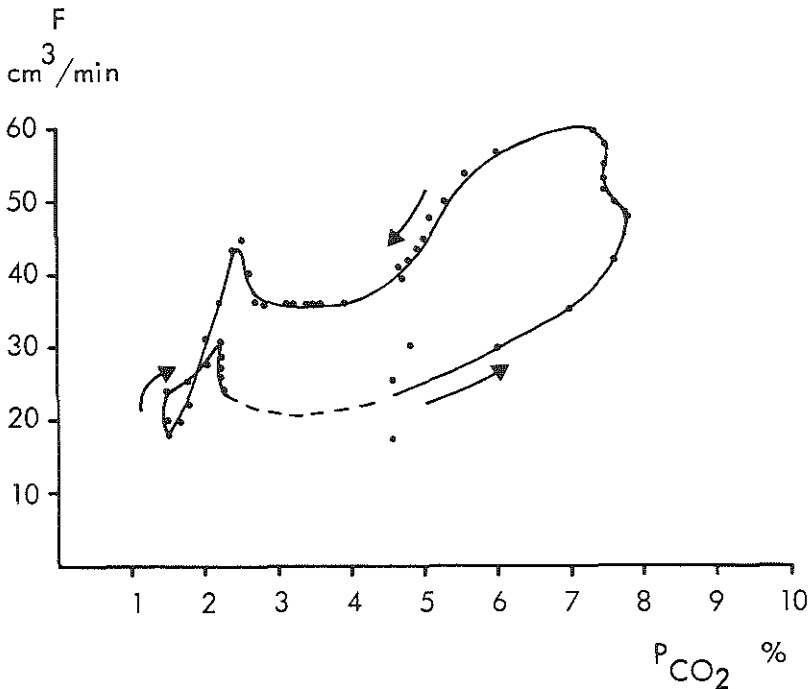


Fig. 34.: Relation between blood flow to the cerebrum, measured by means of an electromagnetic flow probe, and P_{CO_2} .

Left out of regard the contribution of the vertebral artery, we find from the rising limb in Fig. 34 that for P_{CO_2} increasing from 3 to 7%, \bar{f} increases from 36 to 64

$\text{cm}^3/\text{min}/100 \text{ g}$. From the descending limb we find that \bar{f} decreases from 109 to $64 \text{ cm}^3/\text{min}/100 \text{ g}$.

These values are considerably higher than those found with the Xe-clearance technique and in better agreement with the values reported for other animals.

IV-6 Xe-clearance measurements on dogs.

In addition to the experiments on pigs we did two series of Xe-clearance measurements on two mongrel dogs. These experiments were primarily performed to investigate fluctuations in Xe-clearance curves which have been reported by Zwart and Seagrave (1973). For that reason halothane was chosen as the anaesthetic agent. The results of the study of the fluctuations are given in section V-2-1. Here we report the results of the clearance measurements on the dogs, interpreted in terms of the two-compartmental model, to enable a comparison with the results of measurements on the pig.

The dogs, anaesthetized by inhalation of a mixture of halothane and oxygen or carbogene, were mechanically ventilated. No premedication was given. The concentration of halothane in the inspired gas was changed stepwise. The Xe-injection catheter, the same as used for the pig, was advanced through the femoral artery, the descending aorta and the subclavian artery into the left vertebral artery.

The regions supplied with blood by the vertebral artery in the dog has been studied by Reneman et al (1974). The radiation detector was placed on the posterior part of the skull after removal of the skin.

Blood pressure in the aorta was monitored.

Cerebral clearance curves, for both '81-keV' and '31-keV' radiation, were measured for about 20 minutes (short clearance curves), at different levels of halothane and

of carbon dioxide.

After the concentration of halothane had been changed, about 20 minutes was allowed for equilibrium to be reached before the Xe-133 was injected. Because of the study of the fluctuations in the clearance curves, the measurements of the pulse rate were based on a preset time of 2 seconds instead of 4 seconds. The clearance curves were fitted with a sum of two exponentials and a constant. The values of the eccentricities ξ_{81} and ξ_{31} indicate that the quality of fit with this model was no better than in the short clearance curves in the pigs.

Fig. 35 shows the results obtained with one dog. The calculated blood flow values are based on the partition coefficients $\lambda_g = 0.8$ and $\lambda_w = 1.5$. The blood pressure varied during this experiment between 80/55 and 115/85 mm Hg.

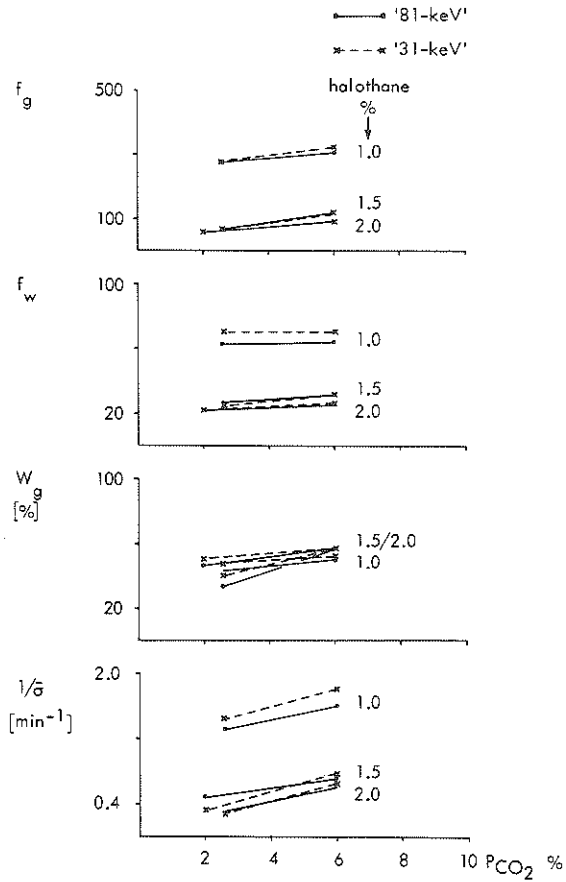
We find that f_g and $1/\bar{t}$ increase with increasing P_{CO_2} . The graphs show also a marked increase in blood flow when the concentration of halothane decreases.

Using the Kr-85 clearance technique, Harper et al (1961) found in dogs, anaesthetized with nembutal, a mean cortical blood flow of $99 \text{ cm}^3/\text{min}/100 \text{ g}$, and a flow in the occipital cortex of $123 \text{ cm}^3/\text{min}/100 \text{ g}$. These values correspond to those in Fig. 35 at a halothane percentage of 1.5%.

The differences between the values derived from the '81-keV' and '31-keV' clearance curves are smaller than those obtained in the pigs.

According to Roth et al (1970) the ratio of flow in grey and white tissue ranges from 4.8-5.2. This is in agreement with the ratios found here.

Fig. 35 shows that W_g is, compared to the findings in the pig, more independent of blood flow over a wide range. The value of this relative weight, about 50%, is close to the values reported.



Sequence (P_{CO_2} , P_{hal}): (6; 2), (6; 1.5), (6; 1), (2.6; 1), (2.6; 1.5), (2, 2)

Fig. 35.: Cerebral blood flow values, derived from Xe-clearance curves in a dog, at different P_{CO_2} levels and levels of halothane.

The constants K_{81} and K_{31} vary between 5 to 10% of the initial values of the clearance curves. The standard deviations of the fitted constants were about 1%.

The mean values and spread of the ratios A_{31}/A_{81} , B_{31}/B_{81} and K_{31}/K_{81} determined from this series of measurements are:

A_{31}/A_{81}	B_{31}/B_{81}	K_{31}/K_{81}
0.49 ± 0.02	0.44 ± 0.03	0.37 ± 0.01

These values justify the conclusion that, on the average the deeper the brain tissue, the slower the clearance rate.

Of inhalation anaesthetics halothane has the most profound effect upon c.b.f. and metabolism, (Purves, 1972). The increase in the cerebral circulation when the percentage halothane is increased, is in contradiction to reported observations by Mischenfelder et al (1968), Wollman et al (1969) and Zwart and Van Dieren (1974). We have no explanation for this discrepancy. Purves (1972), cite however, investigators who found a dependence similar to ours.

Fig. 36 shows the results from a second dog. Here P_{CO_2} was kept constant ($P_{CO_2} = 2.6\%$), while the percentage halothane was varied. In this experiment an increase in the halothane level causes an increase in the c.b.f.. We conclude that the clearance measurements on dogs are in agreement with those reported. This conclusion emphasizes the discrepancies in the results with the pig compared to other animals.

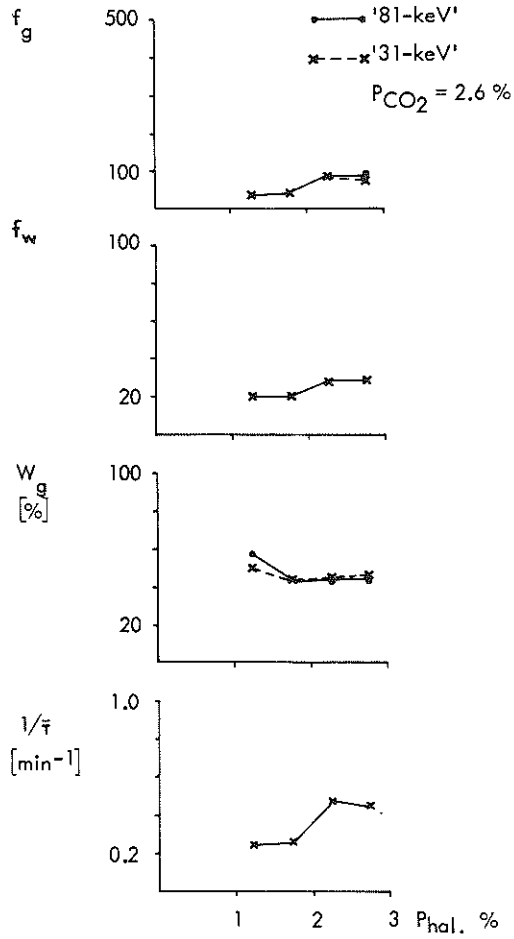


Fig. 36.: Cerebral blood flow values, derived from Xe-clearance curves, measured in a dog, at a certain P_{CO_2} level and different levels of halothane.

IV-7 Summary of conclusions.

From the Xe-clearance experiments on the pig we summarize the following conclusions:

- If '81-keV' and '31-keV' clearance curves are fitted by a sum of two exponentials and a constant, a reasonable quality of fit is obtained judged by eye in most cases. The values of ξ_{81} and ξ_{31} , however, indicate a significant lack of fit.
- Significant differences between the corresponding decay constants of the fitted '81-keV' and '31-keV' clearance curves are obtained, which conflict with the two-compartmental clearance model.
- The values of the constant K_{81} and K_{31} are too large to be ascribed to background radiation.
- The results of analysis depend on the length of the clearance curves, in such a way that the values of the decay constants, the reciprocal value of the mean time constants and the values of the constants K_{31} and K_{81} increase, if the analyses are based on shorter clearance curves. The quality of fit also improves.
- The fact that lower values of the constants K_{81} and K_{31} are obtained if longer clearance curves are analysed, indicates that these constants correspond to a slowly decaying component.
- For long clearance curves (45 minutes), analysed according to a two-compartmental model, and taking $\lambda_g = 0.85$ and $\lambda_w = 1.6$, we find:

$$f_g = 25 - 35 \text{ cm}^3/\text{min}/100 \text{ cm}^3 \text{ grey tissue}$$

$$f_w = 10 - 20 \text{ cm}^3/\text{min}/100 \text{ cm}^3 \text{ white tissue}$$

$$W_g = 0.4 - 0.65$$

$$K_{81} \text{ and } K_{31} \text{ are } 3\% \text{ of initial value of the}$$

clearance curves. No distinct dependence of these values on P_{CO_2} is found.

- For short clearance curves (20 minutes) we find:
 f_g , f_w and $1/\bar{\tau}$ vary in a wide range (Figs 32 and 33) and are related to P_{CO_2} , although not uniquely; a hysteresis phenomenon is observed.
 $W_g = 0.50 - 0.90$, the high values are found with high P_{CO_2} levels.
 K_{81} and K_{31} are about 10% of the initial value of the clearance curves.
- If we take $\bar{\lambda} = 1$ we find, from the values of $1/\bar{\tau}$, for both the short and the long clearance curves, values of mean cerebral blood flow, which are low compared with measurements with the electromagnetic flow probe, compared with clearance measurements on the dogs, and compared with published values.
- We have no indications that the great variability of W_g and the low values of the mean cerebral blood flow result from the type of anaesthesia used or from the preparation of the animals.
- In all cases we find $\bar{\tau}_{81} > \bar{\tau}_{31}$, and for the long clearance curves in the pig and short clearance curves in the dog

$$\frac{K_{31}}{K_{81}} < \frac{B_{31}}{B_{81}} < \frac{A_{31}}{A_{81}}$$

so that, on the average, the deeper the brain tissue, the slower the clearance rate.

V-SUPPLEMENTARY INVESTIGATIONSV-1 Multi-exponential character of the clearance curvesV-1-1 A study of the heterogeneity of cerebral blood flow in the pig

The results of the analyses of Xe-clearance measurements on the pig are not in agreement with the two-compartmental clearance model usually applied. It is known, however, that c.b.f. is more heterogeneous than is suggested by the two-compartmental model, section II-4. Obviously commonly the disagreement between the two-compartmental model and the actual clearance process is supposed not to have consequences which are too serious for the study of c.b.f.

Because the discrepancies which we have found do not justify this assumption, we have studied the heterogeneity of c.b.f. in the pig. This study was carried out by means of radioactive labeled 'carbonized' microspheres (3M-Company), section I-3 and section II-4. We used spheres which had a diameter of $15 \pm 5 \mu\text{m}$, and labeled with Cr-51. The spheres were suspended in a solution of 10% dextran. The density of the microspheres was about 1.4. When shaken in the dextran solution, the spheres remained suspended for about 25 seconds and then slowly settled. To facilitate injection we used a small glass chamber, in which the solution was kept in vibration during the injection.

Because the diameter of the microspheres is larger than the diameters of the capillaries, they will be trapped by the capillaries (nutrient vessels), but will pass through most arterio-venous shunts (non-nutrient vessels), so that they are eventually trapped in the lungs. The

validity of the measurement of total and regional blood flow by the radioactive microsphere technique has been studied by several investigators (Rudolph and Heymann, 1967; Hoffbrand and Forsyth, 1969). Buckberg et al (1971) showed that the reliability of the determination of regional blood flow was improved if each tissue sample contained more than 400 microspheres.

We injected approximately 10^5 microspheres, suspended in 0.1 cm^3 solution, into the common carotid artery, while the external carotid artery was tied off. The fact that the arterial blood pressure did not change significantly after the injection of this large number of microspheres is taken as an indication that these amounts are well tolerated (compare Reneman et al, 1974).

Post mortem the cerebral vascular system was filled with a solution of formalin. Then the skull was removed with the aid of a Stryker saw. The brain was fixed for about 24 hours in a formalin solution. Then it was sectioned along parallel planes. Thus about 100 tissue samples of weight 0.5 to 1.5 g, were obtained. This implies that the mean number of microspheres per tissue sample was about 1000, neglecting microspheres that passed through the arterio-venous shunts.

The Cr-^{51} radioactivity of the tissue samples was measured by means of an automatic sample changer (Nuclear Chicago). About 70% of the microspheres was found in the hemisphere on the injection side. The number of counts per 100 seconds per tissue sample from that hemisphere was 10^3 to 4×10^3 . If the number of counts per tissue sample is divided by the sum of the number of counts from all these samples then, according to the Sapirstein principle, section I-3, this fraction represents the blood flow of that sample divided by the blood flow to all these samples. This fraction divided

by the weight of the tissue sample yields the relative specific blood flow of that sample.

By means of a classification, with a class interval of 0.001 g^{-1} , histograms have been constructed which represent the distribution of the relative specific blood flow in the hemisphere.

Figures 37 and 38 show such histograms, obtained in exp.nr. 83-I and 84-I respectively.

In contrast to the flow distributions found with C-14-antipyrine, which are shown in Fig. 11, these distributions are not bi-modal. The histograms of Fig. 37 and 38, however, are based on samples of mixed grey and white tissue. Because the c.b.f. in white tissue

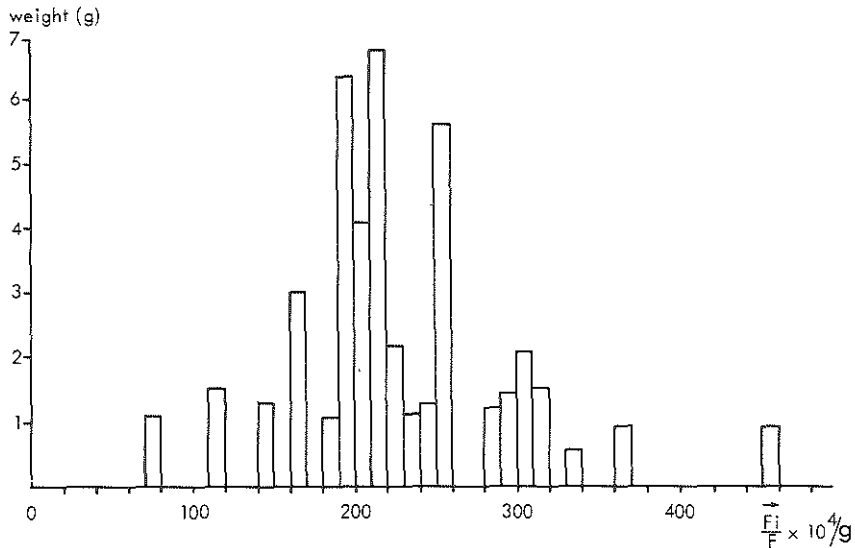


Fig. 37.: Distribution of relative specific blood flow in the brain of a pig (exp. nr. 83-I) as determined with Cr-51-microspheres.

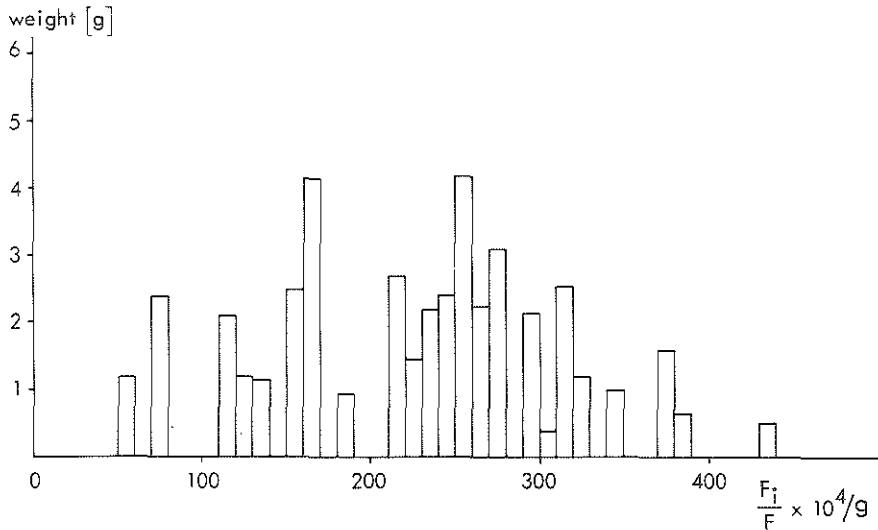


Fig. 38.: Distribution of relative specific blood flow in the brain of a pig (exp. nr. 84-I), as determined with Cr-51 microspheres.

is expected to be smaller than that in grey tissue, the histograms might become bi-modal if they were based on samples of grey and white tissue. However, we did not succeed in making a good separation of grey and white brain tissue.

The mean values and standard deviations of the distributions in Fig. 37 and 38 are given in Table 14.

	mean	st. dev.	% st. dev.
exp.nr. 83-I (Fig. 37)	0.0227	0.0065	28
exp.nr. 84-I (Fig. 38)	0.0225	0.0085	37

Table 14.: Mean and standard deviations of the histograms shown in the Figs 37 and 38.

The injections of the microspheres were preceded by measurements of Xe clearance curves. Between the injection of Xe-133 and the administration of microspheres about 60 minutes elapsed. The physiological parameters in these experiments are given in Table 15.

exp.nr.	sex (m/f) age (w) weight (kg)	bloodpress. S/D (mm Hg)	heart freq. (min ⁻¹)	temp. (°C)	P _{co2} (%)
83-I	f/28/35	135/65	175	36.9	4.4
84-I	m/28/30	125/100	120	37.2	4.4

Table 15.: Physiological parameters of exp. nrs 83-I and 84-I.

The clearance curves of 45 minutes were fitted by a two-exponential model. The results are given in Table 16.

exp.nr.	A	a	$\sigma(a)$	%	B	β	$\sigma(\beta)$	%	K	ξ	$\bar{\tau}$
83-I	1750	0.282	0.014	13	2086	0.052	0.003	15	590	10	12.1
	358	0.320	0.026		392	0.060	0.063		111	0.3	10.2
84-I	8373	0.407	0.010	-9	6688	0.113	0.002	13	474	4	5.3
	5486	0.369	0.009		4770	0.128	0.002		157	13	5.1

Table 16.: Results of a two-exponential analysis.

If we take $\bar{\lambda} = 1$, then it follows from the mean time constants that $\bar{F} = 8 \text{ cm}^3/\text{min}/100 \text{ cm}^3 \text{ tissue}$ in exp. nr. 83-I and in exp.nr. 84-I, $\bar{F} = 19 \text{ cm}^3/\text{min}/100 \text{ cm}^3$.

Both values are extremely low.

After we had performed these measurements, Foreman et al (1976) published their study on the c.b.f. in unanaesthetized pigs, by means of carbonized microspheres

of the same diameter as those that we used. Their microspheres were labeled with Sr-85, Ce-141 or Cr-51. They injected 1.5 to 2.5×10^6 microspheres into the left atrium. Because this is the only reference that we have found concerning the measurement of c.b.f. in the pig, it is useful to summarize some of their conclusions. They found that c.b.f. was about 2% of cardiac output at rest. The mean specific blood flow was $45 \pm 5 \text{ cm}^3/\text{min}/100 \text{ g}$. Although they measured consistently greater flows in grey tissue, the maximum value of the ratio of the flows in grey and in white tissue was 1.7 only (middle brain region), compared with ratios of 4.8 - 5.2 reported in dogs (Roth et al, 1970). The flow in grey tissue ranged from 40 to $65 \text{ cm}^3/\text{min}/100 \text{ g}$, and the flow in white tissue ranged from 32 to $54 \text{ cm}^3/\text{min}/100 \text{ g}$.

Since the grey tissue had much higher metabolic activity, Foreman et al argued, it was not clear why white tissue in the pig received such a relatively large proportion of the c.b.f. Furthermore they found no significant decrease in c.b.f. at exercise, although a sharp decrease in the arterial pressure of carbon dioxide was elicited by such exercise. No significant change in the pattern of the distribution of c.b.f. was found, regardless of the intensity of the exercise, section I-2. The mean c.b.f. measured by Foreman et al (1976) corresponds to values reported for other animals, but not to the considerably lower values we found in the pig using the Xe-clearance technique. We shall discuss this discrepancy later.

Because Forman et al found a range of blood flow in grey and white tissue which overlapped to a considerable extent, we do not expect that the distributions in Fig. 37 and 38 would become distinctly bi-modal, if they were based on grey and white tissue samples separately.

The bi-modal character of the distributions may be less distinct than that found with the antipyrine studies on the cat, shown in Fig. 11.

Because of the large effect of anaesthesia on the c.b.f., as appear e.g. from Fig. 11, it must be noted that Foreman et al performed their measurements on unanaesthetized pigs, while our measurements are performed on anaesthetized pigs.

Let us assume that in the Xe-clearance studies, the ranges of specific blood flow values correspond to ranges of exponential decay constants of exponentials, section V-2-1. Then, if we take for the partition coefficients of grey and white tissue $\lambda_g = 0.85$ and $\lambda_w = 1.6$ respectively, the flow ranges reported by Forman et al correspond to the following ranges of decay constants: $\alpha = 0.47 - 0.76 \text{ min}^{-1}$ and $\beta = 0.20 - 0.34 \text{ min}^{-1}$. Hence, though the blood flow ranges overlap, the ranges of the decay constants do not. The maximum value of f_g/f_w , which is 1.7, implies that α/β is always less than 2. In contrast to this conclusion we found in our measurements that in all cases $\alpha/\beta > 2$.

In section III-3-1 it was shown that, for a reliable separation into exponentials with decay constants, which do not differ greatly in magnitude, such as are to be expected from the measurements of Foreman et al (1976), the errors in the clearance data must be extremely small. The measurements with the microspheres (Figs. 37 and 38) show that c.b.f. in the pig is heterogeneous.

Consequently it is to be expected that cerebral Xe-clearance curves are composed of many exponential terms, instead of only two assumed in the two-compartmental model. Therefore the uncertainty in the parameters, obtained by fitting a two-exponential model, caused in the first place by the ratio of the decay constants, is

then further enlarged by the inadequacy of the model in describing a multi-exponential clearance process. This is a part at least of the explanation of the discrepancies found between the parameters to the clearance curves and the two-compartmental model. We shall deal with some aspects of this discrepancy between the mathematical model and the actual clearance process in the next sections.

V-1-2 Some features of multi-exponential clearance curves

Van Liew (1962, 1967) studied the graphical fitting of decay curves which were constructed according to a mono-modally distributed multi-exponential process. He reported that the concavity of semi-logarithmic plots of such curves was determined by the magnitudes of the standard deviation relative to the mean of the time constants in the distribution.

The larger the ratio $\sigma(\tau)/\bar{\tau}$, the greater the concavity. The smaller this ratio is, the more the composite curve resembles a single exponential process.

In Fig. 39 standard curves for multi-exponential processes are plotted on a semi-logarithmic scale. These curves, taken from Van Liew (1967), are constructed from 50 exponential terms, which approximate a normal distribution, $A(\tau)$. It appears that a distribution with a standard deviation of 30%, which is approximately equal to the value found in the distribution of the micro-spheres, deviates significantly from a straight line, so that it cannot be fitted well with one exponential term, but a good fit is attained with a sum of two exponentials (Fig. 39).

If A_i and τ_i are the coefficients and time constants of the exponentials that fit the decay curve, then according to Van Liew, the formula:

$$s(\tau) = \sqrt{\sum A_i (\tau_i - \bar{\tau})^2} \quad (82)$$

yields estimations of the standard deviation of the actual multi-exponential process, provided that distribution is symmetric in τ .

If the distribution is skewed with a mean to the right of the mode, the semi-logarithmic plot is more concave,

and has a more pronounced two- or three-exponential character, then in the case that the distribution is symmetric with the same equal $\sigma(\tau)/\bar{\tau}$.

If the analysis is applied to nearly straight semi-logarithmic curves, given by distributions with small ratios, they separate so that the largest derived component has a time constant approximating the mean time constant of the distribution. Curves which are concave tend to result in two or three components of similar magnitude. Such results may thus be misleading since, if the exponential process responsible for the curve is distributed with a large $\sigma(\tau)/\bar{\tau}$ ratio, the derived components suggest two or three separate processes of similar magnitude.

For the 45-minute clearance curves, analysed in section IV-2, we find that $\bar{\tau}$ is about 5.5 minutes. If we assume that the clearance curves are composed of many exponentials, distributed over τ according to a Gaussian distribution with $\bar{\tau} = 5.5$ minutes, then 45 minutes correspond to about 12 half-value times. According to the graphs of Fig. 39, a decay curve with $\sigma(\tau)/\bar{\tau} = 0.30$ has then decayed to about 0.1% of its initial value. The clearance curve, however, is then at a value equal to the fitted constant, which is about 3% of the initial value.

Much larger values of $\sigma(\tau)/\bar{\tau}$, however, imply that the distribution $A(\tau)$ should be truncated at $\tau = 0$, since no increasing exponentials are involved in the clearance process.

We conclude that the clearance curves are not composed of exponentials distributed over τ according to a symmetric, Gaussian distribution function.

The distribution of microspheres corresponds to a distribution of c.b.f. The decay constants of the

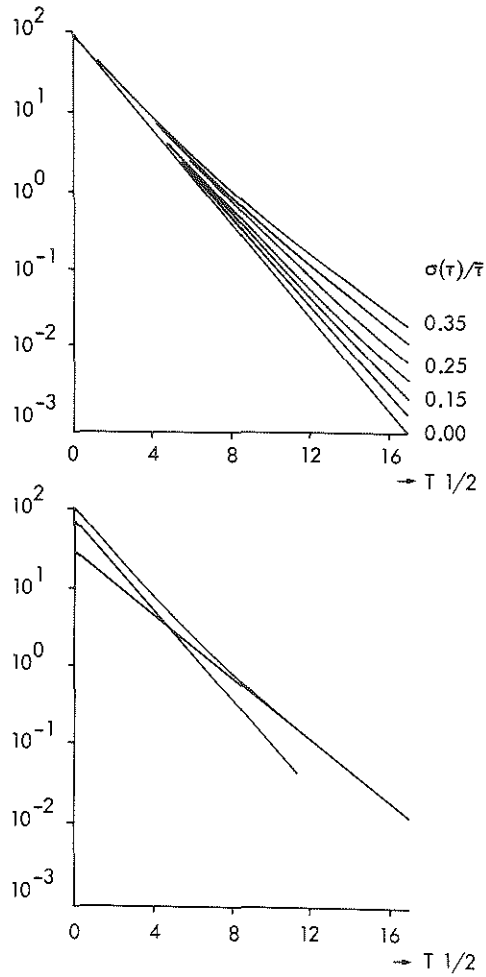
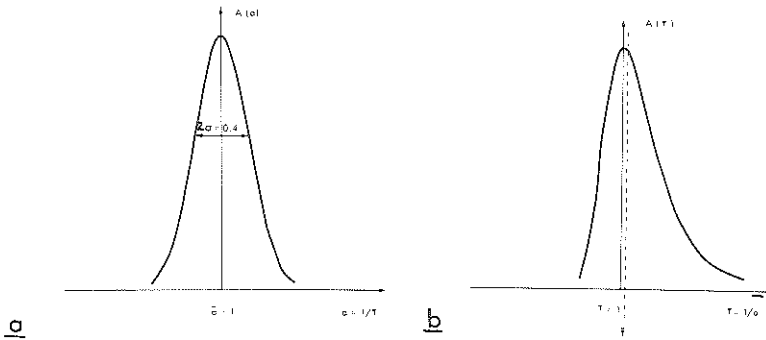


Fig. 39.: Upper: multi-exponential decay curves composed of normally distributed time constants.
 Lower: separation of a decay curve, with $\sigma(\tau)/\bar{\tau} = 0.30$, into two-exponential components.

exponentials constituting the clearance curves are proportional to the specific blood flow values. Therefore the distribution of microspheres corresponds more directly to a distribution of decay constants than to a distribution of time constants. In this connection it is important to note that a distribution expressed in terms of decay constants, $A(\alpha)$, has a shape which differs from that of the same distribution expressed in terms of time constants, $A(\tau)$.

Figure 40a shows a Gaussian distribution of decay constants, with a mean value $\bar{\alpha} = 1$ and a standard deviation $\sigma(\alpha) = 0.2$.



*Fig. 40 a: Gaussian distribution of decay constants, $A(\alpha)$, for a multi-exponential decay process.
b: Distribution of time constants, $A(\tau)$, for the same multi-exponential process.*

Figure 40b shows the corresponding distribution of time constants, where $\alpha = 1/\tau$. It appears that, when $A(\alpha)$ is a symmetrical distribution, $A(\tau)$ is an asymmetrical one, and vice versa. According to Van Liew, referred to above, the skewness of $A(\tau)$ has consequences for the exponential character of the decay curves.

We conclude that a multi-exponential clearance curve can be described by a sum of two or three exponentials, and that the values of the parameters obtained by fitting that model, are determined by the shape of the distribution of the exponentials which generate the clearance curve.

Another important aspect of multi-exponential clearance curves concerns the difference between the mean time constant $\bar{\tau}$ (59) and the mean decay constant $\bar{\alpha}$. We define the mean decay constant as follows:

$$\bar{\alpha} = \frac{\sum A_i \alpha_i}{\sum A_i} = \frac{\sum A_i / \tau_i}{\sum A_i} \quad (83)$$

Because generally:

$$\frac{\sum A_i \tau_i}{\sum A_i / \tau_i} \neq 1$$

this implies that:

$$\bar{\tau} \neq 1/\bar{\alpha} \quad (84)$$

For the distribution in Figs. 40a and 40b, where $\bar{\alpha} = 1$ and thus $1/\bar{\alpha} = 1$, it is shown that $\bar{\tau} > 1$. (83) expresses the fact that exponentials in the distribution with relatively large time constants contribute relatively less to the value of $\bar{\alpha}$. On the other hand, these exponentials contribute relatively more to the value $\bar{\tau}$. In other words the mean time constant of a clearance curve emphasizes the slow clearance components, while the mean decay constant of that curve emphasizes the fast clearance components.

A consequence of this fact is that the mean decay

constants of the clearance curves are less affected by tracer recirculation than the mean time constants, section II-2.

Since the clearance rate of the faster components in the clearance curves are more sensitive to variations in P_{CO_2} (section I-2) the mean decay constants are more sensitive to these variations than the mean time constants. Applying (83) to the fitted parameters of the clearance experiments reported in section V-1, we find:

exp.nr. 83-I	$\bar{\alpha}_{81}=0.16$	$\bar{\alpha}_{31}=0.18$	$\bar{\alpha}_{81} \cdot \bar{\tau}_{81}=1.9$	$\bar{\alpha}_{31} \bar{\tau}_{31}=1.9$
exp.nr. 84-I	$\bar{\alpha}_{81}=0.28$	$\bar{\alpha}_{31}=0.26$	$\bar{\alpha}_{81} \cdot \bar{\tau}_{81}=1.4$	$\bar{\alpha}_{31} \bar{\tau}_{31}=1.3$

The values of $\bar{\alpha}$ are considerable larger than the corresponding values of $1/\bar{\tau}$. This means that the mean blood flow calculated from the mean decay constant yields a considerably larger value than that calculated from the mean time constant.

It was found in section IV-4 that larger values of the constants are obtained with short clearance curves than with long clearance curves, indicating that these constants in fact correspond to a slowly decaying component. In the long clearance curves the fitted exponentials account for more of this slow component than in the short clearance curves. Because the slow component has a smaller contribution relatively to the value of $\bar{\alpha}$ than to the value of $\bar{\tau}$, $\bar{\alpha}\bar{\tau}$ will be smaller if based on a shorter first part of the clearance curves.

Figure 41 shows the values of $\bar{\alpha}$, based on the analyses of the short '81-keV' and '31-keV' clearance curves of exp.nr. 87-I to 5, described in section IV-5. The values of $1/\bar{\tau}$ are taken from Fig. 32. It appears that $\bar{\alpha}$ is systematically larger than $1/\bar{\tau}$. The value of $\bar{\alpha}\bar{\tau}$ decreases

from 2.7 to 1.3 with increasing P_{CO_2} .

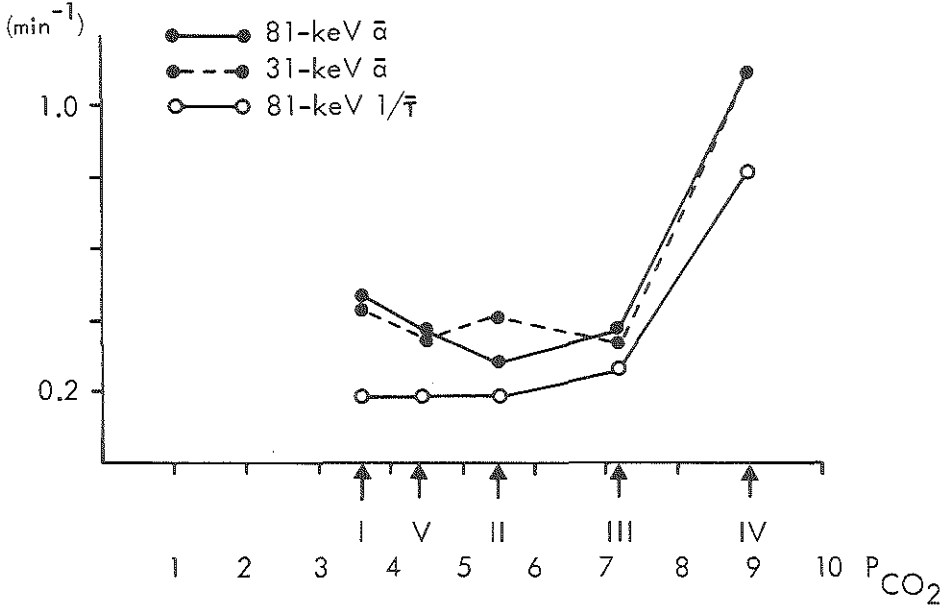


Fig. 41.: Dependence of mean decay constants and mean time constants on P_{CO_2} , derived from exp. nrs 87-I to V.

The dependence of $\bar{\alpha}$ to P_{CO_2} shows a maximum in the low P_{CO_2} range, like f_g in Fig. 32. The dependence of mean c.b.f. calculated from $\bar{\alpha}$, is similar also to the dependence of blood flow measured by means of the electromagnetic flow probe (Fig. 34).

Because of the great difference between $\bar{\alpha}$ and $1/\bar{\tau}$ it is important to specify on which parameter the mean blood flow is based.

In section II-6 it is shown that the mean time constant corresponds to the mean transit time $\bar{\tau}$ of the tracer gas,

which can be derived also by the 'height-over-area' method of Zierler. From this mean time constant we calculate the mean c.b.f. via the relation $\bar{t} = \bar{\lambda}\bar{f}$. In other words, the 'height-over-area' method for determination of mean c.b.f. is based on determination of \bar{t} .

In the model proposed by Reivich et al (1969), section II-4, for the analysis of multi-exponential clearance curves, the aim is to determine two mean decay constants $\bar{\alpha}$ and $\bar{\beta}$, each corresponding to one mode of a bi-modal distribution of decay constants.

Another method of determination of the mean c.b.f., namely the initial-slope-index (I.S.I.), described in section II-6, is based on the initial part of the clearance curves. Because:

$$\left(\frac{dr}{dt}\right)_{t=0} = \frac{d}{dt} \sum_{i=1}^n A_i e^{-\alpha_i t} = - \sum_{i=1}^n A_i \alpha_i = - \bar{\alpha} \sum_{i=1}^n A_i \quad (85)$$

the initial slope (I.S.) is determined by the mean decay constant. Hence, the I.S.I. is based on $\bar{\alpha}$.

The power series method of analysing clearance curves as proposed in section V-1-5 is also based on $\bar{\alpha}$.

To our knowledge differences that we find in the pig, between the results of the analyses of the clearance curves, according different methods, are greater than reported for other animals. Obviously the greater discrepancies are consequences of the relative larger contributions of slowly decaying components to the clearance curves measured in the pig, compared to the situation in other animals.

V-1-3 A study of a multi-exponential clearance model

In the analyses of the '81-keV' and '31-keV' clearance curves, we found differences between the corresponding decay constants α_{81} and α_{31} and the decay constants β_{81} and β_{31} . In section V-1-1 we showed that the clearance is caused by c.b.f., which is very heterogeneous.

The following model is intended to illustrate that the differences in corresponding decay constants can be explained by a multi-exponential character of the clearance curves.

In order to derive the distribution of exponentials that constitute the Xe-133 clearance curve from the distribution of blood flow values in the cerebrum, two operations must be performed.

The blood flow values f must be divided by the partition coefficients of the tissue regions concerned to obtain the decay constants.

We must allow for the radiation absorption in the tissue in order to obtain the coefficients of the exponentials. Therefore we must know the geometrical distribution of specific blood flow in the cerebrum. This geometrical distribution of blood flow varies with the physiological circumstances and is not known. In our model we assume a simple distribution, which corresponds roughly with experimental observations. One of these observations is that the clearance rate is lower for the deeper regions of the brain. In the model we assume that the blood flow in a plane tissue layer at a certain distance d from the collimator face, is homogeneous, and that it decreases linearly with increasing d . This relation is expressed by the values shown on the X-axis of the graph of Fig. 42. Furthermore we assume that the initial distribution of

the isotope, after the Xe-injection, which is related to the distribution of the blood flow, can be approximated by a parabolic function, as shown in Fig. 42.

The model represents a relatively small amount of highly perfused cortical tissue, a large amount of tissue with moderate perfusion rates, situated beneath the first layer, and a small amount of tissue in deep brain regions with low perfusion rates. The upper region corresponds to the highly perfused cortical tissue, e.g. as found by Lassen (1965) and to the fast decaying component if a three-exponential model is fitted to the clearance curves (section IV-2). The moderately perfused region corresponds to widely overlapping values of the blood flow in grey and white tissue, reported by Foreman et al (1976). Finally the relatively poor perfused deep brain region may correspond to the values of the constant K obtained when an exponential model is fitted to the clearance curves. The mean value of the parabolic distributed specific blood flow is 0.5 min^{-1} and the standard deviation is 0.15 min^{-1} .

With this distribution ten exponentials are chosen, corresponding with the stars in the graph of Fig. 42. It was assumed that the boundary between grey and white tissue was situated at a distance $d = 28 \text{ mm}$.

To allow for the different partition coefficients the decay constants of exponentials corresponding to grey tissues were divided by 0.8 and those corresponding to white tissue by 1.5. Thus the original distribution became a bi-modal distribution. In order to account for the absorption of the '81-keV' and '31-keV' radiation of Xe-133, the coefficients were reduced by multiplying them by $e^{-\mu_{81}d}$ and $e^{-\mu_{31}d}$, respectively μ_{81} and μ_{31} being the linear attenuation coefficients in water.

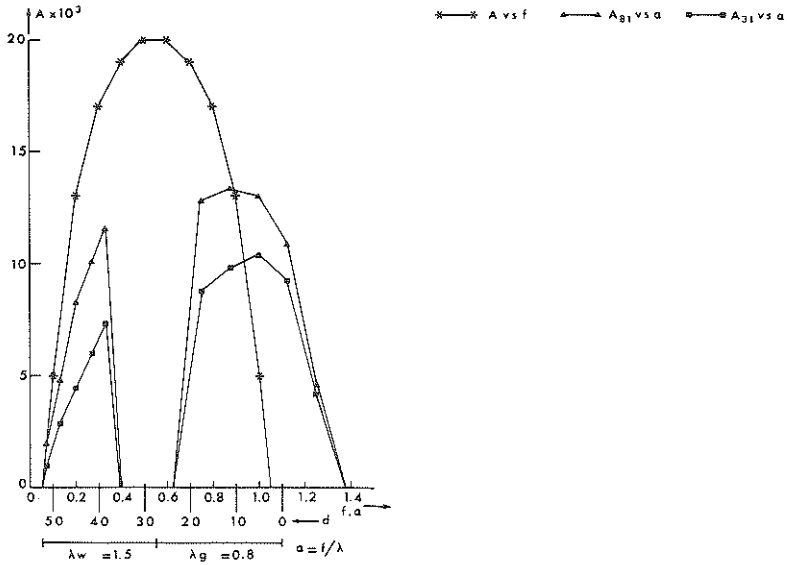


Fig. 42.: Distribution of exponentials according to a multi-exponential cerebral clearance model for Xe-133.

Taking $\mu_{81} = 0.18 \text{ cm}^{-1}$ and $\mu_{31} = 0.36 \text{ cm}^{-1}$, we obtained the coefficients of the bi-modal distributions of the '81-keV' and '31-keV' exponentials which are shown in Fig. 42. It appears that the shape of the bi-modal distribution of '81-keV' exponentials is different from the shape of the distribution of the '31-keV' exponentials. The difference in shape is dependent on the geometrical distribution of flow and not on the flow distribution in itself. In Table 14a the mean decay constant $\bar{\alpha}$, its standard deviation $\sigma(\alpha)$, the mean time

grey tissue					
81-keV			31-keV		
distribution	fit	error	distribution	fit	error
$\bar{a} = 0.957$	$a = 0.879$	8%	$\bar{a} = 0.972$	$a = 0.916$	5.7%
$\sigma_a = 16.5\%$			$\sigma_a = 16.4\%$		
$\bar{\tau} = 1.07$			$\bar{\tau} = 1.06$		
$1/\bar{\tau} = 0.931$	$a = 0.879$	5.5%	$1/\bar{\tau} = 0.946$	$a = 0.916$	3.1%

"Discrepancy" between \bar{a}_{31} and \bar{a}_{81} : 1.5%

between a_{31} and a_{81} : 4.2%

a

white tissue					
81-keV			31-keV		
distribution	fit	error	distribution	fit	error
$\bar{\beta} = 0.242$	$\beta = 0.196$	19%	$\bar{\beta} = 0.249$	$\beta = 0.207$	16.8%
$\sigma_{\beta} = 33.6\%$			$\sigma_{\beta} = 31.8\%$		
$\bar{\tau} = 4.97$			$\bar{\tau} = 4.75$		
$1/\bar{\tau} = 0.201$	$\beta = 1.96$	2.5%	$1/\bar{\tau} = 0.210$	$\beta = 0.207$	1.4%

"Discrepancy" between $\bar{\beta}_{31}$ and $\bar{\beta}_{81}$: 2.8%

between β_{31} and β_{81} : 5.5%

b
Table 14 a and b: Results of a two-exponential analysis of a decay curve, generated according to the model represented in Fig. 42.

constant $\bar{\tau}$ and its reciprocal value $1/\bar{\tau}$, calculated for that mode of the distribution which is related to grey tissue, are given for both 81-keV and 31-keV radiation. Table 14b shows these values for the mode related to white tissue.

The composite '81-keV' and '31-keV' clearance curves were generated for a period of 32 minutes, i.e. more than twice the longest time constant in the distributions. These clearance curves were fitted by a sum of two exponentials. The fitted decay constants α_{81} and α_{31} in Table 14a, and the fitted decay constants β_{81} and β_{31} are given in Table 14b. These tables also show the percentage differences between the fitted decay constants and the mean decay constants of the distributions and the reciprocal values of the mean time constants of the distribution. It appears that the differences between the fitted decay constants and the mean decay constants of the distributions are greater than the difference between the fitted decay constants and the reciprocal value of the mean time constants of the distributions. Furthermore we find differences between the corresponding decay constants of the '81-keV' and '31-keV' clearance curves, just as in the experiments in-vivo.

We conclude that the discrepancies between results of the fit of a two-exponential model and a two-compartmental model, as found in the in-vivo experiments, are qualitatively in agreement with this simplified multi-exponential clearance model.

Therefore we take the differences between the corresponding decay constants of the fitted two-exponential model to the '81-keV' and '31-keV' clearance curves, as a consequence of a multi-exponential character of the clearance curves, which is different for both energies caused by different absorption in the tissue. This interpretation implies that the clearance rate is heterogeneously distributed as a function of depth in the cerebrum.

V-1-4 Inverse Laplace transformation methods for the
analysis of multi-exponential clearance curves

A multi-exponential function may be expressed by means of a Laplace integral equation, as follows:

$$r(t) = \sum_{i=1}^n A_i e^{-\alpha_i t} = \int_0^{\infty} \tilde{A}(\alpha) e^{-\alpha t} d\alpha \quad (87)$$

where $A(\alpha)$ is a sum of delta functions. According to this representation of a multi-exponential function $A(\alpha)$ can be determined by means of an inverse Laplace transformation. A problem is that such an inverse Laplace transformation must be performed on experimental data.

Gardner and Gardner (1962) published a method for performing such a numerical inverse Laplace transformation for multi-exponential decay curves. The goal of their method is to get plot of the distribution density function $A(\alpha)/\alpha$ versus α . The presence of a peak in this plot indicates an exponential component, the abscissa value at the centre of the peak is the decay constant α_1 , while the height of the peak is proportional to the coefficient A_1 . We shall summarize their method by presenting the essential steps in the analysis. In order to perform the transformation they introduce two variables x and y , so that:

$$t = e^x \quad \text{and} \quad \alpha = e^{-y}$$

With these variables the Laplace integral can be written as a convolution, namely:

$$e^x f(x) = e^{(x-e^x)} * A(e^{-x})$$

By performing a Fourier transformation on these functions, this convolution can be simplified to the expression:

$$F(\mu) = K(\mu)G(\mu)$$

where μ is a frequency variable.

Hence:

$$G(\mu) = \mathcal{F} \left\{ A(e^{-x}) \right\} = F(\mu)/K(\mu)$$

where \mathcal{F} symbolizes the Fourier transformation. It can be shown analytically that $K(\mu)$ is the complex gamma function (Abramowitz and Stegun, 1965), namely:

$$K(\mu) = \frac{1}{\sqrt{2\pi}} \Gamma(1 + i\mu)$$

Hence, the method proposed by Gardner and Gardner is as follows.

Find $F(\mu)$ by performing a Fourier transformation on the function $tr(t)$, where $r(t)$ is the measured clearance function. Determine $G(\mu)$ by dividing $F(\mu)$ by the known function $K(\mu)$. Finally perform an inverse Fourier transformation on $G(\mu)$ to obtain the density function, $A(e^{-y})$, which is equivalent to the function $A(\alpha)/\alpha$, to be plotted versus α .

Gardner and Gardner pointed out that their method has the following advantages.

In contrast to non-linear curve fitting procedures, no initial estimation of parameters is necessary.

The number of exponential components follow automatically from the analysis in their method, while in the other procedures the number of exponentials is presupposed in

the model to be fitted.

Furthermore they claim that full use is made of the accuracy that is inherent in the data, since the data are treated as a whole, as opposed to some methods of the subtraction type wherein all but the shortest-lived components are determined, using fewer points than actually are available.

Finally, the occurrence of α values very close together does not endanger the entire solution as it does in other methods.

Because of these advantages we wished to use their method for the analysis of the multi-exponential clearance curves. The method was evaluated by Van Poelgeest (1971). He found that its applicability was seriously limited by errors which are introduced by the numerical integrations and by the finite range of integration needed to perform the convolution integral and the Fourier transformations.

Because of the approximations involved in the method, the peaks in the plots are broadened, so that the resolution of the separate exponential components is reduced. If the range of integration is made larger, noise and sampling errors cause additional peaks, which interfere with the reliable identification of the real components. Therefore a compromise had to be made in the range of integration.

Figures 43a and 43b show the results of an inverse Laplace transformation, performed according to the method of Gardner and Gardner (1962) on the '81-keV' and '31-keV' clearance curves of exp.nr. 43-II. In these plots the decay constants found by regression analysis with the two- and three-exponential models, section IV-2, are indicated by arrows. It appears that there is no agreement with the results of the two-exponential

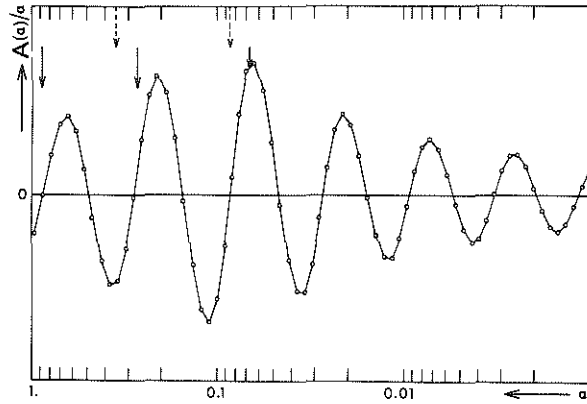


Fig. 43 a: 81-keV.

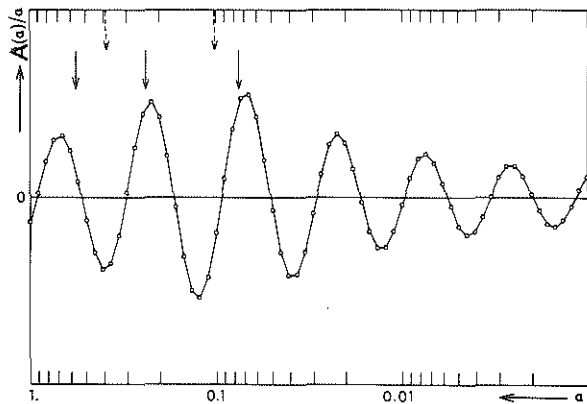


Fig. 43 b: 31-keV.

Fig. 43.: Inverse Laplace transformation performed to the clearance data of exp. nr. 43-II.

- indicate decay constants found with a three-exponential model (Table 6).
 -----→ indicate decay constants found with a two-exponential model (Table 5).

model. The decay constants found with the three-exponential model, however, correspond more or less with the first three peaks in the plots. Because of this correspondence we are inclined to conclude that the other peaks are falsely and introduced by the computing procedure.

To distinguish true peaks from error ripples Gardner and Gardner suggested that the analyses should be repeated with another boundary to the range of integration; then the true peaks will remain in the same position as in the first analysis.

In that case then, however, repeated regression analyses of the clearance curves, with an increasing number of exponentials, might be more attractive.

With regard to the resolution of exponentials, in our opinion their method offers no advantages, because it is merely a transformation of the data, so that the problem of identification is changed into the problem of interpretation of the plots obtained.

Papoulis (1973) claimed that he had improved the method of Gardner and Gardner. The method of Papoulis was evaluated for our purpose by Pfaff (1975) and turned out to be very sensitive to noise. It was concluded that this method was not useful either.

Finally, Lauw (1976) evaluated a method based purely on Fourier transformation, published by Prost et al (1974). This method was too unsuccessful with our data.

A more detailed evaluation of these three transformation methods of analysis of multi-exponential decay curves has been given by Sparreboom et al (1976).

It must be concluded that these complicated methods of analysis offer no advantages, that justifies their use in place of the regression analysis.

V-1-5 The use of positive power series of time for the analysis of clearance curves

In section V-1-2 it has been shown that the mean decay constant is a valuable measure for c.b.f., especially if one is mainly interested in the highly perfused tissue. This mean decay constant can be calculated from the parameters obtained by fitting an exponential model.

Because the clearance curves have a multi-exponential character, it is useful to search for methods that yield other parameters, besides the mean decay constant, to characterize the distribution of exponentials.

One common method of characterizing a distribution in statistics is based on the moments of the distribution. Using normalized distribution density functions $A'(\tau)$ and $A'(\alpha)$, we introduce the moments:

$$M_n(\tau) = \int_0^{\infty} \tau^n A'(\tau) d\tau; \text{ with } \int_0^{\infty} A'(\tau) d\tau = 1 \quad (88)$$

and

$$M_n(\alpha) = \int_0^{\infty} \alpha^n A'(\alpha) d\alpha; \text{ with } \int_0^{\infty} A'(\alpha) d\alpha = 1 \quad (89)$$

Here $M_1(\tau) = \bar{\tau}$, and $M_1(\alpha) = \bar{\alpha}$.

The second moment yields the variance of the distribution and is related to the standard deviation about the mean value:

$$\sigma(\tau) = \sqrt{M_2(\tau) - M_1^2(\tau)} \quad (90)$$

$$\sigma(\alpha) = \sqrt{M_2(\alpha) - M_1^2(\alpha)} \quad (91)$$

All the moments characterize different features of the shape of the distribution function, and it may therefore be useful to evaluate them from the clearance curves. For example the standard deviation of the time constant is a measure for the dispersion suffered by the tracer particles as they pass through cerebral tissue. Theoretically all the moments can be calculated from the parameters obtained by fitting an exponential model. An alternative method for the determination of the moments, not based on the fitting of an exponential model, is as follows.

For the distribution $A'(\tau)$ we find that:

$$\int_0^{\infty} t^{n-1} H^*(t) dt = (n-1)! \int_0^{\infty} \tau^n A'(\tau) d\tau = (n-1)! M_n(\tau) \quad (92)$$

where $H^*(t)$ is the tracer residue function, introduced in section II-6. This relationship can be used to extend the 'height-over-area' method of analysis, described in section II-6.

For the distribution $A'(\alpha)$ we find that:

$$\left(\frac{d^n H^*(t)}{dt^n} \right)_{t=0} = (-1)^n \int_0^{\infty} \alpha^n A'(\alpha) d\alpha = (-1)^n M_n(\alpha) \quad (93)$$

This relationship can be used to extend the I.S. method. If we write $H^*(t)$ in the form of a Taylor series:

$$H^*(t) = \sum_{n=0}^{\infty} \frac{1}{n!} \left(\frac{d^n H^*(t)}{dt^n} \right)_{t=0} t^n$$

we note that:

$$H^*(t) = \sum_{n=0}^{\infty} \frac{(-1)^n}{n!} M_n(\alpha) t^n \quad (94)$$

This means that, if the clearance curve is represented by a series of positive powers of time, the coefficients yield just the moments of the α -distribution function; in particular the coefficient of t yields $\bar{\alpha}$, and that of t^2 yields the variance $\sigma^2(\alpha)$. We may thus conclude that, if clearance curves are generated by a multi-exponentially distributed process, the use of a power series model instead of the traditional exponential model may offer advantages.

The fit of a power series to experimental data can be performed by a computer. Because this model is linear in the parameters to be fitted, the regression analysis is simpler than the non-linear regression analysis used to fit an exponential model.

The use of the power series model for our experimental data has not yet been evaluated. To obtain an impression of the theoretical meaning of this model, we synthesized decay curves generated by a Gaussian distribution of $A(\alpha)$, by means of the power series.

For this Gaussian distribution (Abramowitz and Stegun, 1965):

$$\begin{aligned}
 M_0(\alpha) &= 1 \\
 M_1(\alpha) &= \bar{\alpha} \\
 M_2(\alpha) &= \sigma^2 + \bar{\alpha}^2 \\
 M_3(\alpha) &= 3\sigma^2\bar{\alpha} + \bar{\alpha}^3 \\
 M_4(\alpha) &= 3\sigma^4 + 6\bar{\alpha}\sigma^2 + \bar{\alpha}^4 \\
 M_5(\alpha) &= 15\sigma^4 + 10\bar{\alpha}^3\sigma^2 + \bar{\alpha}^5
 \end{aligned} \tag{95}$$

Hence, the residue function $H^*(t)$ generated by this process, is given by the power series:

$$\begin{aligned}
 H^*(t) = 1 - \bar{\alpha}t + \frac{\sigma^2 + \bar{\alpha}^2}{2!}t^2 - \frac{3\sigma^2\bar{\alpha} + \bar{\alpha}^3}{3!}t^3 + \\
 + \frac{3\sigma^4 + 6\sigma^2\bar{\alpha}^2 + \bar{\alpha}^4}{4!}t^4 + \frac{15\sigma^4 + 10\sigma^2\bar{\alpha}^3 + \bar{\alpha}^5}{5!}t^5 + \dots (96)
 \end{aligned}$$

The residue curve has been synthesized from this power series for two cases, namely $\bar{\alpha} = 0.2$ with $\sigma(\alpha) = 0.6$ and $\bar{\alpha} = 1$ with $\sigma(\alpha) = 0.15$. Figure 44 shows semi-logarithmic plots of the first two minutes of these curves. In order to construct these two-minute curves, terms up to the third power of t were needed for the first case and up to the sixth power of t in the second case.

The two-minute curves are approximately mono-exponential, like was found for $A(\tau)$ in section V-1-2, Fig. 39.

Using a mono-exponential model, we find that the decay constant is 0.19 min^{-1} in the first case and 0.97 min^{-1} for the second case. These values are close to the mean decay constants of the distributions.

The I.S.I.-index which was proposed by Paulson et al (1969), described in section II-6, and is based on the assumption that the decay is mono-exponential during the first two minutes, is equal to the decay constant of this exponential. For the multi-exponential curve assumed here, this approach is justified, though it yields a slight underestimate of the mean decay constant of the distribution. The fitting of a power series model, however, yields in theory the correct value of the mean decay constant, even in cases where the first part of the curves cannot be well approximated by a mono-exponential model, and thus the I.S.I.-method is therefore bound to fail.

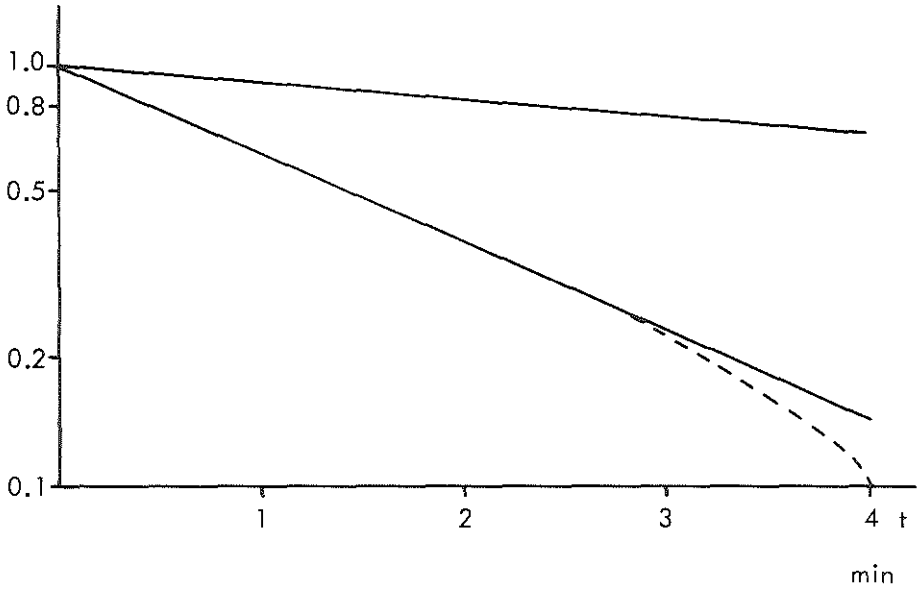


*Fig. 44.: Courses of the decay curves generated according to a positive power series of the time, approximating a multi-exponential process with normally distributed decay constants.
 ---- course deviating from —, caused by the limitation of the degree of the power series to 5.*

V-2 Diffusion effects on the clearance curvesV-2-1 Phenomena related to intertissue transport of Xe-133

In the sections II-4, V-1-1 and V-1-3 it was assumed that the clearance rates of Xe in the cerebrum is as heterogeneous as the blood flow. According to the theoretical treatment of Kety (1951) the diffusion of Xe in cerebral tissue is so fast that the clearance rate is not limited by diffusion. Thus the clearance of one tissue type should follow a mono-exponential function, corresponding to one compartment, section II-1.

If the clearance rates are heterogeneously distributed in the cerebrum, Xe-concentration gradients between tissue regions will exist. These concentration gradients cause interregional diffusion and consequently makes the clearance rates less heterogeneous than c.b.f. Theoretically the diffusivity of Xe could be so great, that it could even reduce the clearance of the hemisphere to that of a one-compartmental system. However, the clearance curves appear to be composed of at least two exponentials, section II-2 and IV-7. Usually the 'fast' exponential is ascribed to the clearance of grey tissue and the 'slow' exponential to the clearance of white tissue. Our study, based on the simultaneous recording of the '81-keV' and '31-keV' clearance curves, affirms that the rapidly cleared tissue is situated more peripherally than the more slowly cleared tissue, section IV-7. Hence, in spite of the high diffusivity of Xe in cerebral tissue, the clearance rate as a function of depth in the cerebrum is heterogeneous. By means of multi-probe systems it is demonstrated that the clearance rate is also distributed heterogeneously,

along the cortex, section II-4.

Obviously the diffusivity of Xe in the tissue is small enough to preserve some heterogeneity in clearance rates.

A model, in which fast diffusion within an undefined tissue region is assumed, but the consequences of interregional diffusion are excluded, gives ambivalent results. It follows that the identification of the distribution of c.b.f. with the corresponding multi-compartmental system may not be justified, section II-4.

In other words, diffusion may affect the clearance curves more than assumed in such multi-compartmental models.

An example of intertissue diffusion is given by Perl et al (1965), who accounted for differences between the rate of uptake of N_2O and cyclopropane in man by diffusion from lean to neighbouring adipose tissue. The rate of uptake of cyclopropane into adipose tissue by diffusion initially is large compared to the uptake by perfusion. If the rate of uptake was directly interpreted as the result of perfusion of adipose tissue, the perfusion is overestimated.

If the clearance curves are affected by diffusion, the clearance rate will be different for tracer gases with different diffusion coefficients, apart from the differences in their partition coefficients. Such differences have been reported by Valois et al (1976), using Xe-133, Kr-85 and I-125-Antipyrine in the rabbit. Intertissue diffusion has also been seen as a possible explanation for the continuously decreasing ratio r_{31}'/r_{81}' , described in section IV-2 (Van Duyl et al, 1975). A study of an analog computer model of the cerebral clearance process has shown that the various courses of r_{31}/r_{81} , found in the in-vivo measurements, can be simulated in the model by intercompartmental diffusion (Tukker, 1974).

These ideas led us to perform the following experiment. A bolus of Xe-133 was injected into the internal carotid artery of a pig. Immediately after the injection the blood circulation was arrested. Both the 81-keV and 31-keV radiation of Xe-133 were recorded. The results of this measurement are given in Fig. 45.

During the first minute, the circulation was not fully arrested. After this period a very slow decay in the '81-keV' recording can be observed. A slightly faster decay can be seen, however, in the recording of the 31-keV radiation. This decay cannot be due to clearance by perfusion. The difference between the decay rates of the '81-keV' and '31-keV' recordings indicates a gradual increase in the absorption of radiation in cerebral tissue, which is different for the two radiation energies. Of course any increase in the distance between Xe-source and detector would yield such recordings. However, it might be a consequence of intertissue

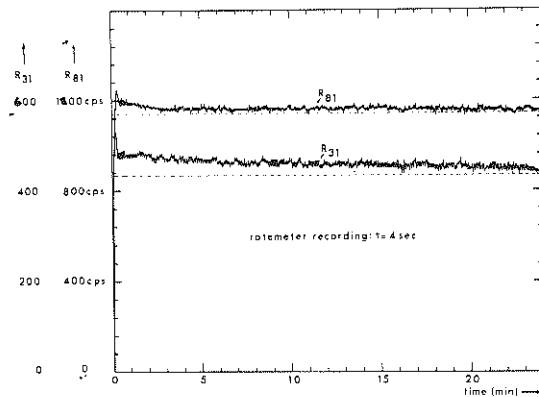


Fig. 45 : Radioactivity of the cerebrum measured after arrest of circulation.

diffusion, because immediately after an injection the partial pressure of Xe in the highly perfused cortical tissue is higher than in the more slowly perfused deeper brain tissues.

For a two-compartmental model with intercompartmental diffusion, it can be shown (Van Duyl et al, 1975; Bakker, 1976), that the relative weight W_g , calculated by (20), depends on the ratio of the clearance rates in both compartments. If the dependence of the relative weight on the c.b.f. is ascribed wholly to intercompartmental diffusion, one can derive an estimate of this intercompartmental diffusion.

Several other investigators (Wollman et al, 1965; Bozzao et al, 1969; Valois and Peperkamp, 1970; Kasoff, 1970; Cliff et al, 1973; Heiss et al, 1975) have reported that the relative weight of the faster clearance compartment is lower when the mean c.b.f. is lower. We encounter this dependence of W_g on c.b.f. more distinctly in the pig, section IV-5.

It has been taken as a consequence of problems in separation of exponential components.

Because the multi-exponential character of the clearance curves is taken as the main cause of the false interpretation of W_g , the estimate of intercompartmental diffusion is doubtful.

Intercompartmental transport of Xe was assumed by Zwart and Van Dieren (1974), also in order to explain both the shift in the relative weights of grey and white tissue and the oscillations they observed in the clearance curves. To account for these oscillations, the intercompartmental Xe-transport was assumed to have an oscillatory behaviour.

To explain oscillations of the sort that they observed in the clearance curves, it is necessary to suppose that

the transport is caused by an active mechanism. The simplest way that they could find of obtaining oscillations was the addition to the two-compartmental model of an on-off flow of blood, equilibrated with the slow compartment, into the fast compartment. This type of clearance they called the series release. Some physiological support for their postulate is derived from the observations described by Misrahy and Clark (1958), section I-2.

Because any transport of Xe-133 in the direction of the detector implies that there is a decrease in the absorption length of the radiation in the tissue, such transport also implies an increase in the pulse rate. Thus the fluctuations in the clearance curves can be ascribed to the oscillatory character of intercompartmental transport of Xe. The oscillations they observed had no fixed frequency, but varied with cycles of about 8 and 30 seconds.

The statistical nature of radioactivity might lead to apparent oscillations in the clearance curves.

To search for these oscillations, we performed experiments on two dogs under conditions similar to those in the experiments of Zwart and Van Dieren. In order to detect the oscillations with more certainty, however, we measured the '81-keV' and '31-keV' clearance curves simultaneously. To reduce the effect of the finite sample time on the oscillations a preset time of 2 seconds was chosen instead of the 4 seconds we used in the other experiments. The results of the analyses of the clearance curves by a two-compartmental model have been described in section IV-6.

To detect the oscillations we first fitted a sum of three exponentials and a constant to the clearance curves.

In most cases the eccentricity of the weighted sum of

residuals was less than 1, so that this model yields a good fit. Because the oscillations cannot be fitted by the exponential model, they contribute to the residual sum of squares. Hence, the small values of ξ indicate, that the oscillations, if present, cannot be large. To perform a statistical investigation of the residuals, the fitted model was subtracted from the clearance data. According to the theory of the Poisson statistics of the pulse rate data, these residuals, divided by the square root of the fitted pulse rate figure, are normally distributed for high enough pulse rates, with a constant standard deviation. This has been checked on data measured from a constant Xe-source at different pulse rate levels (Dreschler, 1975).

If the fluctuations in the pulse rate, about a fitted clearance curve, are purely of a statistical nature, the weighted residuals are distributed normally, section III-4. If there exists a periodic component in the residuals, with a certain periodic time, it will produce a peak in the autocorrelation function. However, the more the period of the oscillations varies, the more difficult it is to detect such a component by means of the autocorrelation function.

If there is a component in the residuals that is associated with Xe-transport, it must be found both in the '81-keV' and '31-keV' residuals at the same time. Therefore a more sensitive method for the detection of any non-statistical component in the residuals is by means of the crosscorrelation between the weighted residuals of the '81-keV' and '31-keV' clearance curves. Correlation coefficients, originating from N values distributed normally, have a mean equal to zero and a variance equal to $1/N$, if N is large enough (Jenkins and Watts, 1968). Hence, we can define a 95% confidence

interval for certain values of the correlation coefficient originating from noise, namely $\pm 1.96/\sqrt{N}$. Of course the only relevant cross correlation in our analysis is that between residuals of '81-keV' and '31-keV' clearance curves at the same moment, $\rho(0)$. However, because there may be some time shift in the replay of the '81-keV' and '31-keV' recordings of the clearance data, we determined also the cross correlation between the residuals shifted by 2 seconds with respect to one another $\rho(+2)$ and $\rho(-2)$.

Table 15 gives the cross correlation coefficients for a series with clearance curves measured in the dog, and for two measurements made on a constant Xe-133 source (Dreschler, 1975).

In this table + and - refer respectively to positive and negative values of the correlation coefficient, within the confidence interval, while p and n indicate that positive or negative values lying outside this interval. The table shows that there are no significant differences between $\rho(0)$, $\rho(+2)$ and $\rho(-2)$, and that in most cases the cross correlation coefficients are within the confidence interval. Furthermore there is no significant difference between the results with the clearance curves and those with the constant Xe-133 source.

We conclude that there is no correlation between the fluctuations in the '81-keV' and '31-keV' clearance curves, so that Xe-transport phenomenon of the type described by Zwart and Van Dieren (1974) cannot be detected in the clearance curves of our experiments.

clearance curves												constant source	
cross-correlation coefficient	I-1	I-2	I-3	I-4	II-3	II-4	II-5	II-6	II-7	II-8	II-9	C-1	C-2
$\rho(-2)$	+	+	+	p	+	-	+	+	-	-	-	-	n
$\rho(0)$	-	-	+	n	p	-	+	-	-	-	+	-	p
$\rho(+2)$	-	n	+	-	p	-	+	p	+	+	+	+	+

Table 16: Correlation coefficients between fluctuations in 81-keV and 31-keV clearance curves

V-2-2 Determination of the solubility coefficient and diffusion coefficient of Xe in cerebral tissue of the pig

In section II-1, in discussing the measurement of c.b.f. by the Xe-clearance technique, the crucial assumption is explained that the clearance rate is not limited by diffusion (Kety, 1951). The theoretical validity of this assumption is based on calculations of the time required for inert, non-polar gases to attain equilibrium in the Krogh cylinder, section I-2, after a stepwise change of the concentration of the gas in the capillary. Kety concluded from these calculations that equilibrium is reached in about one second. In the calculation it is assumed that tissue is a homogeneous diffusion medium with a diffusion coefficient in the range $D = 1 \text{ to } 3 \times 10^{-5} \text{ cm}^2/\text{sec.}$, which is approximately equal to the diffusion coefficients of these gases in water. Then the diffusion rate is so fast compared to the rate of change of the concentration in the blood, that during the clearance the gas concentration remains approximately in equilibrium throughout the tissue.

The equilibrium ratio of the concentrations of the gas, in tissue and blood, the tissue-blood partition coefficient λ , is related to the solubility coefficients of the gas in tissue β_t and blood β_b , by the formula $\lambda = \beta_t/\beta_b$ (2). Table 16 shows values of solubility and diffusion coefficients of Xe in human cerebral tissue and in olive oil. Yeh and Peterson (1963) have shown that, at body temperature, the solubilities of Xe and Kr are essentially the same in olive oil and in animal fats. For that reason Osborn et al (1969) chose olive oil as a representative substance for studying the diffusivity of these gases in fats.

Solubility coefficients for the cerebral tissue of the pig are not known. In section IV-7 it is concluded that low c.b.f. values are obtained if the fitted decay constants of the Xe-clearance curves are multiplied by the partition coefficients taken from the literature. Therefore we decided to measure the solubility coefficient of Xe in the cerebral tissue of the pig.

No experimental values of diffusion coefficients in cerebral tissue are found in literature. This gap has become particularly important in view of the criticisms of Hills (1967). Hills' criticisms concern the value of the diffusion coefficient assumed in the calculations of Kety and the geometry of the diffusion medium. From measurements of blood flow in the muscle of the rabbit, made by the Kr-85 clearance technique, Hills concluded that this tissue was not a homogeneous diffusion medium, but encompasses a cellular phase and an extra-cellular phase (interstitial fluid). He found that the diffusion coefficient in the cellular phase was approximately 0.01 of the value in the interstitial fluid. As a consequence the clearance of tissue is limited by the diffusion rate in the cellular phase. Furthermore this

substance	temp. (°C)	β	$D \times 10^5$ (cm ² /sec)	reference
human cerebral grey tissue	37	0.1196	-	Veall and Mallett (1969)
human cerebral white tissue	37	0.2253	-	Veall and Mallett (1969)
human cerebral tissue homogenate	37	0.1616	-	Veall and Mallett (1969)
human fat	37	1.8345	-	Yeh and Peterson (1963)
olive oil	37	1.8532	25.8	Osborn et al (1969)
	30	1.9749	18.9	
	25	2.0725	15.8	

Table 16: Solubility coefficients and diffusion coefficients of Xe

implies that the clearance from a single type of tissue is not mono-exponential.

Hills argues that for the determination of the diffusion coefficient of a heterogeneous diffusion medium, methods based on measurements transport under steady-state conditions are not appropriate, because solute molecules would mostly by-pass regions with low diffusivity when traversing the medium under the constant concentration gradient stipulated in steady-state methods. For heterogeneous diffusion media transient methods must be applied, in which the transfer function of the solute is determined. Hills (1967) directed attention to the fact that the values of the diffusion coefficients for various gases, referred to by Kety (1945), were one third to one fifth of the corresponding values for water. This is of the order of magnitude to be anticipated for

the fraction of the cross sectional area of the tissue occupied by extra-cellular fluid. Because of Hills' remarks we combined measurements of the solubility of Xe in cerebral tissue with measurement of the diffusion coefficient by a transient method. The method we used is based on the measurement of sorption of Xe-133 into or desorption of Xe-133 from a small amount of the cerebral tissue of the pig. We preferred to measure the desorption for two reasons. Firstly the desorption process is more resembling the Xe-clearance process in the experiments in-vivo. Secondly the sorption method has the disadvantage that the beginning of sorption is difficult to measure, because then only a small amount of Xe is in the tissue, while after a long sorption process the radioactivity is reduced by the physical decay of the isotope. Obtaining tissue in which Xe-133 is homogeneously distributed, is a problem in using the desorption method. This was solved doing experiments in-vivo. After an intra-arterial injection of Xe-133 the circulation was arrested. Then a small amount of cerebral tissue was sucked into a syringe, the small tip of which had been removed. From the syringe a tissue layer of about 10 mm was pushed on to the bottom of a glass tube, without contaminating the inner surface of the tube with radioactive tissue. To ensure that no bubbles remained trapped in the tissue, the tube was centrifuged. To ensure that equilibrium was attained between Xe desorbed into the air and that remaining in the tissue, the tube was closed by a second glass tube placed on top of it. In this way putrefaction and drying of the tissue were prevented also. To minimize rediffusion of Xe from the air space into the tissue, the volume of the air space in the glass tube was made about 15 times

larger than the volume of the tissue sample. Thus, compared to the initial partial pressure of the Xe in the tissue, the partial pressure will be low in the equilibrium situation.

Figure 46 shows the set-up for the measurement of the desorption curves.

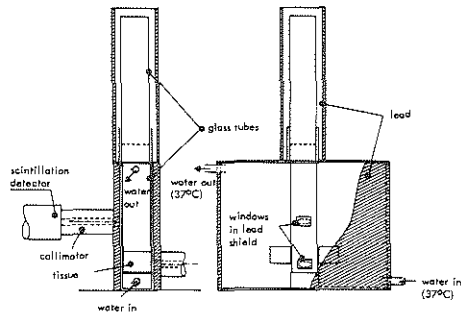


Fig. 46: Set-up for the measurement of solubility and diffusion coefficient of Xe in cerebral tissue

The closed specimen tube is placed in a plastic box, and is kept at 37°C , by water circulating around it. Box and tube were shielded by lead. In the lead shields on both sides there was a window. Via the windows the radiation from the tissue and from the air space above the tissue were measured by two scintillation detectors. The 'field of vision' of each detector was limited by narrow collimators, resulting in responses of both detectors, from a spherical source of Xe-133, with a diameter of about 3 mm, placed at different distances from the bottom of the tube, as shown in Fig. 47.

It appears that the radioactivity measured via one window is well separated from the radioactivity measured via the other window.

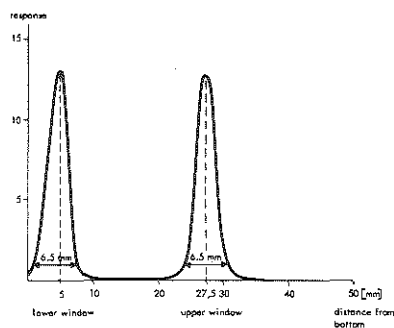


Fig. 47: Separation of 'fields of vision' of the detectors via both windows in the set-up of Fig. 46.

To allow for a difference between the pulse rates, originating from equal concentrations of Xe-133 in the field of vision of each detector, the response to some Xe-gas in a glass tube was measured. The gas in the tube was homogeneously distributed. This was checked by shifting the tube with respect to one scintillation detector. The ratio of the pulse rates of the two detectors, referred to as the efficiency ratio, was used as a correction factor in the determination of the solubility coefficient of Xe in cerebral tissue. During the desorption process the pulse rates originating from the radioactivity of the tissue and of the air space were measured alternately at preset time intervals of 20 minutes.

Figure 48 shows the results of measurements of desorption taken over a period of 160 hours. These data are obtained from the measured pulse rates, by subtracting the background radiation and multiplying by $e^{t/182.5}$ in order to correct for the physical decay of Xe-133. Data points at intervals of 2 hours only are

shown in the graphs. In this experiment the layer of tissue was 0.9 cm thick and was a mixture of grey and white tissue. It appears that after 100 hours both phases are in equilibrium.

The equilibrium ratio of the pulse rate estimated from the fitted curves is $r_t/r_g = 0.663$. The efficiency ratio in this measurement is 0.89. The ratio of the radio-

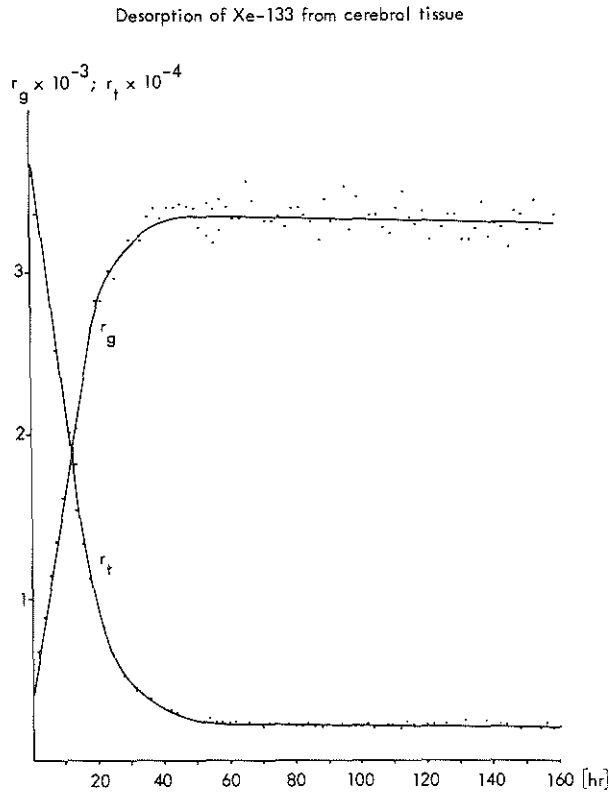


Fig. 48: Desorption of Xe-133 from cerebral tissue:
 r_g pulse rate from Xe-133 in air
 r_t pulse rate from Xe-133 in tissue

activities of the Xe in air and in tissue is the $0.663/0.89 = 0.745$.

To allow for the absorption of the radiation in the tissue, we assume that the radiation detected by the scintillation detector originates from a tissue layer of thickness 1.5 cm, which is equal to the inner diameter of the specimen tube, and that the linear attenuation coefficient $\mu_{81} = 0.15 \text{ cm}^{-1}$ (Appendix I). According to (73) the correction factor is then $1.5 \times 0.15 (1 - e^{-0.15 \times 1.5}) = 1.10$.

Hence, the solubility coefficient, found in this measurement equals $0.745 \times 1.10 = 0.82$. In a second experiment we found $\beta = 0.77$.

The values of the solubility coefficient found in this way, are more than four times larger than those reported by Veall and Mallett (1965) for human cerebral tissue homogenate, and more than three times larger than those for human cerebral white tissue.

The equilibrium values are subtracted from the data in Fig. 48 and the resulting points are plotted on a semi-logarithmic scale in Fig. 49. For $t > 10$ hours, the points can be fitted with a straight line, so that this part of the desorption curve is practically mono-exponential. From the slope of the semi-logarithmic plot we find that $\tau = 9.8$ hours.

In Appendix II it is shown that the concentration of Xe in tissue in this desorption process eventually follows a practically mono-exponential function, with a time constant equal to $4a^2/\pi^2D$, where a is the thickness of the tissue column. Hence, the pulse rate originating from the non-homogeneously distributed Xe in the wedge-shaped field of vision, also eventually becomes a practically mono-exponential function with that time constant. Since the thickness of the tissue column was

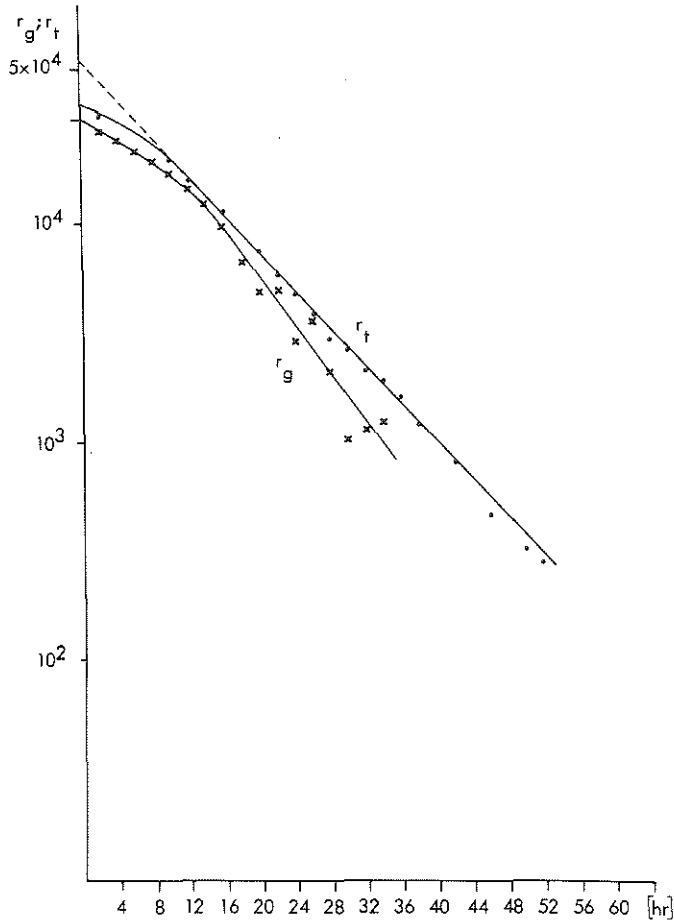


Fig. 49: Semi-logarithmic plot of curves in Fig. 48.

0.9 cm in this experiment, we find $D = 0.9 \times 10^{-5} \text{ cm}^2/\text{sec}$. In the second experiment, referred to above, we find $D = 1.0 \times 10^{-5} \text{ cm}^2/\text{sec}$. These values are in agreement with those reported by Kety (1951).

Because of the large difference between the solubility coefficient found by the desorption method and the results

of Veall and Mallett, it is useful to compare the two methods of determination. Veall and Mallett (1965) obtained samples of grey and white human cerebral tissue weighing 0.5 to 1.0 g. They added 1.0 ml of distilled water to each sample. The mixture was ground with a close-fitting glass pestle to produce a uniform fluid with the consistency of thin cream. Approximately 1 ml of the tissue suspension was introduced into a glass specimen tube (outer diameter 7 mm). Then about 0.1 ml containing approximately 10 μ Ci of Xe-133 was introduced in each syringe, and the tube was quickly sealed. The tubes were left overnight in a water bath at 37°C.

Immediately before the radioactivity measurements were performed, each tube was shaken vigorously for a few seconds and then spun briefly in a centrifuge to ensure that no bubbles were trapped in the liquid phase. The specimen tubes were kept in water at 37°C during the measurements.

The measurements were performed by bringing the tissue phase and the gas phase alternately in the field of vision of a collimated detector. Allowing for the added amount of water, the solubility coefficient of the tissue was calculated from the ratio of measured radioactivity. We note that Veall and Mallett did all they could to obtain equilibrium between the Xe in the tissue and that in the gas phase. The higher values of solubility that we find with the desorption method indicate that equilibrium has not yet been reached during our observation time.

The published values of solubility coefficients are determined from equilibrium situations reached via sorption of Xe in the tissue. Therefore we also measured the process of sorption of Xe-133 in cerebral tissue, in

spite of the disadvantages of this method described previously. We used the same set-up, as for the desorption measurement.

Figure 50 shows the result of such measurement. In Appendix II it is shown that desorption and sorption curves can be analysed in a similar way. In one experiment we found $\beta = 0.22$ and $D = 1.7 \times 10^{-5} \text{ cm}^2/\text{sec}$. In another experiment, performed on a sample that contained more grey tissue than the first sample, we found $\beta = 0.20$ and $D = 1.6 \times 10^{-5} \text{ cm}^2/\text{sec}$.

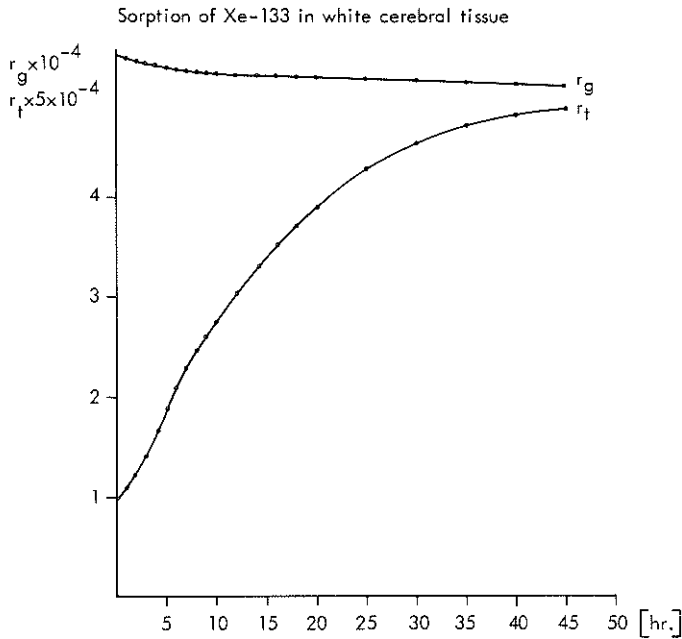


Fig. 50: Sorption of Xe-133 in white cerebral tissue

These values of the solubility coefficients are considerably closer to the reported values. It appears that the sorption method yields larger values of the

diffusion coefficient than the desorption method. This means that the uptake of Xe in cerebral tissue is faster than its release.

Now the question arises as to the cause of the significant differences between the values of the solubility coefficient and the diffusion coefficient found by the sorption and the desorption methods. This is an important question, because the desorption method is more in accordance with the situation in cerebral blood flow measurements, while the values of the solubility coefficients, which are generally used in the analysis of clearance curves, rely on a complete equilibrium between the Xe in the tissue and that in the gas phase.

The value of the solubility coefficient of Xe in pig cerebral tissue homogenate, which is derived from the sorption measurements is about 0.22. The value of the solubility coefficient of Xe in blood with Hct = 32%, is $\beta_b = 0.13$ (Fig. 3). With these values the mean partition coefficient $\bar{\lambda}$ is about 1.7. Therefore, if the mean transit time is about 0.2 min., section IV-5, the mean c.b.f. is about $34 \text{ cm}^3/\text{min}/100 \text{ cm}^3$ tissue.

Hence, the solubility coefficient of Xe in pig cerebral tissue, being larger than reported values, contributes to the explanation of the low c.b.f.-values we find if partition coefficients taken from the literature, are used.

If the desorption process contains a second component with a decay constant which is 100 times larger than the decay constant of the component that we have measured, then this second component appears to be a constant during our observation time. Hills (1967) found such a slow diffusion component and ascribed it to the cellular phase of the tissue.

A histological study of our tissue samples before and after the desorption measurement showed that the cellular structure had been lost. Hence, any slow diffusion component, which may exist in the desorption curves, cannot be due to a cellular structure in our experiments. The tissue, however, is not homogeneous and may contain structural elements, e.g. myeline, that cause a delay in diffusion. In that case, however, it is remarkable that then these structural elements not cause a similar delay in sorption.

Let us assume that cerebral tissue is composed of two substances, water and fat. The solubility coefficient of Xe in water is 0.0834 (Ladefoged and Anderson, 1967). Because the solubility coefficient in human cerebral tissue homogenate is 0.1616, and the solubility coefficient in human fat is 1.8345 (Table 16), we can derive that 4.5% of cerebral tissue only is fat. If tissue contains only 1% more fat then we find, that $\beta = 0.1796$, i.e. more than 11% increase in solubility of cerebral tissue.

Osborn et al (1969) reported values of the diffusion coefficient of Xe in olive oil which are about 25 times larger than the values referred to by Kety (1951) and the values we calculated from the fast diffusion component in cerebral tissue. However, because of the relative small amount of fat and because it is surrounded by water, the rate of diffusion of Xe in cerebral tissue is mainly limited by the water.

In the desorption method high initial concentrations in both the water and the fat are obtained via the microcirculatory system. It appears that a large proportion diffuses out of the tissue sample at a rate corresponding to that for water, and that a small proportion remains. This small proportion, however, is

too large to ascribe it to water in equilibrium with the gas. It is likely to assure that fatty structures are responsible for it.

We must assume then that diffusion out of these structures meets high resistance. Furthermore, because the sorption method yields values of the solubility coefficients which are close to the reported values, the diffusion resistance is smaller in this case, or else the fat component that offers a high diffusion resistance is a small fraction only of the total fat in the tissue. Because of the consequences for c.b.f. measurement, it is important to emphasize that our observations are similar to those described by Hills (1967), although the situation during the desorption process is not equivalent to the situation during clearance with the microcirculation intact. Our findings are consistent with the conclusion that c.b.f. is underestimated if partition coefficients taken from the literature are used.

Because we do not know the diffusion coefficient associated with the slow diffusion component, we cannot quantify its consequences for the analysis of the clearance curves. If the slow diffusion component limits the clearance rate partly, it contributes slow components to the clearance curves. These components cause an underestimation of c.b.f., especially if the flow is based on the calculation of the mean time constant of the clearance curve. Furthermore they may contribute to the values of the fitted constants.

Although our findings may explain the low c.b.f. values we find with the Xe-clearance technique in the pig, compared to those in man, it is hard to believe that the difference between the sorption and desorption processes that we have observed is typical only of the

cerebral tissue of the pig. Therefore, it is important that further research on the solubility and diffusion of Xe in cerebral tissue also in pigs and in other animals should be carried out.

APPENDIX ICharacteristics of the collimator for 81-keV and 31-keV radiation of Xe-133

With the nuclide Xe-133, 99.95% of the disintegrations involve a transition energy of 81 keV. A fraction of 65% of these disintegrations produces conversion electrons, which are followed by emission of X-rays, predominantly at 31 keV. The other 35% of the disintegrations involve emissions of a 81-keV gamma ray. Hence the ratio of the emission rate of 31-keV and of 81-keV photons of Xe-133 is 1.86.

In practice the ratio of the detected photons is much smaller, because the absorption of the 31-keV radiation in the medium between source and detector is greater than the absorption of the 81-keV radiation.

We measured the response of our scintillation detector (III-2-1) to a plane source of Xe-133 placed at various distances from the collimator face. The plane source was constructed from two glass discs of diameter 60 mm and thickness 1 mm, held 3 mm apart by a glass ring. The space between the discs was filled with Xe-133. In each measurement about 50.000 pulses of both energies were counted. The ratio of the pulse rates of the 31-keV radiation r_{31} and of the 81-keV radiation r_{81} , calculated for each measurement, is plotted in Fig. 1A.

The variation of about 1% in this ratio can be fully ascribed to the statistical nature of the radioactivity. It appears that at distances between 0 - 50 mm the ratio r_{31}/r_{81} is independent of the distance. The value of this ratio, here 0.86, depends on the widths and situations of the electronic windows of the pulse height analysers. We used symmetric windows of 5/4 W.H.M. (III-2-1).

Not only the ratio r_{31}/r_{81} is independent of distance, but so are the separate pulse rates r_{31} and r_{81} . This independence is a characteristic of narrow beam collimators, and it is caused by the cancelling out of an increase of the amount of isotope in the detector field, which increase is proportional to the square of the distance from the crystal, by decrease of the contribution from each point source, which decrease is inversely proportional to the square of that distance. The effect of absorption of radiation in air appears to be negligible.

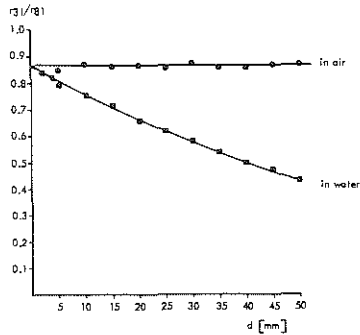


Fig. 1 A: Ratio of the pulse rates of 31-keV and 81-keV radiation from a plane source of Xe-133 at various distances from collimator face, with air or water between source and collimator.

Steyn et al (1974) published an analytical study of the response of a narrow beam pipe collimator to a plane source. From their publication we take the formula for the plane sensitivity:

$$r = a \epsilon_E \left(\frac{b}{2l} \right)^2 e^{-\mu d} \quad (1A)$$

where

- r is the pulse rate
- a is the density of the plane source, i.e. the number of photons of energy E , emitted per cm^2 per second
- ϵ_E is the detection efficiency for photons of energy E
- $2b$ is the inner diameter of the collimator
- l is the length of the collimator to the face of the crystal
- d is the distance between plane source and collimator face
- μ is the linear attenuation coefficient

The response of the detector to the plane source was measured at various distances from the collimator face, with water as an absorber between plane source and collimator. The linear attenuation coefficients for 81-keV and 31-keV radiation in water are $\mu_{81} = 0.18 \text{ cm}^{-1}$ and $\mu_{31} = 0.36 \text{ cm}^{-1}$ (Weber and Rasmussen, 1972). Because of the mono-exponential relationship between pulse rate and distance, we expect a mono-exponential decay of r_{31}/r_{81} with increasing distance, which has a decay constant $\mu_{31} - \mu_{81} = 0.18 \text{ cm}^{-1}$.

The results of the measurements with the plane source in water are shown in Fig. 1A. When these data are plotted on a semi-logarithmic scale it appears that the ratio can approximately be described with the function:

$$\frac{r_{31}}{r_{81}} = 0.84 e^{-0.12 d} \quad (2A)$$

The coefficient in this formula is affected by the absorption of the radiation in the upper glass disc of the plane source. In a separate measurement we found

that a layer of 0.21 cm of glass reduces r_{31}/r_{81} by a factor 0.70. Hence the disc of 0.1 cm thick causes a reduction determined by the factor:

$$e^{(\frac{1}{0.21} \ln 0.7) 0.1} = 0.84$$

Hence the experimental relationship between r_{31}/r_{81} and the distance of a plane source from the collimator face, corrected for the absorption in the glass disc, is:

$$\frac{r_{31}}{r_{81}} = 1.0 e^{-0.12 d} \quad (3A)$$

We may wonder about the difference between the theoretically expected decay constant and the measured one. Figure 2A shows the contributions of circular areas of the plane source, as functions of radius, with the plane source placed in water at various distances from the collimator face. About 85% of the detected radioactivity originates from regions limited by the cone drawn in the figure.

Hence if Xe-133 is homogeneously distributed in a volume the 'field of vision' of the collimator is in practice limited by the cone.

Figures 3A and 4A, the pulse rates for 81-keV and 31-keV radiation, have been plotted on a semi-logarithmic scale. It appears that the attenuation coefficients are $\mu'_{81} = 0.15 \text{ cm}^{-1}$ and $\mu'_{31} = 0.27 \text{ cm}^{-1}$. These attenuation coefficients differ from the linear attenuation coefficients μ_{81} and μ_{31} , reported above. We determined the contribution to the pulse rate from those regions of the plane source, that are limited by the cone illustrated in Fig. 2A. These values have been plotted

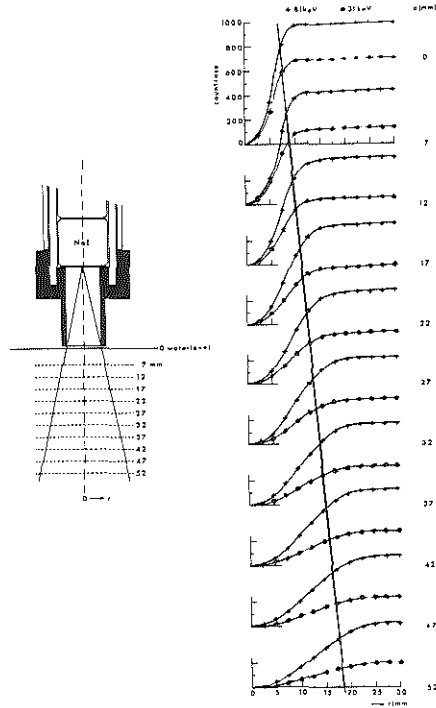


Fig. 2 A: Response to a plane source of Xe-133 in water, at various distances from collimator face.

in Figs. 3A and 4A also. It appears that here the attenuation coefficients μ_{81} and μ_{31} are close to the reported linear attenuation coefficients of 81-keV and 31-keV in water referred to above.

We conclude that the differences between μ_{81} and μ_{81}' and between μ_{31} and μ_{31}' are consequences of the geometry of the collimator, which is not an ideal narrow beam collimator.

If we assume a plane source with thickness dx and Xe concentration c , then the density of the plane source

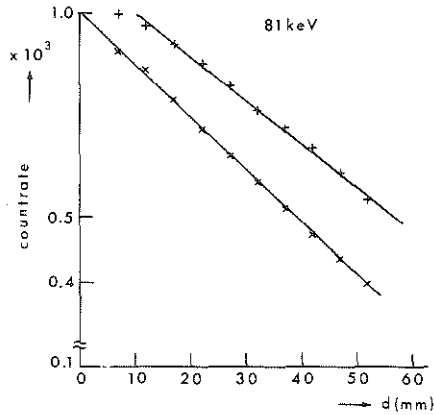


Fig. 3 A ++: r_{81} measured for a plane source of Xe-133 in water at various distances from collimator:

$$\mu'_{81} = 0.15 \text{ cm}^{-1}$$

xx: contribution to pulse rate from regions of the plane source determined by the cone in Fig. 1 A:

$$\mu''_{81} = 0.18 \text{ cm}^{-1}$$

is cdx. Hence, according to our results of the measurements, the response for such an infinitesimally thin plane source, placed in water at a distance d from collimator face, can be approximated by the formulas:

$$dr_{81} = g_{81} c e^{-\mu'_{81} d} dx \quad (4A)$$

$$dr_{31} = g_{31} c e^{-\mu'_{31} d} dx \quad (5A)$$

where g_{81} and g_{31} are proportionality factors, which depend on the units in which c is expressed.

Formulas (4A) and (5A) are used in section III-3-2 to

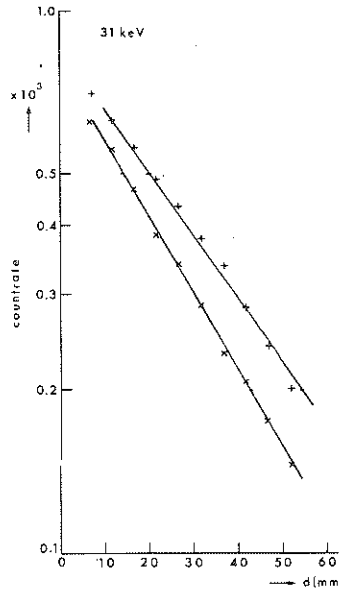


Fig. 4 A: ++: r_{31} measured for a plane source of Xe-133 in water at different distances from collimator:

$$\mu'_{31} = 0.27 \text{ cm}^{-1}$$

xx: contribution to pulse rate from regions of the plane source determined by the cone in

$$\text{Fig. 1 A: } \mu''_{31} = 0.34 \text{ cm}^{-1}.$$

derive the collimator response to a compartment.

APPENDIX IIAnalysis of the sorption and desorption curves

The one-dimensional diffusion of gas in a solute is governed by the differential equation (Fick's second):

$$\frac{\delta c_s}{\delta t} = D \frac{\delta^2 c_s}{\delta x^2} \quad (6A)$$

where c_s is the concentration of the gas in the solute as a function of time t and position x , and D is the diffusion coefficient.

In order to separate c_s into a function of position only, denoted by $X(x)$, and a function of time only, denoted by $T(t)$, we introduce:

$$c_s(x, t) = T(t)X(x)$$

Then:

$$\frac{\delta c_s}{\delta t} = X(x) \frac{dT}{dt} \quad \text{and} \quad \frac{\delta^2 c_s}{\delta x^2} = T(t) \frac{d^2 X}{dx^2}$$

so that:

$$\frac{1}{T} \frac{dT}{dt} = \frac{D}{X} \frac{d^2 X}{dx^2}$$

This relation implies that the left- and right-hand sides of this equation are each equal to a constant independent of x . We write for this constant $\lambda^2 D$ (Hsu Hwei, 1970). Then the solutions of both differential equations are:

$$T(t) = e^{-\lambda^2 Dt} \quad \text{and} \quad X(x) = A \sin \lambda x + B \cos \lambda x$$

Because there may be a number of values of λ , that satisfies these equations, a more general solution is:

$$c_s(x,t) = \sum_n e^{-\lambda_n^2 Dt} (A_n \sin \lambda_n x + B_n \cos \lambda_n x) \quad (7A)$$

The values of λ_n are determined by the boundary conditions of the experimental situation.

In the desorption experiment we assume that the gas initially is homogeneously distributed in the solute (Fig. 5A), so that:

$$c_s(x,0) = C_{s,0} \quad \text{with} \quad -a \leq x < 0$$

When this value of c_s is substituted in (7A), with $t = 0$, we find:

$$C_{s,0} = \sum (A_n \sin \lambda_n x + B_n \cos \lambda_n x) \quad \text{with} \quad -a \leq x < 0$$

We assume that the concentration of the gas at $x > 0$ is kept zero during the desorption of the gas from the solute.

If we extend this concentration function to a periodic function, as shown in Fig. 5A, we can perform a Fourier analysis and thus determine λ_n , A_n and B_n . The periodic function chosen implies that $\left(\frac{\delta c_s}{\delta x}\right) = 0$ at $x = -a$.

This boundary condition satisfies the fact that no diffusion takes place across the boundary $x = -a$. The discontinuity in c_s at $x = 0$ is approximated by the Fourier series.

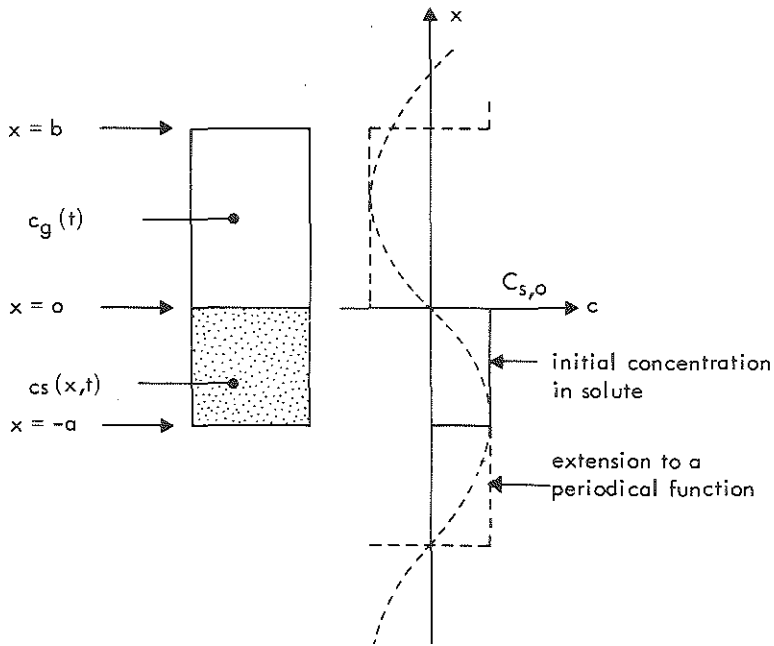


Fig. 5 A: Diagram of the initial concentration of the gas in the solute and in the gas space, and the approximation of the concentration function in the solute by means of a periodic function.

The Fourier expansion of the block function is:

$$c_s(x, 0) = \frac{-4C_0}{\pi} \sum_{n=0}^{\infty} \frac{1}{2n+1} \sin(2n+1) \frac{\pi}{2a} x$$

Hence:

$$\lambda_n = \frac{(2n+1)\pi}{2a}; \quad A_n = \frac{-4C_0}{\pi(2n+1)}; \quad B_n = 0$$

Substitution of these parameters in (7A) yields:

$$c_s(x,t) = \frac{-4C_0}{\pi} \left[\sum_{n=0}^{\infty} \frac{1}{2n+1} \sin \frac{(2n+1)\pi}{2a} x e^{-(2n+1)^2 t/\tau} \right] \quad (8A)$$

where:

$$\tau = \frac{4a^2}{\pi^2 D} \quad (9A)$$

For values of t/τ which are not too small, the convergence of this series is rapid. For $t = 0.5 \tau$ and $x = -a$, the absolute value of the second term in this series is less than 0.6% of the absolute value of the first term. In other words, for high enough values of t/τ the desorption curves become mono-exponential. For small values of t/τ a rapidly converging series is (Crank, 1970):

$$c_s(x,t) = C_0 \left[\sum_{n=0}^{\infty} (-1)^n \operatorname{erfc} \frac{(2n+1)a-x}{2\sqrt{Dt}} + \sum_{n=0}^{\infty} (-1)^n \operatorname{erfc} \frac{(2n+1)a+x}{2\sqrt{Dt}} \right] \quad (10A)$$

In Fig. 6A normalized desorption curves are plotted on a semi-logarithmic scale. These curves are constructed for different values of x/a by means of both types of series (Tukker, 1974). Depending on the value of x/a , the first part of the curves show either a convex or a concave course. Eventually all the curves become linear with equal slope.

It appears that for $t > 0.5 \tau$ the curves with $0.3 \leq x/a \leq 0.7$ are approximately mono-exponential and have the time constant τ defined in (9A). Hence, by

determination of τ from an exponential desorption curve, we can calculate the diffusion coefficient D , provided the length of the column of the solute, a , is known. In our experimental situation (section V-2-2) the space above the solute is closed. As a consequence, the concentration of the gas in this space ($x > 0$) rises during the desorption of the gas from the solute. Because the diffusion process is governed by linear differential equations, we can find $c_s(x,t)$ by superposition of the concentration in the solute as calculated previously and the concentration built up by sorption from the gas space. Therefore we need to analyse the sorption process. In the situation where the concentration in the gas space, c_g , is kept at a constant value, while the initial concentration of the gas in the solute is zero, it can be shown that the concentration in the solute builds up according to the formula:

$$c_s(x,t) = \frac{4C_0}{\pi} \left\{ \frac{\pi}{4} + \sum_{n=0}^{\infty} \left[\frac{1}{2n+1} \sin \frac{(2n+1)\pi}{2a} x e^{-(2n+1)^2 t/\tau} \right] \right\} \quad (11A)$$

Disregarding the constant, this sorption function is similar to the desorption function (8A). Hence, we can use sorption curves also to determine the diffusion coefficient.

In the experimental situation the gas space is closed, so that the gas concentration will not be constant but will decrease during sorption. This of course will affect the sorption curves.

To calculate the sorption into the solute when the concentration in the space is an arbitrary function $c_g(t)$ of the time, we use Laplace transformed functions (Abramowitz and Stegun, 1965).

Fick's second law, expressed in Laplace transformed

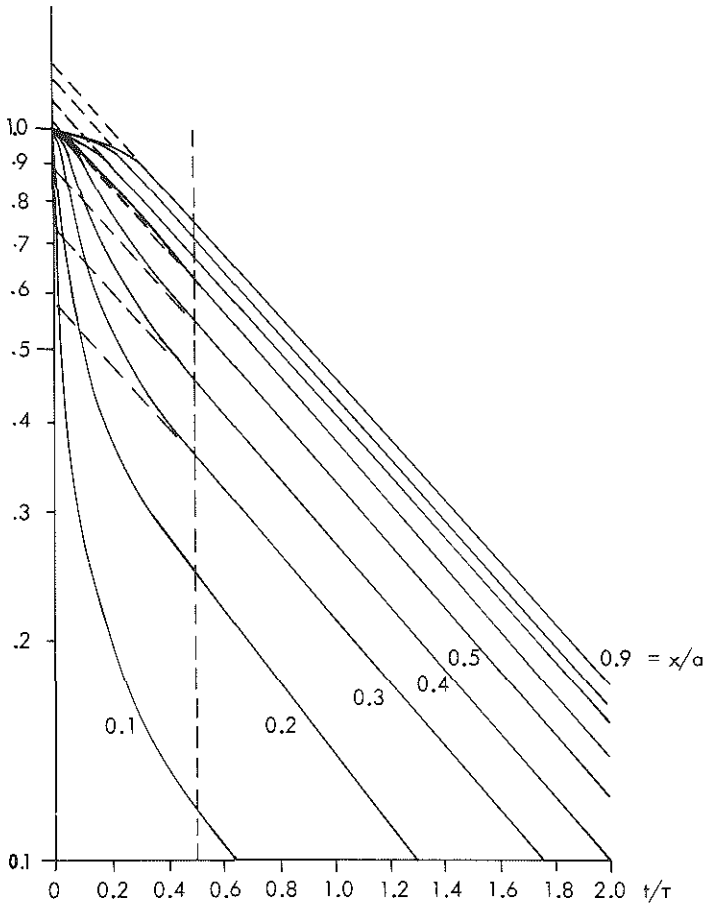


Fig. 6 A: Theoretical desorption curves (normalized), plotted on a semi-logarithmic scale, for various values of x/a (defined in text).

functions, is:

$$\frac{\delta^2 C_s(x,p)}{\delta x^2} - q^2 C_s(x,p) = 0$$

where:

$$C_s(x,p) = \int_0^\infty c_s(x,t) e^{-pt} dt$$

and

$$q^2 = \frac{p}{D}$$

The solution of this equation is (Crank, 1970):

$$C_s(x,p) = Ae^{-qx} + Be^{qx}$$

From the boundary condition at $x = a$:

$$\left(\frac{\delta C_s(x,p)}{\delta x} \right)_{x=a} = 0$$

it follows, that:

$$B = Ae^{2qa}$$

We assume further that, at $x = 0$, the concentration rises stepwise from zero at time $t = 0$, hence, $C_s(0,p) = 1/p$. In that case $A + B = 1/p$, so that the sorption curve can be described by the function:

$$C_s(x,p) = \frac{1}{p} \frac{\cosh q(x+a)}{\cosh qa}$$

Because this is a response to a unit step function at $x = 0$, the response to a unit pulse function is:

$$\frac{\cosh q(x+a)}{\cosh qa} \quad (12A)$$

In the desorption experiments we found that the concentration in the gas space can be described by an exponentially increasing function. This concentration function, Laplace transformed, can be represented by:

$$C_g(p) = \frac{K_1}{p} + K_2 \left(\frac{1}{p} - \frac{1}{p+1/\tau_g} \right)$$

where K_1 and K_2 are constants. At the interface between the solute and the gas space ($x = 0$) the concentrations are in equilibrium; hence:

$$C_s(0,p) = \frac{\beta K_1}{p} + \beta K_2 \left(\frac{1}{p} - \frac{1}{p+1/\tau_g} \right) \quad (13A)$$

where β is the solubility coefficient.

The concentration function $C_s(x,p)$, caused by the exponentially increasing concentration at $x = 0$, is found by multiplying (13A) with (12A):

$$\begin{aligned} C_s(x,p) = & \frac{\beta K_1 + p K_2}{p} \frac{\cosh q(x+a)}{\cosh qa} + \\ & - \frac{\beta K_2 \cosh q(x+a)}{(p+1/\tau_g) \cosh qa} \end{aligned} \quad (14A)$$

We can express this function as a series of exponential terms by using Heaviside's expansion theorem, i.e.:

$$c_s(x,t) = \sum_{k=1}^{\infty} \frac{T(p_k)}{N'(p_k)} e^{p_k t}$$

where p_k are the roots of $N(p) = 0$.

According to Crank (1970) the poles of $\cosh x$ are

$x_k = \pm (2n+1)\pi j/2$, ($n = 0, 1, \dots$). Hence, the poles of the concentration function (14A) are:

$$p = 0; -1/\tau_g; (2n+1)^2 t/\tau$$

Hence, the expansion theorem yields:

$$c_s(x,t) = K_3 + \sum_{n=0}^{\infty} K_{n,4} e^{-(2n+1)^2 t/\tau} + K_5 e^{-t/\tau_g} \quad (15A)$$

where K_3 , $K_{n,4}$ and K_5 are constants.

We note that, when the concentration in the gas space increases exponentially with a time constant τ_g , then the concentration function for the solute increases according to a series of exponential terms, with time constants equal to those in formula (8A), plus an extra exponential term with the time constant τ_g .

In the desorption experiment this course of the concentration function is superimposed on the course of the concentration calculated with the condition that c_g is kept zero.

In the experiments it turns out that the difference between τ and τ_g is small. This is a consequence of the fact that the concentration in the gas space builds up at a rate that is determined by the rate of desorption from the solute.

Therefore we conclude finally that, although the

concentration in the gas space is not kept at zero during the desorption experiment, the variation of the concentration in the solute will eventually become mono-exponential, with a time constant that is approximately equal to $\frac{4a}{\pi^2 D}$.

This is the theoretical background to the determination of the diffusion coefficient described in section V-2-2, using desorption and sorption methods.

REFERENCES

- Abramowitz, M. and Stegun, J.A. eds., Handbook of mathematical functions. Dover Public. Inc. New York 1965.
- Allan, L., Smith, G., Neufeld, R., Ominsky, J. and Wollmann, H., Interrelations among cerebral blood flow mean transit time and vascular volume. *Federative Proc.* 29-I, 519, Abstr. 1526, 1970.
- Bakker, L., Simulatie van de relatieve gewichten van de witte en grijze hersenen als functie van de gemiddelde cerebrale doorbloeding onder aanname van intercompartimentele diffusie, Cand.-thesis, T.H.-Delft, M 149, 1976.
- Barl, Ph., ed. *Medical Physiology* 14, 11th ed. The C.V. Mosby Comp., 1961.
- Boulay, G.H. du, and Verity, P.M., The cranial arteries of mammals. William Heinemann Medical Books Limited, 1973.
- Bozzao, L., Agnoli, A., Bartolini, A., and Fierchi, C. Local cerebral flow measured by clearance curves of hydrogen gas. Third Intern. Salzburg Conference, Ch. 7, 1969.
- Brans, J.M., Diskrete deconvolutie t.b.v. clearance curves. Cand. thesis, T.H.-Delft, M 136, 1975.
- Brown, A.S. and Donaldson, A.A. The effect of X-rays contrast medium (angiografin) on regional cerebral blood flow. In: *Brain and Blood Flow*. R.W. Ross Russell, e.a., Ditman London, 289-293, 1970.
- Bruin, M. de, X-ray fluorescent thyroid scanning; determination of the depth distribution of radio-activity. Paper presented at the 10th International Symposium on "Radio-active isotopes in clinical Medicine and Research", Report I.R.I.: 133-72-02, January 1972.
- Buckberg, G.D., Luck, J.C., Payne, D.B., Hoffman, J.I.E., Archie, J.P. and Fixler, D.E. Some sources of error in measuring regional blood flow with radio-active microspheres. *J. Appl. Phys.* 31, 598-604, 1971.
- Bustad, L.K. and McClellan, R.O., eds. *Swine in biomedical research*. Seattle Frayn Printing Co., 1966.
- Bijl en Salet, *Analytische Meetkunde II*, Delftsche Uitgevers Maatschappij, Delft, 1964.
- Crank, J., *The mathematics of diffusion*. Oxford University Press 1970.
- Crawley, J.C.W. and Veall, N., The gamma spectrum subtraction technique for measurement of activity in body organs and its use for cerebral blood flow studies. Symp. on dynamic studies with radio-isotopes in clinical medicine and research. Rotterdam, I.A.E.A., September 1970.
- Crone, C., The permeability of brain capillaries to non-electrolytes. *Acta Physiol. Scand.* 64, 407-417, 1965.
- Cummings, J.N., Harris, W.H. and Agar, J.L. Anaesthetic regime for prolonged operations in swine. *Canad. Anaesth. Soc.* 19, 557-566, 1972.
- Daniel, P.M., Dawes, J.D.K. and Prichard, Marjorie M.L. Studies of the carotid rate and its associated arteries. *Philos. Trans. Roy. Soc. London. B.* 237, 173-208, 1953.

- Diemer, K., Eine verbesserte Modellvorstellung zur Sauerstoffversorgung des Gehirns. Die Naturwissenschaften, Heft 19, 1963.
- Douglas, W.R. On pigs and men and research. Space Life Sciences 3, 226-234, 1972.
- Doyle, T.F., Martinas, A.N. and Kobrine, A.J. Estimating total cerebral blood flow from the initial slope hydrogen washout curves. Stroke, 6, 149-152, March-April 1975.
- Draper, N. and Smith, H. Applied Regression Analysis. John Wiley and Sons Inc. New York, 1967.
- Dreschler, W.A. Onderzoek naar fluctuaties in uitwascurves bij het hersenschorsdoorbloedingsonderzoek. Cand-thesis, T.H.-Delft, M. 141, November 1975.
- Duy1, W.A. Van, Zwart, A. Van der, Rikken, H. and Roggeveen, H. An electronic device for a quick analysis of exponential decay curves. Accepted for publication, Urologia Internationalis, 1977.
- Duy1, W.A. Van, Mechelse, K., Sparreboom, D. and Volkers, A.C.W. Interpretation of differences between "81-keV" and "31-keV" decay curves recorded during clearance of Xe-133 in cerebral tissue of the pig. In "Cerebral circulation and metabolism" eds. Th.W. Langfitt, L.C. Mc Henry, Jr., M. Reivich and H. Wollman. Springer Verlag, 409-412, 1975.
- Duy1, W.A. Van and Brenninkmeyer, P.J.J. Gain instability of scintillation detectors and consequences for dynamic tracer studies. Brit.J.Rad., 48-1037, 1975.
- Duy1, W.A. Van, Dynamische pulstempometing aan stochastische pulsreeksen. Internal report T.H. Delft, M.E. 72, October 1970.
- Duy1, W.A. Van, Measurement of cerebral circulation. Physical and mathematical aspects in using radio-active clearance methods. Accepted chapter in "Cardiovascular Physics", Vol. II, Ghista, D.N., Yang, W.J. and Van Vollenhoven eds., 1975.
- Duy1, W.A. Van, Volkers, A.C.W., and Sparreboom, D. Indications and consequences of diffusion effects on the measurement of cerebral blood flow based on the clearance method of diffusable gases. 16th Dutch Federative Meeting, 1975.
- Duy1, W.A. Van, Volkers, A.C.W. and Sparreboom, D. Cerebral circulation of the pig. The failure of the two-compartmental clearance model. 18th Dutch Federative Meeting, 1977.
- Duy1, W.A. Van, The measurement of cerebral blood flow in man. Paper read at Int.Symp.Nucl. Med., Bunnik, 1969.
- Duy1, W.A. Van, Sparreboom, D. and Volkers, A.C.W. Compartmental models of cerebral blood flow. Analysis using the "81-keV" and "31-keV" photons of "Xe-133". J. Nucl. Med. 17, 596-602, 1976.
- Duy1, W.A. Van, Tukker, J. and Volkers, A.C.W. Determination of the diffusion coefficient of Xe-133 in cerebral tissue. 17th Dutch Federative Meeting, 1976.
- Eckman, W.W., Phair, R.D., Fenstermacher, J.D., Patlak, C.S., Kennedy, C. and Sokoloff, L. Permeability limitation in estimation of local brain blood flow with C-14 antipyrine. Am. J. Phys. 229, 1, 215-221, July 1975.
- Edlich, R.F. et al. Radioactive microspheres; effect of their physical properties on vascular distribution. Proc. Soc. Exp. Biol. and Med. 128, 909-913, 1968.

- Ellenberger-Baum. Handbuch der vergleichende Anatomie der Haustiere. 18e Auflage, Springer Verlag 1943.
- Flehsig, G. und Zintzsch, J. Die Arterien der Schädelbasis des Schweines. Anat. Anz. Bd 125, 206-219, 1969.
- Foreman, D.L., Sanders, M. and Bloor, C.M. Total and regional cerebral blood flow during moderate and severe exercise in miniature swine. Appl. Phys. 40, 2, 191-195, 1976.
- Gardner, D.G. and Gardner, J.C. Analysis of multicomponent decay curves by use of Fourier transforms. Report N.A.S.-NS-3107-U.S. Atomic Energy Commission, 1962.
- Gardner, D.G., Gardner, J.C., Laush, G. and Wayne, Meinke W. Method for the analysis of multicomponent exponential decay curves. The Chem. Physics, 31, 4, 978-987, October 1959.
- Glass, H.J. and Harper, A.M. Measurement of regional blood flow in cerebral cortex of man through intact skull. Brit. Med. i 593, 1963.
- Grubb, R.L., Raichle, M.E., Eichling, J.O. and Ter-Pogossian, M.M. The effects of changes in P_{CO_2} on cerebral blood volume, blood flow and vascular mean transit time. Stroke 5, 632-639, Sept.-Oct. 1974.
- Haggendal, E., Nilsson, N.J. and Norback, B. Effect of blood corpuscle concentration on cerebral blood flow. Acta Chir. Scand. Suppl. 364, 13-21, 1966.
- Harper, A.M. Autoregulation of cerebral blood flow: influence of the arterial pressure on the blood flow through cerebral cortex. Journ.Neurol. Neurosurg.Psychiat, 29, 398-403, 1966.
- Harper, A.M., Glass, H.J. and Glover, M.M. Measurement of blood flow in the cerebral cortex of dogs by the clearance of Kr-85. Scot. Med. J. 6, 12-17, 1961.
- Harper, A.M. and Glass, H.J. Effect of alterations in the arterial carbon dioxide tension on the blood flow through the cerebral cortex at normal and low arterial blood pressure. J.Neurol. Neurosurg. Psychiat. 28, 449-452, 1965.
- Haskins, J.R. Monoenergetic absorption peaks obtained with a scintillation spectrometer. Rev.Sc.Instr. 28, 6, 425-426, 1957.
- Hedlund, S., Nyhn, G. and Regiström. The behavior of the cerebral circulation during muscular exercise. Acta Physiol. Scand. 54, 316-324, 1962.
- Heiss, W.D., Reisner, T. and Hoyer, J. Changes of Compartmental weight in the course of stroke. In: Blood Flow and Metabolism in the Brain. Harper, M. et al, eds. A viemore 1975.
- Held, K., Gottstein, U. and Niedermayer, W., C.B.F. in non-pulsatile perfusion. In: Cerebral Blood Flow. Brock, M., Fieschi, C., Ingvar, D.H., Lassen, N.A. and Schürmann, K. eds. 94-95, 1969.
- Hengst, D. Onderzoek naar het gebruik van Geranium Lithium halfgeleider-detectors voor bijzondere toepassing en in de nucleaire geneeskunde. Ir.-theis, T.H.-Delft, M. 81, 1971.
- Henneberg, R. Messungen der Oberflächenanschnung der Grosshirnrinde. J. Psych. Neurol. (Lpz), 17, 144, 1910-1911.
- Hills, B.A. Diffusion versus blood perfusion in limiting the rate of uptake of inert non-polar gases by skeletal rabbit muscle. Clin.Sci. 33, 67-87, 1967.

- Høedt-Rasmussen, K., Sveinsdottir, E. and Lassen, N.A. Regional cerebral blood flow in man determined by intra-arterial injection of radio-active inert gas. *Circ.Res.* XVIII, 3, 237-247, March 1966.
- Høedt-Rasmussen, K., Kr-85 and Xe-133 injected intra-arterially to measure regional blood flow in brain. K. Fellerger and R. Höfer, eds. Radio-active isotope in clinic Forschung Band VI, München/Berlin, Urban und Schwarzenberg, p. 232, 239, 1965.
- Hoffbrand, B.J. and Forsyth, R.P. Validity studies of the radio-active microspheres method for the study of the distribution of cardiac output, organ blood flow and resistance in the conscious rhesus monkey. *Cardiovasc. Res.* 3, 426-432, 1969.
- Hsu Hwei, P. Fourier Analysis. Simon and Schuster, N.Y. 1970.
- Iiliff, L., Zilkha, E., Bull, J.W.D., Boulay, G.H. du, Marshall, J., Ross Russel, R.W. and Symon, L. Effect of changes in C.B.F. on compartmental weight W . In: Cerebral Circulation and Metabolism, Philadelphia, Bangfitt, Th.W. et al, eds. 1975.
- Ingvar, D.H., Cronquist, S., Ekberg, R., Risberg, J. and Høedt-Rasmussen, K. Normal values of regional cerebral blood flow in man including flow and weight estimates of grey and white matter. *Acta Neurol. Scand.* 41, Suppl. 14: 72, 1965.
- Ingvar, D.H. and N.A. Lassen. Regional blood flow of cerebral cortex determined by Krypton-85. *Acta Physiol. Scand.* 54, 325-338, 1962.
- Jenkins, G.M. and Watts, D.G. Spectral analysis and its applications. Holden-Day Series in time series analysis, 1968.
- Jensen, K.B., Høedt-Rasmussen, K., Sveinsdottir, E., Stewart, B.M. and Lassen, N.A. Cerebral blood flow evaluated by inhalation of Xe-133 and extracranial recording: A methodological study. *Clin. Sci.* 30, 485-494, 1966.
- Julius, R.S. The sensitivity of exponentials and other curves to their parameters. *Computers and Biomedical Research* 5, 473-478, 1972.
- Kanno, Iwao and Kazuo, Uemura. Some experimental errors in calculating regional cerebral blood flow from the Intracarotid Xe-133 clearance curve: A quantitative evaluation employing a digital model. *Stroke*, 6, 370-375, 1975.
- Kasoff, S., Zingesser, L.H. and Shulman, K. Compartmental abnormalities of regional flow in children with head trauma. In: Brain and Blood Flow. R.W. Ross Russell ed., Pitman Med. and Scientific Publ. Co. Ltd. London, 1971.
- Kerkhoff, M. Over het registreren van stochastisch in de tijd verdeelde pulsen op een magnetische band bij lage bandsnelheid en het ontwerpen van een derandomizer om dit mogelijk te maken. Ir.-thesis, T.H.-Delft, M.E. 66, June 1970.
- Kety, S.S. and Schmidt, C.F. The effect of altered arterial tensions of carbon dioxide and oxygen on cerebral blood flow and cerebral oxygen consumption of normal young men. *J. Clin. Invest.* 27, 484-492, 1948.
- Kety, S.S. The theory and applications of the exchange of inert gas at the lungs and tissues. *Pharm. Rev.* 3, 1, 1951.
- Kirkegaard, P.A. A Fortran IV version of the sum of exponential square code exposum. Report Risø-M-1279, Research Establ. Risø, Danish Atomic Energy Commission, Sept. 1970.

- Kitani, K. Solubility coefficients of 85-Krypton and 133-Xenon in water, saline, lipids and blood. *Scand. J. Clin. Lab. Invest.* 29, 167-172, 1972.
- Krogh, A. Capillaries and oxygen in muscle. *J. of Physiol.* 52, 409, 1918.
- Lagerwey, E. Anaesthesie van het varken voor experimentele doeleinden. Dr.-thesis, Utrecht 1973.
- Ladefoged, J. and Andersen, A.M. Solubility of Xe-133 at 37°C in water, saline, olive oil, liquid paraffin, solutions of albumin and blood. *Phys. Med. Biol.* 12, 9, 353-358, 1967.
- Lanczos, C. Applied analysis. Prentice Hall Inc. Englewood Cliffs, N.Y. 1956.
- Landau, W.M., Freygang, W.H. Jr., Rowland, L.P., Sokoloff, L. and Kety, S.S. The local circulation of the living brain: values in the unanaesthetized and anaesthetized cat. *Trans. Am. Neurol. Assoc.* 80, 125, 1955.
- Lassen, N.A. Blood flow of the cerebral cortex calculated from 85-Krypton- β -clearance recorded over the exposed surface: evidence of inhomogeneity of flow. In: *Regional Cerebral Blood Flow*, Ingvar, D.H. and Lassen, N.A. eds. Lund, March 1965.
- Lassen, N.A. and Høedt-Rasmussen, K. Human cerebral blood flow measured by two inert gas techniques. Comparison of the Kety-Schmidt method and the intra-arterial injection method. *Circ.Res.* XIX, 681-688, Oct. 1966.
- Lassen, N.A. and Klee, A. Cerebral blood flow determined by saturation and desaturation with Kr-85. An evaluation of the validity of the inert gas method of Kety and Schmidt. *Cir.Res.* XVI, 26-32, 1965.
- Lauw, T.H. Identificatie van systemen bestaande uit N parallel geschakelde 1e orde systemen waarbij N niet vooraf bekend is, en de toepassing in het hersendoorbloedingsonderzoek. Ir-thesis, T.H. Delft, M. 152, 1976.
- Lesser, G.T. and Deutsch, S. Measurement of adipose tissue blood flow and perfusion in man by uptake of Kr-85. *Journ. Appl. Physiol.* 23, 621-6 0, 1967.
- Lewis, B.M., Sokoloff, L., Wechsler, R.L., Wentz, W.B. and Kety, S.S. A method for continuous measurements of cerebral blood flow in man by means of radio-active Krypton (Kr-85). *J. Clin. Invest.* 39, 707, 1960.
- Lierse, W. Die Kapillardichte in Wirbeltiergehirn. *Acta Anat.* 54, 1-31, Basel, 1963.
- Liew, H.D. Van, Graphic analysis of aggregates of linear and exponential processes. *J. Theor. Biol.* 16, 43-53, 1967.
- Liew, H.D. Van, Semilogarithmic plot of data which reflects a continuum of exponential processes. *Science*, 138, 682, 1963.
- Luginbuhl, H. and Detweiler, D.K. Animal models for the study of cerebro-vascular disease. In: *animal models for biomedical research*, Nat. Ac. of Sciences. Proc. of Symp. Dallas, Texas, 35-41, July 1967.
- Mallett, B.L. and Veall, N. The measurement of regional cerebral clearance rates in man using Xenon-133 inhalation and extra-cranial recording. *Clin. Sci.* 29, 179-191, 1965.

- Mallett, B.L. and Veall, N. Investigation of cerebral blood flow in hypertension using radioactive xenon inhalation and extracranial recording. *Lancet* i, 1081-1082.
- Marquardt, D.W. Solution of nonlinear chemical engineering models. *Chem. Eng. Progr.* 55, 6, 65-70, 1959.
- Marquardt, D.W. An algorithm for least-squares estimation of nonlinear parameters. *J. Soc.Industr.Appl. Math.* 11, 2, 431-441, 1963.
- Meier, P. and Zierler, K.L. On the theory of the indicator-dilution method for measurement of blood flow and volume. *J. Appl. Phys.* 6, 12, 1954.
- Mischenfelder, J.D., Messick, J.M. and Theyne, R.A. Simultaneous cerebral blood flow measured by direct and indirect methods. *J. Surg. Res.* 8, 475-481, 1968.
- Mishary, G., Clark, L.C. and Fox, R.P. Chronically implanted polarographic electrodes. *J. Appl. Physiol.* 13, 85, 1958.
- Myhill, J. Investigation of the effect of data-error in the analysis of biological tracer-data. *Biophys. J.* 7, 1967.
- Myhill, J. Investigation of the effect of data-error in the analysis of biological tracer-data from three-compartment systems. *J. Theor. Biol.*, 23, 218-231, 1968.
- Obrist, W.D., Thompson, H.K. Jr., King, C.H. and Wang, H.S. Determination of regional cerebral blood flow by inhalation of ¹³³Xenon. *Circ. Res.* XX, 124-135, 1967.
- Obrist, W.D., Thompson, H.K. Jr., Wang, H.S. and Wilkinson, W.K. Regional cerebral blood flow estimated by Xe-133 inhalation. *Stroke* 6, 245-255, May-June, 1975.
- Olesen, J. Contralateral focal increase of cerebral blood flow in man during arm work. *Brain* 94, 635-646, 1971.
- Olesen, J., Paulson, O.B., Lassen, N.A. Regional cerebral blood flow in man determined by the initial slope of the clearance of intra-arterially injected Xe-133. *Stroke* 2, 519-540, Nov./Dec. 1971.
- Osborn, J.O., Stitzell, J.A. and Peterson, R.E., Diffusion of argon krypton and xenon in olive oil. *J. Appl. Phys.* 27, 5, 624-629, 1969.
- Papoulis, A. A different approach to the analysis of tracer data. *S.J.A.M. J. Control.* 11, 3, 466-474, 1973.
- Paulson, O.B., Lassen, N.A., Skinhøj, E. Regional cerebral blood flow in apoplexy without arterial occlusion. *Neurology (Minneapolis)* 20, 125-138, 1970.
- Paulson, O.B., Cronquist, S., Risberg, J. et al. Regional cerebral blood flow: A comparison of 8 detector and 16 detector instrumentation. *J. Nucl. Med.* 10, 164-173, 1969.
- Perl, W. A method for curve-fitting by exponential functions. *Int. J. Appl. Radiat. Isot.* 8, 211, 1960.
- Perl, W., Rackow, H., Salanitro, E., Wolf, G.L. and Epstein, R.M. Intertissue diffusion effect for inert fat-soluble gases. *J. Appl. Physiol.* 20, 4, 621-627, 1965.
- Pfaff, R. Een analysemethode voor meetgegevens van het hersenschorsdoorbloedingsonderzoek. Ir-thesis, T.H. Delft, M.135, Aug. 1975.
- Poelgeest, R. Van. Digitale compartimentele analyse m.b.v. de inverse Laplace-transformatie van de meetgegevens die verkregen worden bij het hersenschorsdoorbloedingsonderzoek m.b.v. Xe-133.

- Ir.-thesis, T.H.-Delft, M. 85, June 1971.
- Price, W.J. Nuclear radiation detection. Mc. Graw-Hill series in nuclear engineering, 1964.
- Prost, R., Azencot, J., Goutte, R. Identification des fonctions de transfert de systèmes linéaires de premier ordre associés en parallèle. *Automatisme*, Tome XIX, no 8/9, 1974.
- Purves, M.J. The physiology of the cerebral circulation. Cambridge University Press, 1972.
- Rainwater, L. Applications of probability theory to nuclear particle detection. *Nucleonics*, Oct. 1947.
- Reivich, M. Observations on exponential models of cerebral clearance-curves. In: Research on cerebral circulation. Third Salzburg Conf. Ch. 13, 1969.
- Reivich, M. Slater, R. and Sano, N. Further studies on exponential models of cerebral clearance curves. *Proc. C.B.F.* 1969.
- Reivich, M., Jehle, J., Sokoloff, L. and Kety, S.S. Measurement of regional cerebral blood flow with antipyrine-C-14 in awake cats. *J. of Appl. Phys.* 27, 2, 1969.
- Reivich, M., Obrist, W., Slater, R., Greenberg, J. and Goldberg, H.J. A comparison of the Xe-133 intracarotid injection and inhalation techniques for measuring regional cerebral blood flow. In: *Blood Flow and Metabolism in the Brain*, Harper, M. et al eds., 1975.
- Reneman, R.S., Wellens, D., Jagenau, A.H.M. and Stynen, L. Vertebral and carotid blood distribution in the brain of the dog and the cat. *Cardiovasc. Res.* VIII, 1, 65-72, 1974.
- Risberg, J. and Ingvar, D.H. Patterns of activation in the grey matter of the dominant hemisphere during memorization and reasoning. *Brain*, 96, 737-756, 1973.
- Risberg, J. Zenob, A. Wilson, E.M., Wills, E.L. and Halsey, J.H. Regional cerebral blood flow by Xe-133 inhalation. Preliminary evaluation of an initial slope index in patients with unstable flow. *Stroke*, 6, 142-147, March-April 1975.
- Roberts, G.W., Larson, K.B. and Spaeth, E.E. The interpretation of mean transit time measurements for multi-phase tissue systems. *J.Theor. Biol.*, 39, 447-475, 1973.
- Roth, J., Greenfield, A., Kaihara, S. and Wagner, H. Jr. Total and regional cerebral blood flow in the unanesthetized dog. *Am.J. Physiol.* 219, 96-101, 1970.
- Rudolph, A.M. and Heyman, M.A. The circulation of the fetus in utero. Methods for studying distribution of blood flow, cardiac output and organ blood flow. *Circ. Res.* 21, 163-184, 1967.
- Sapirstein, L.A. Regional blood flow by fractional distribution of indicators. *Am. J. Physiol.* 193, 161-168, 1958.
- Smalhout, B. Capnography, its importance in diagnosis operation and after treatment of neurological patients. Dr.-thesis, Utrecht, 1967.
- Smith, A., Neufeld, G.R., Ominsky, A.J. and Wollman, H. Effect of arterial CO₂ tension on cerebral blood flow, mean transit time and vascular volumes. *J. Appl. Physiol.* 31, 701-707, 1971.
- Sokoloff, L. The action of drugs on the cerebral circulation. *Pharmac. Rev.* 11, 1-85, 1959.

- Sparreboom, D., Duyl, W.A. Van, Lauw, T.H., Pfaff, R. and Poelgeest, R. Van. An evaluation of three transform methods for the analysis of multicomponent exponential decay curves. In preparation, 1976.
- Steyn, J.J., Andrews, D.G. and Dixmier, M. Collimated detector response to point, line and plane source. Nucl. Instr. and Methods 74, 123-131, 1969.
- Stortenbeek, W. Het zuur-base evenwicht bij de mens. De erven F. Bohn. nv. Haarlem, 1970.
- Sveinsdottir, E., Thorlöf, P., Risberg, J. et al. Calculation of regional cerebral blood flow (r.C.B.F.): initial-slope-index compared to height-over-area values. In: Russell R.W.R. (ed.). In: Brain and blood flow, London, Pitman Co Ltd, p. 85-93, 1971.
- Tschetter, T.H., Klassen, A.C., Resch, J.A. and Meyer, M.W. Blood flow in the central and peripheral nervous system of dogs using a particle distribution method. Stroke 1, 370-374, 1970.
- Tschetter, T., Meyer, M., Klassen, A. and Resch, J. Regional cerebral blood flow using labeled microspheres. Proc. Int. Union of Physiol. Sci. 7, 441, 1968.
- Tukker, J. Modelvorming van de hersenschorsdoorbloeding. Ir.-thesis, T.H.-Delft, M. 112, April 1974.
- Valois, J.C. De, and Groot, P. De. Discrepancies in the results of flow measurements using different isotopes, Kr-85, Xenon-133 and C-114, antipyrine. In: Cerebral Circ. and Metabolism. Langfitt, W., McHenry, L.C., Reivich, M., Wollman, H. eds., New York, Springer, 1975.
- Valois, J.C. De and Peperkamp, J.P.C. The influence of some drugs upon the regulation of cerebral blood flow in the rabbit. In: Brain and Blood Flow, Russell, R.W. ed., Pitman Med. and Sc. Publ. Co., London, 1971.
- Veall, N. and Mallett, B.L., The partition of trace amounts of Xenon between human blood and brain at 37°C. Phys. Med. Biol. 10, 375-380, 1965.
- Veall, N. and Mallett, B.L. Regional cerebral blood flow determination by Xe-133 inhalation and external recording. The effect of arterial recirculation. Clin. Sci. 30, 353-369, 1966.
- Wagner, H.N. ed. Principles of Nuclear Medicine. W.B. Saunders Company. Philadelphia, London, Toronto, 1968.
- Weber, J. en Rasmussen, C.E. Inleiding tot de stralingshygiëne. Ver. Studie en Studentenbelangen, Delft, 1972.
- Wilde, D.J. Optimum seeking methods. Prentice Hall, Englewood Cliffs, New York, 1964.
- Wilkinson, J.M.S., Bull, J.W.D., Boulay, G.H. du, Mashall, J., Ross Russell, R.W. and Symon, L. The heterogeneity of blood flow throughout the normal cerebral hemisphere. In: Cerebral Blood Flow. Springer, Mainz, 17-18, 1969, Brock et al. ed.
- Winsor, Travis. Electrocardiografie voor de medicus practicus. C.I.B.A. publ. 1968.
- Wollman, H., Smith, A.L. and Alexander, S.C., Effects of general anesthetics in man on the ratio of cerebral blood flow to cerebral oxygen consumption. In: Cerebral Blood Flow, Brock et al eds., Springer Berlin, 242-243, 1969.

- Wollman, H., Alexander, S.G., Cohen, P.J., Stephen, G.W. and Zeiger, L.S. Two-compartmental analysis of the blood flow in the human brain. In: Regional Cerebral Blood Flow. Lund. Ingvar, D.H. and Lassen, N.A. eds. Munksgaard, Copenhagen, 1965.
- Worsley, B.H. Analysis of decay-type data, Communications of the A.C.M., 7, 1, Jan. 1964.
- Yeh, S.Y. and Peterson, R.E. Solubility of carbon dioxide, krypton and xenon in lipids. J. Pharm. Sc. 52, 5, 453-458, 1963.
- Yeh, Shu-Yuan and Peterson, R.E. Solubility of krypton and xenon in blood, protein solutions and tissue homogenates. J. Appl. Physiol. 20, 1041-1047, 1965.
- Zobl, E.G., Talmers, F.N., Christensen, R.C. and Baer, L.J. Effect of exercise on the cerebral circulation and metabolism. J. Appl. Physiol. 20, 1289-1293, 1965.
- Zwart, A. and Dieren, A. Van. Monitoring and control aspects during halothane anesthesia: some results of combined model simulation and animal experiments. Progress Report 4, Inst. Med. Phys., 70-82, 1974.
- Zwart, A. and Seagrave, R. Oscillations in cerebral concentrations during flow measurement and halothane anesthesia. Digest of the 10th Int. Conf. Med. Biol. Eng. 33-7, Dresden, 1973.
- Zwart, A.J. Van der. Modelvorming van de visco-elastische eigenschappen van de urineblaas en het ontwerp van een apparaat om de parameters van dit model te bepalen. Ir.-thesis, T.H.-Delft, M. 106, 1973.

SUMMARY

The measurement of blood flow in the cerebrum is important both clinically and for research. A method which is often used is based on the measurement of the clearance of the radioactive inert gas Xe-133 from cerebral tissue via the blood. The Xe-133 is administered either by injection into an artery in the neck (injection technique) or via the lungs (inhalation technique). The clearance is measured by means of a radiation detector placed over the skull.

The injection technique is more attractive from a measurement point of view, but traumatic for the patient. The inhalation technique is atraumatic, but yields less reliable results.

After a survey of various methods for the measurement of cerebral blood flow, this thesis gives a description of the clearance techniques. Experience with the inhalation technique is discussed. The results of the injection technique, applied to the pig, are then described.

A study of the usual two-compartmental model for the interpretation of the clearance curves is included. The model study is based on simultaneous registration of the 81-keV and 31-keV radiation of Xe-133. It is found that the model cannot account for the results. Problems of interpretation arise when the clearance curves are analysed as a sum of exponential terms. It is proposed that the curves may be analysed as a series of positive powers of the time.

The fallacy of the two-compartmental model is more manifest in the measurements in the pig than in measurements in other animals. This is a consequence of the remarkably low rate of clearance of Xe-133 in the

pig, compared to published observations on other animals. Therefore this study is a model for the characteristic problems to be expected in situations where the cerebral blood flow is pathologically reduced.

From a small series of measurements of the diffusion coefficient and the solubility coefficient of Xe-133 in cerebral tissue, based on sorption and desorption measurements, remarkable results are obtained, which deviate from published data.

An interesting relation between the cerebral blood flow and the carbon dioxide in the expired air is observed, namely a hysteresis effect and a relative maximum in the flow at low concentrations of carbon dioxide.

SAMENVATTING

Het meten van de doorbloeding van de hersenen is van belang zowel voor de kliniek als ook voor wetenschappelijk onderzoek. Een veel toegepaste methode is gebaseerd op de meting van de uitwas van het radioactieve edelgas Xe-133 uit het hersenweefsel door het bloed. Het Xe-133 wordt toegediend d.m.v. een injectie in een halsslagader (injectie-techniek) of via de longen (inhalatie-techniek). De uitwas wordt gemeten m.b.v. stralingsdetectoren geplaatst op de schedel. De injectie-techniek is meettechnisch aantrekkelijker, maar traumatisch voor de patiënt. De inhalatie-techniek is atraumatisch, echter de meetresultaten zijn minder betrouwbaar.

Dit proefschrift geeft, na een overzicht van een aantal andere methoden om de hersendoorbloeding te meten, een beschrijving van de uitwastechnieken. Hierbij komen enige ervaringen met de inhalatie-techniek ter sprake. Vervolgens worden de resultaten beschreven van de toepassing van de injectie-techniek op het varken. Hierin is opgenomen een studie van het gebruikelijke twee-compartimenten model voor de interpretatie van de uitwascurven. Deze modelstudie is gebaseerd op een, gelijktijdige registratie van de 81-keV en 31-keV straling van het Xe-133. Gebleken is, dat dit model tot strijdige resultaten leidt.

Interpretatie-problemen ontstaan, indien de curven geanalyseerd worden volgens een som van e-machten. Voorgesteld is de uitwascurven te analyseren volgens een positieve macht-reeks van de tijd.

Het falen van het twee-compartimenten model manifesteert zich sterker bij metingen aan het varken dan bij metingen aan andere proefdieren. Dit is een gevolg van

een opvallend lage uitwassnelheid van het Xe bij het varken, vergeleken met gepubliceerde waarnemingen. Hierdoor staat deze studie model voor karakteristieke problemen die te verwachten zijn bij lage hersendoorbloeding b.v. in pathologische gevallen.

Op grond van een kleine serie metingen van de diffusiecoëfficiënten en oplosbaarheidscoëfficiënten van Xe-133 in hersenweefsel, gebaseerd op sorptie en desorptie metingen, zijn opmerkelijke, van de literatuur afwijkende, resultaten verkregen.

Voorts is aan het varken een bijzondere relatie geobserveerd tussen de hersendoorbloeding en de koolzuurspanning in de uitademingslucht, t.w. een hysteresiseffect en een relatief maximum in de doorbloeding bij lage koolzuurconcentraties.

CURRICULUM VITAE

(Op verzoek van de Erasmus Universiteit Rotterdam)

De auteur van dit proefschrift werd geboren op 14 mei 1939 te Rotterdam. Hij behaalde in 1956 het M.U.L.O.-B diploma. Daarna bezocht hij de H.T.S. te Rotterdam, waar hij in juli 1960 het diploma 'electrotechniek' behaalde. Van juli 1960 tot november 1960 was hij in dienst van Philips N.V. te Eindhoven. Daarna vervulde hij de militaire dienstplicht tot september 1962. Vervolgens studeerde hij aan de Technische Hogeschool te Delft. Hij studeerde af in de electrotechnische meettechniek o.l.v. Prof.Dr.Ir. F.A. Heyn en legde in 1968 het doctoraal examen af in de electrotechniek. Tijdens zijn T.H.-studie werkte hij enige maanden bij de Elektrizitätswerk Wesertal in Hameln en bij The British Broadcasting Corporation te Londen. Van 1966 tot 1968 was hij student-assistent bij het Laboratorium voor Electrotechnische Meettechniek. In 1968 werd hij bij dit Laboratorium aangesteld als wetenschappelijk medewerker met een 0,5 deeltaak bij de werkgroep voor Medische Electrotechniek. Tevens werd hij voor 0.5 deeltaak aangesteld bij de Afdeling Biologische en Medische Natuurkunde (hoofd Prof.Dr. G. van den Brink) van de Medische Faculteit te Rotterdam, aanvankelijk bij het Praktikum Natuurkunde, later voor onderzoek. Bij de werkgroep voor Medische Electrotechniek was hij belast met het begeleiden van studenten bij kandidaats- en afstudeeropdrachten. De onderwerpen kwamen voort uit onderzoek van de auteur, verricht aan de Medische Faculteit. Een belangrijk deel hiervan had betrekking op het thema van dit proefschrift. Naast onderzoek van de meting van de hersendoorbloeding

heeft de auteur onderzoek verricht op het gebied van de Urologie.

Sinds oktober 1976 is de auteur voor 0,8 deeltaak als wetenschappelijk hoofdmedewerker verbonden aan de Faculteit der Geneeskunde van de Erasmus Universiteit Rotterdam en voor 0,2 deeltaak aan de Afdeling der Electrotechniek van de Technische Hogeschool te Delft. Sinds 1971 verzorgt hij jaarlijks een serie colleges 'Inleiding in de systeemtheorie voor de geneeskunde'.